Application of the Jost-matrix Theory to the Lambda-nuclear and Multi-Lambda systems

by

Ishmael Mmusi Gopane

Submitted in partial fulfilment of the requirements for the degree

Doctor of Philosophy

in the Faculty of Natural & Agricultural Sciences

University of Pretoria

Supervisor: Prof. S.A Rakitianski

February 27, 2024

UNIVERSITY OF PRETORIA

DECLARATION OF ORIGINALITY

**This document must be signed and submitted with every
essay, report, project, assignment, dissertation and/or thesis.**

Full names of student: Ishmael Mmusi Gopane

Student number: 24209148

Personal number: 04361482

Declaration

1. I understand what plagiarism is and am aware of the University's policy in this regard.

2. I declare that this thesis is my own original work. Where other people's work has been used (either from a printed source, Internet or any other source), this has been properly acknowledged and referenced in accordance with departmental requirements.

3. I have not used work previously produced by another student or any other person to hand in as my own.

4. I have not allowed, and will not allow, anyone to copy my work with the intention of passing it off as his or her own.

SIGNATURE STUDENT:..

SIGNATURE SUPERVISOR:..

Summary

This study involves the investigation into the hypernuclear and multi-lambda systems using the Jost-function method, as well as the recovery of the two-body potential from the two and three-body systems using the approximate(guessed) wavefunction.

The Schrodinger equation describing the quantum system of interest is solved by being replaced with a system of first-order differential equations, which enable one to obtain the Jost functions. These Jost functions are multi-valued energy functions which can be treated as single-valued functions defined on a complex energy surface called the Riemann surface. Direct calculations of the Jost functions, the S-matrix, for all complex momenta of physical interests including the spectral points corresponding to the bound states and resonance states can be obtained. In this work, this method was used to locate the spectral points for the wide range of Λ-nuclear systems within the two-body ΛA-model. The S-matrix residues as well as the corresponding Nuclear-Vertex and Asymptotic-Normalization constants (NVC's and ANC's) for the bound states are also found.

For scattering parameters the Jost functions were factorized in such a way that they contain certain combination of the channel momenta times an analytic single-valued function of the energy E. The remaining energy-dependent factors were now defined on single energy plane which does not have any branching points anymore. For these energy-dependent functions, a system of first-order differential equations is obtained. Then, using the fact that the functions are analytic, they were expanded in the power series to obtain a system of differential equations that determine the expansion coefficients. When the expansion coefficients are obtained for the expansion around the energy $E_0 = 0$,

the coefficients are then used to calculate the effective range parameters. For the same hypernuclear systems, the scattering lengths, effective radii, and the other effective-range parameters (up to the order $\sim k^8$) for the angular momentum $\ell = 0, 1, 2$ are calculated.

Possible bound and resonant states of the multi-lambda systems $\Lambda\Lambda(0^+)$, $\Lambda\Lambda\Lambda(\frac{1}{2}^-)$ and $\Lambda\Lambda\Lambda\Lambda(0^+, 1^+, 2^+)$ are sought as zeros of the corresponding Jost functions calculated within the framework of the hyperspherical approach with local two-body S-wave potentials describing the $\Lambda\Lambda$ interactions. Bound $\Lambda\Lambda(0^+)$, $\Lambda\Lambda\Lambda(\frac{1}{2}^-)$ and states only appears if the two-body potentials are multiplied by a minimum factor of ~ 1.461 and 3.449. For $\Lambda\Lambda\Lambda\Lambda(0^+, 1^+, 2^+)$ systems the bound states appear when the two-body potentials are multiplied by the factors ~ 3.018, 4.360 and 3.419.

A method for deducing the two-body potential from a given two- or three-body wave function is suggested. This method makes it possible to numerically obtain an unknown potential acting between the particles A and B when we know the potentials of their interaction with a third particle C and know the characteristics of the three-body bound state (ABC). The systems (nnp) and $(\Lambda\Lambda\alpha)$ were used to show that a three-body wave functions can be constructed using the knowledge of the binding energies and sizes of these systems to deduce reasonable and realistic nn and $\Lambda\Lambda$ potentials.

3

Acknowledgments

I would like to acknowledge the following:

- Prof. Sergei Rakitianski for his patience, help and guidance throughout this journey

- My family and friends for their support and encouragement during my studies

- The staff and fellow students of the Department of Physics of the University of Pretoria for their support

- The National Research Foundation, University of Pretoria, and Sol Plaatje university for their financial support

Contents

iii

List of Figures

List of Tables

viii

Chapter 1

Introduction

1.1 Hypernuclear physics

In 1952 Marian Dansyz and Jerzy Pniewski used the nuclear emulsion technique to see two stars connected by thick track and that led them to the conclusion that the experimental evidence depicted a hypernucleus, in particular a nucleus consisting of a Λ-hyperon and nucleons. Many hypernuclei were discovered up until 1955 [1][2]. After more than 65 years of research on hypernuclei, our knowledge of the interaction of hyperons with nucleons or with other hyperons still remains limited and this situation is not good given the important role that hyperons play in various aspects of nuclear physics as well as for astrophysics[3, 4, 5, 6, 7, 8].

The Λ-Particle belongs to the group of particles called hyperons (eg, $Y = \Lambda, \Sigma, \Xi$) which are heavier than nucleons and made up of the up quark, the down quark and the strange quark. The Λ-particle is the lightest hyperon with the mass of 1115.684MeV and a mean life of $2.60 \times 10^{-10}s$. Its properties are listed in Table 1.1.

Table 1.1: Λ-particle properties taken from [9].

Λ-particle property	Quantum number
Isospin(I)	0
Spin(Parity)	$1/2^+$
Charge(Q)	0
Strangeness(S)	-1
Charm(C)	0
Bottomness(B)	0

The nucleus consisting of one or more nucleons replaced by Λ-hyperons is referred as hypernucleus. Currently, only single-Λ (or $S = -1$ single-strange) and double-Λ (or $S = -2$ double-strange) hypernuclei have been found experimentally. In the first case the physical properties of the hyperon-nucleon interaction can be studied, while in double-Λ hypernuclei the hyperon-hyperon interaction is also accessible [10]. In this case, $S = -2$ nuclei such as double-Λ hypernuclei and Ξ hypernuclei represent the way to the multi-strangeness systems[10]. Due to lack of knowledge regarding the $S = -2$ scattering data we have very little knowledge of the $\Lambda\Lambda$ and ΛN interactions. When nucleons are added to the core nucleus, they can only be outside the core nucleus due to the Pauli exclusion principle. But, when a Λ hyperon is added to the core nucleus, due to no Pauli principle between the nucleon and Λ, then the Λ particle can penetrate inside, and attract the surrounding nucleons towards the interior of the core nucleus [11].

The hyperon-nucleon (YN) and the hyperon-hyperon (YY) interactions are important to explore the strange nuclear systems, in which hyperons (or strange quarks) are added in a normal nuclear systems as "impurities"[11, 12]. Despite their importance, YN and YY interactions have still large uncertainties because direct YN and YY scattering experiments are either difficult or impossible due to the short life-time of hyperons [13]. Hence, the knowledge of the hyperon-nucleon (YN) interaction is crucial for further development of the hypernuclear physics. For instance, studies of very neutron rich hypernuclei are important to understand the nature of neutron stars because several model calculations predict that hyperons might be dominating in the core of neutron stars [14, 15].

Around 1960, two double-Λ hypernuclei were experimentally observed and reported, $^{10}_{\Lambda\Lambda}$Be [16, 17], and the other was $^{6}_{\Lambda\Lambda}$He[18]. In 1991, a new double-Λ hypernucleus was found in an emulsion-counter experiment [18] at KEK, which was difficult to identify the event uniquely. One interpretation of the observation was $^{10}_{\Lambda\Lambda}$Be with a repulsive $\Lambda\Lambda$ interaction [19], and another was $^{13}_{\Lambda\Lambda}$B with an attractive $\Lambda\Lambda$ interaction. In 2001, the KEK $E373$ experiment [20] reported the observation of the double-Λ hypernucleus $^{6}_{\Lambda\Lambda}$He (called the Nagara event), which was uniquely identified as a double-Λ hypernucleus. The experiment extracted a two-Λ removal energy of 6.91 ± 0.16 MeV [20, 21]. This event demonstrated that the $\Lambda\Lambda$ interaction should be less attractive than the ΛN interaction, significantly influencing the study of the $S = 2$ sector interaction. Another important observation was that of the hypernucleus identified as $^{10}_{\Lambda\Lambda}$Be, termed the Demachi-Yanagi event [22] with the binding energy from this hypernucleus reported to be 11.90 ± 0.13 MeV. However, whether this event should be interpreted as the ground state or as an excited state remains ambiguous. Furthermore, in 2010, another double-Λ hypernucleus was observed for the first time, known as the Hida event [22]. However, again, there are two possible interpretations of this event (see the next section for details): The hypernucleus is either $^{11}_{\Lambda\Lambda}$Be, whose two-Λ removal energy is 20.83 ± 1.27 MeV, or $^{12}_{\Lambda\Lambda}$Be, whose two-Λ removal energy is 22.48 ± 1.21 MeV. Therefore, whether this event should be interpreted as a ground state or an excited state is unclear.

2

The other important aspect of the $S = -1$ hypernulear systems is the knowledge regarding the $\Lambda N - \Sigma N$ coupling, which affects Λ and Σ hypernuclei. $\Lambda N - \Sigma N$ coupling is also important for understanding the equation of state (EoS) that governs the size and mass of neutron stars. To understand the mechanism of gravitational waves from two–neutron star mergers, we first need to understand the structure of neutron stars. For this purpose, the EoS is essential. It is crucial to construct the EoS with strangeness. That is why this observation is important from the perspective of hypernuclear physics. This $\Lambda N - \Sigma N$ coupling effect is thought to play a significant role in neutron-rich Λ hypernuclei due to the total isospin becoming larger[10].

Several theoretical methods have been used over the past years to study hypernuclei systems. For local interactions, configuration space methods suh as, e.g. hyperspherical harmonics, Green's function Monte Carlo, expansion in Gaussians or stochastic variational method (SVM), have been successfully used to predict properties of light hypernuclei [3, 23, 24, 25, 26, 27]. For very light systems, the same goal can be achieved by solving the Faddeev or Yakubovsky equations in momentum space [3, 28, 29, 30, 31, 32, 33]. Those methods allow one also to deal with non-local two-body interactions, but it is difficult to extend the approaches to larger systems. Alternatively, shell model calculations have been a quite successful tool to understand properties of hypernuclei, in particular the energy level splittings [3, 34, 35, 36, 37]. However, that approach requires specific effective interactions that are not easily related to free-space baryon-baryon interactions. The same disadvantage also holds for density functional approaches, which have been applied to rather complex hypernuclei [38, 39]. Recently, nuclear lattice effective field theory (NLEFT) has been extended to hypernuclei using the impurity lattice Monte Carlo technique [40]. Although this first study has been performed with somewhat simplified (spin-independent) interactions, that method promises the application of free-space interactions up to medium-heavy hypernuclei. One specifically interesting approach to tackle bound baryon systems is the no-core shell model (NCSM) [41].

There are three different types of physical problems associated with the Schrödinger equation in a non-relativistic quantum mechanical system, namely, bound, scattering, and resonant state problems which differs in the boundary conditions imposed on their corresponding wave function at large distances.

A method used in this Thesis for locating central short range potential spectral points, is based on a direct calculation of the Jost functions for single channel case or Jost matrices for multichannel case in the complex mometum k-plane, has recently been developed [42, 43, 44, 45]. When defined for all complex values of the momentum, these functions contain complete information about the underlying physical system. Within this method, the bound, resonant, and scattering states can be found by calculating the Jost solutions and the Jost functions on the appropriate domain of the k-plane. The bound and resonant state energies, for example, can be found by locating the zeros of the Jost function on the positive imaginary axis and in the fourth quadrant respectively. To obtain the Jost functions, the second-order Schrödinger equation is transformed into

the coupled first-order differential equations whose solutions asymptotically tend to the Jost functions, using an appropriate boundary conditions starting from $r = 0$ up to a distance where the potential vanishes.

The S-matrix can be constructed as the ratios of the Jost functions and therefore is singular at each spectral point where the Jost functions is zero. Firstly, the Jost functions are multivalued energy functions and thus are defined on an appropriate number of layered Riemann energy surface consisting of physical sheets and unphysical sheets.

Bound states and resonance states parameters are determined by finding the poles of the S-matrix in an appropriate domain of the Riemann surface of energy. We move around a threshold point E_n, from one layer to another. The threshold points $E_n (n = 1, 2, ..., N)$ are the branching points on this manifold[46]. Bound states correspond to negative energy , $E_b < 0$, poles on the physical sheets of the Riemann surface of energy and the resonances corresponds to the S-matrix poles at complex energies, $E_i = E_r - i\Gamma/2$, on the unphysical sheets of the energy Riemann surface.

At the spectral points the S-matrix residues can be calculated together with their corresponding Nuclear vertex constants and the Asymptotic normalization constants.

In quantum scattering theory, Taylor power-series expansion is used in what is known as the effective-range expansion. For short range potential, it represented by this type of a function which contains the scattering phase shift $\delta_\ell(k)$ in this form,

$$k^{2\ell+1} \cot \delta_\ell(k) = \sum_{n=0}^{\infty} c_{\ell n} k^{2n}, \tag{1.1}$$

where sum of terms proportional to even powers of the collision momentum k, and $c_{\ell n}$ are energy independent expansion coefficients corresponding to the low-energy parameters.

A method within the phase variable approach was developed at least 60 years ago to calculate the low-energy scattering parameters accurately, called phase-variable method(see Ref.[46] and Refs. within). The technique of canonical quantization was used recently to re-derive the same equations [47]. The low-energy parameters were now obtained via the asymptotic values($r \to \infty$) of the corresponding radial functions $a(r), r_0(r), P(r), ...$ obeying a system of first-order differential equations. However, the problem arises when the potential that supports the bound states is being used.This leads to the function $a(r)$ to have singularities and difficulties when the system of the differential equations is solved numerically leading to numerical difficulties. This problem is resolved when we use the expansion coefficients of the Jost functions which also obeys the system of the differential equations. The Jost functions expansion coefficients can be used to obtain the low-energy parameters.

1.2 Aims and Objectives

1.2.1 The Lambda-hypernuclear systems

The first part of this study involves the investigation into the single Lambda-nuclear systems. We would like to find their corresponding spectral points (i.e the bound and resonance states) and the scattering parameters. We will try to do so for several orbital angular momentum. The S-matrix residues at the bound state energies as well as their corresponding Asymptotic normalization and Nuclear vertex constants would also be calculated.

There are several reasons that motivate the studies of the Lambda-nuclear interactions. First of all, they constitute the major part of the research devoted to the strangeness in nuclear physics [48]. In addition to that, the low-energy collisions of Λ-particles with nuclei and the formation of their bound states (hyper-nuclei) play an important role in the description of massive celestial bodies such as the neutron stars [49, 50, 51].

At low collision energies the Λ-nucleus scattering phase-shift $\delta_\ell(k)$ can be accurately parametrized with the help of the scattering length a_ℓ, effective radius r_ℓ, and few other parameters (P_ℓ, Q_ℓ, L_ℓ, etc.) of the effective-range expansion,

$$k^{2\ell+1}\delta_\ell(k) = -\frac{1}{\mathsf{a}_\ell} + \frac{\mathsf{r}_\ell}{2}k^2 - \mathsf{P}_\ell \mathsf{r}_\ell^3 k^4 + \mathsf{Q}_\ell \mathsf{r}_\ell^5 k^6 - \mathsf{L}_\ell \mathsf{r}_\ell^7 k^8 + \cdots \tag{1.2}$$

Therefore the knowledge of these parameters for the hyper-nuclear systems is helpful in the analysis of various Λ-nuclear collision processes.

In addition to the elastic collisions, the Λ-particle can be captured by a nucleus with the emission of a γ-quantum. Theoretical description of such a capture involves an integral, $\langle u_{\ell'}^{\mathrm{b}}|\mathcal{O}|u_\ell^{\mathrm{sc}}\rangle$, of a certain electromagnetic operator $\mathcal{O}$ sandwiched between the bound and scattering state wave functions with the initial and final angular momenta ℓ and ℓ'. It can be shown (see, for example, Ref. [52]) that astrophysically relevant radiative captures are mainly peripheral and therefore the major contribution to this integral comes from the distances that are much greater than the typical size of a hypernucleus. This means that in many cases a sufficient accuracy can be achieved if, instead of the exact wave functions, one uses their asymptotic forms,

$$u_\ell^{\mathrm{b}} \underset{r\to\infty}{\longrightarrow} \mathcal{A}_\ell \frac{e^{-\kappa r}}{r} \;, \qquad u_\ell^{\mathrm{sc}} \underset{r\to\infty}{\longrightarrow} \mathcal{N}_\ell \frac{e^{i\delta_\ell}}{r}\sin(kr - \ell\pi/2 + \delta_\ell) \;, \tag{1.3}$$

where the phase shift $\delta_\ell(k)$ can be expressed via the effective-range parameters, the normalization factor $\mathcal{N}_\ell$ is determined by the intensity of the incoming flux of the colliding

5

particles, while the Asymptotic Normalization Constant (ANC), $\mathcal{A}_\ell$, of the bound state needs to be determined separately.

The above reasons make it clear that the values of the effective-range parameters for hyper-nuclear scattering as well as the ANC's for the bound states are necessary for simple and quick calculations of various processes in nuclear astrophysics. To the best of our knowledge, Ref. [53] is the only paper where these values were calculated for a wide range of nuclei.

Using the same ΛA-potential (Here A stands for a nucleus with the mass number A) as in Ref. [53], we will re-calculated the effective-range parameters and for the same set of nuclear targets. In addition to the S-wave scattering lengths and effective radii reported in Ref. [53], we will calculate the higher-order parameters in the expansion (1.2) as well as obtained them for higher partial waves.

1.2.2 The multi-Lambda systems

The second part of this study involves the investigation into the multi-hyperon systems. We will consider the three systems $\Lambda\Lambda$, $\Lambda\Lambda\Lambda$, and $\Lambda\Lambda\Lambda\Lambda$. We would like to find out if many Λ-particles are placed close to each other, is it possible for them to form a bound state? Of course, we cannot answer such a question in full. Hence only estimated calculations for a limited number of Λ-particles in the system will be done.

The multi-particle system will be described within the hyperspherical theory, because the set of the hyperradial equations will be formally be the same as the one for coupled partial waves in a two-body problem. Once the lowest resonance (or pole of the S-matrix) on the complex energy plane is obtained, we can move that S-matrix pole on the Riemann surface of the energy by changing the strength of the potential then move from unphysical sheet to physical or otherwise passing through the threshold(zero energy) to get an idea on how far a multi-Λ system is from being bound, we therefore multiply the $\Lambda\Lambda$-potential by a numerical factor $g > 1$, and gradually increasing it, trace the movement of the corresponding resonance pole until it reaches the threshold energy. The critical value of g (with which a bound state just appears) can be found.

1.2.3 Reconstruction of the Multi-Lambda systems potential

In this third study, a suggested way to directly obtain the two-body potential, using available information on a three-body system where the two bodies in question are included is explored.

There is a kind of the three-body information that we need. Suppose we want to find out how particles A and B interact with each other and for some reason it is not possible to study the AB-scattering, at the same time we know the potentials that describe

the interactions of these particles with a third particle, C, and they form a bound state (ABC) whose energy can be determined experimentally. As we will show shortly, in such a situation, in order to obtain the AB-potential, we need to know the three-body wave function. Of course, one cannot calculate the (ABC) wave function if all the two-body forces keeping this system together, are not known. Very often, however, one can make a reasonable assumptions to the size of the system and its density distribution. Guessing the wave function in this way, one then can obtain a reasonable guess for the two-body potential. We will use the three body system, $\Lambda\Lambda\alpha$, experimental data (binding energy) to try and recover the singlet $\Lambda\Lambda$-potential and compared it with the already existing potentials.

1.3   Thesis Structure

This thesis is structured in following manner:

- Chapter 2 presents the theoretical background for multichannel Jost matrices for two-body spinless system. It covers the theory behind transforming the two-body Schrödinger equation into the coupled first-order differential equations and use an appropriate boundary condition to obtain Jost matrices numerically.

- Chapter 3 present the background theory used to calculate the effective range parameters. This is done by use of the multichannel Jost matrices obtained in Chapter 2. It also presents the calculations done on a wide range of ΛA-hypernuclear systems for different orbital angular momenta. Some of the results obtained were compared and published, See Ref.[54]

- In Chapter 4, the background theory used to solve the many-body Schroödinger equation within the hyperspherical approach to obtain it's corresponding Jost matrices for non-zero spin systems is presented.

- In Chapter 5 the background theory presented in Chapter 2 is used for the study of various ΛA-hypernucleus systems. Some of the results obtained were compared and published, See Ref.[54]

- In Chapter 6 the method present in Chapter 4 is used to study various multi-lambda systems. Their spectral points were calculated and presented.

- Chapter 7 introduces an approach that can be used to recover the two-body potential from its corresponding three-body system data using an approximated wave function. The method was tested by regenerating the already known two-body potential of known systems.

- The general conclusions are presented in Chapter 8

Chapter 2

Multi-channel Jost matrices for spinless systems

The theoretical framework to be used in this study is introduced. The two-body spinless multi channel problem is discussed using the Jost matrix theory. We first introduce the Schrodinger equation in section 2.1, then present the multi-channel radial Schrodinger equation for the two-body systems in Section 2.2. In Section 2.2.1, the multi-channel Schrodinger equation is transformed into the first-order coupled differential equations called the multi-channel Jost matrices with the boundary conditions. Section 2.3 explains how the Jost matrices are used to locate the spectral points (bound and resonance states). In Section 2.4 the scattering states and the S-matrix are defined in terms of the Jost matrices. Section 2.5 introduces the S-matrix residues and followed by it's relationship with the Asymptotic normalization constants and nuclear vertex constants in Section 2.5.

2.1 Introduction

We firstly look at the general quantum system within a Schrodinger picture by fully describing it using a state vector, $|\Psi_a(t)\rangle$ (which belongs to Hilbert space), at a time, t. It is characterized by a full set of quantum numbers, $a = \{\alpha_1, \alpha_2, \alpha_3, ..., \alpha_N\}$, which are the eigenvalues of a set of Hermitian commuting operators.

The state vector $\Psi_a(t)$ is also orthogonal and can be normalized such that,

$$\langle \Psi_a(t)|\Psi_{a'}(t)\rangle = \delta_{aa'}, \tag{2.1}$$

where $\delta_{aa'}$ is the Kronecker Delta. Generally the state vector changes with time, and its evolution is governs by the Schrodinger equation,

$$i\hbar \frac{d}{dt}|\Psi_a(t)\rangle = \hat{H}|\Psi_a(t)\rangle, \tag{2.2}$$

8

provided that the initial state is known at time $t = t_0$, where the Hamiltonian operator,

$$\hat{H} = \hat{H}_0 + \hat{U}, \tag{2.3}$$

is the combination of kinetic energy operator $\hat{H}_0$, and the potential energy operator $\hat{U}$. The Hamiltonian $\hat{H}$, is the total energy operator, and for most physical systems it is time independent and its corresponding total energy, i.e $E \in \{a\}$, is conserved. The possible discreet energies corresponding to certain system, described by $|\boldsymbol{\Psi}_a(t_0)\rangle = |\boldsymbol{\Psi}_a\rangle$, becomes a solution of the following time independent eigenvalue problem,

$$\hat{H}|\psi_a\rangle = E|\psi_a\rangle. \tag{2.4}$$

The state vector can be written in terms of the exponential function of the Hamiltonian operator as [55],

$$|\boldsymbol{\Psi}_a(t)\rangle = e^{-i(t-t_0)\hat{H}/\hbar}|\boldsymbol{\Psi}_a(t_0)\rangle, \tag{2.5}$$

where t_0 is a reference time, and it can be taken to be $t_0 = 0$. Quantum state vectors are normally presented using the space coordinates configuration where the basis of this representation consists of continuous states $|\boldsymbol{r}\rangle$ where the system's particles have a certain space configuration determined by the full set $\boldsymbol{r}$ of the particles coordinates($\boldsymbol{r}$, taken to be a multi-dimensional vector in the $N-$body configuration space, $\boldsymbol{r} \equiv (\boldsymbol{r}_1, \boldsymbol{r}_2, \boldsymbol{r}_3, ..., \boldsymbol{r}_N)$. Now the state vector dynamics is described by the complex-valued wavefunction

$$\langle \boldsymbol{r}|\boldsymbol{\Psi}_a\rangle_t = \Psi_a(\boldsymbol{r}, t),$$

depending on the space-time coordinates. Hence the equations (2.4 and 2.5) can be re-written as,

$$\hat{H}\psi_a(\boldsymbol{r}) = \hat{E}\psi_a(\boldsymbol{r}), \tag{2.6}$$

and

$$\Psi_a(\boldsymbol{r}, t) = \exp\left(-\frac{i}{\hbar}Et\right)\psi_a(\boldsymbol{r}). \tag{2.7}$$

The quantum states represented by wave functions of equation (2.7) are now called the stationary states, where $\psi_a(\boldsymbol{r})$ is the stationary state that obeys the stationary Schrodinger equation (2.6).

For any particle moving in the local diagonal matrix potential U, in the coordinate representation, it's stationary Schrodinger equation is given by,

$$-\frac{\hbar^2}{2\mu}\Delta_{\boldsymbol{r}}\psi_a(\boldsymbol{r}) + U(\boldsymbol{r})\psi_a(\boldsymbol{r}) = E\psi_a(\boldsymbol{r}). \tag{2.8}$$

In cases of central potential that doesn't depend on the direction of vector $\boldsymbol{r}$, and for spinless particles, the wave functions can be factorized into the radial and angular parts,

$$\psi_a(\boldsymbol{r}) = \frac{u_a(r)}{r}Y_{\ell m}(\theta, \varphi), \tag{2.9}$$

9

where $Y_{\ell m}(\theta, \varphi)$, are so called spherical harmonics depending on the spherical angles θ and φ as well as the angular momentum ℓ and its third component m forms part of set of conserving parameters together with the energy E. The , $u_a(r)$, is radial wave function that satisfies the following radial Schrodinger equation

$$\left[\frac{d^2}{dr^2} + k^2 - \frac{\ell(\ell+1)}{r^2} - V(r) \right] u_a(r) = 0, \tag{2.10}$$

where $k^2 = 2\mu E/\hbar^2$ and $V(r) = 2\mu U(r)/\hbar^2$.

We will extend the radial Schrodinger equation (2.10) to the multi-channel two body case in the next section of this Chapter.

2.2 Multi-Channel two-body radial Schrodinger equation

The two-body multi-channel quantum mechanical problem for particles with masses m_1 and m_2 having positions $\boldsymbol{r}_1$ and $\boldsymbol{r}_2$, relative to a specific frame of reference, is described using the two-body Hamiltonian given by:

$$\hat{H} = \hat{H}_1^0 + \hat{H}_2^0 + \hat{U}(r_1 - r_2) + \hat{h} \tag{2.11}$$

with,

$$\hat{H}_i^0 = \frac{\hat{\boldsymbol{p}}_i}{2m_i}, \quad i = 1, 2 \tag{2.12}$$

where, $\hat{\boldsymbol{p}}_i$ is the momentum operator for each individual particles. The Hamiltonian also includes the interaction operator which depends on the particles coordinates $\boldsymbol{r}_1$ and $\boldsymbol{r}_2$, and the operator $\hat{h}$ that describes the internal dynamics of the particles in the moving system. This system can be reduced to an effective one-body problem after the separation of the motion of its center of mass, and assuming that the center of mass frame of reference is stationary relative to the laboratory frame. The two-body total Hamiltonian similar to that of a single particle in a central potential is given by:

$$\hat{H} = \frac{\hat{\boldsymbol{p}}^2}{2\mu} + \hat{U}(\boldsymbol{r}) + \hat{h}, \tag{2.13}$$

with the relative position and reduced mass given by:

$$\boldsymbol{r} = \boldsymbol{r}_1 - \boldsymbol{r}_2, \tag{2.14}$$

$$\mu = \frac{m_1 m_2}{m_2 + m_1} \tag{2.15}$$

The eigenvalues of the two-body Hamiltonian correspond to the discrete bound state energy spectrum of the two particles interaction.

10

The internal dynamics, such as the internal states of the colliding particles, correspond to a different channel of the scattering process. Generally, there are infinite number of the internal states, which are eigenstates of, $\hat{h}$,

$$\hat{h}|n\rangle = E_n|n\rangle, \quad n = 1, 2, 3, \ldots \infty \tag{2.16}$$

Considering only the important N internal states, we can approximate the internal Hamiltonian by N terms,

$$h \approx \sum_{n=1}^{N} |n\rangle E_n \langle n|. \tag{2.17}$$

The total Hamiltonian (2.13) representation using the relative coordinates $\boldsymbol{r}$ is now given by the following $N \times N$ matrix,

$$\langle n|\hat{H}|n'\rangle = \langle n|\hat{H}^0|n'\rangle + \langle n|\hat{U}(\boldsymbol{r})|n'\rangle + \langle n|\hat{h}|n'\rangle$$

$$\therefore \hat{H}_{nn'} = \delta_{nn'}\frac{\langle n|\hat{\boldsymbol{p}}^2|n'\rangle}{2\mu_n} + U_{nn'}(\boldsymbol{r}) + \sum_{n=1}^{N}\langle n||n\rangle E_n \langle n||n'\rangle$$

$$\therefore \hat{H}_{nn'} = -\delta_{nn'}\frac{\hbar^2}{2\mu_n}\Delta_{\boldsymbol{r}} + U_{nn'}(\boldsymbol{r}) + E_n\delta_{nn'}, \tag{2.18}$$

where the μ_n is the reduced mass in the channel n. When we replace the Hamiltonian in the time-independent Schrodinger equation (2.6) by multi-channel two-body Hamiltonian (2.18), we get the following system of coupled differential equations for channel wave functions in the position representation:

$$\left[\frac{\hbar^2}{2\mu_n}\Delta_{\boldsymbol{r}} + (E - E_n)\right]\psi_n(E, \boldsymbol{r}) = \sum_{n=1}^{N} U_{nn'}(\boldsymbol{r})\psi_{n'}(E, \boldsymbol{r}), \tag{2.19}$$

where n is the channel number with $n = 1, 2, \ldots, N$ with $\psi_n(E, \boldsymbol{r})$, their corresponding time-independent wave-function, and E_n are the energy thresholds for their corresponding channels. An eigenstate of the Hamiltonian (2.18) corresponding to the eigenvalue E, is a column-matrix,

$$\Psi_a(E, \boldsymbol{r}) = \begin{pmatrix} \psi_1(E, \boldsymbol{r}) \\ \psi_2(E, \boldsymbol{r}) \\ \vdots \\ \psi_n(E, \boldsymbol{r}) \end{pmatrix}. \tag{2.20}$$

The channels are characterized by complete set of channel quantum numbers, $a = \{\alpha_1, \alpha_2, \alpha_3, \ldots, \alpha_N\}$, which includes threshold energies. If the spin or angular momentum forms part of quantum numbers, then the states that differs by one of them becomes new channels. Any states of the system that differ by at least one quantum number are considered as different channels, even if they share the same energy thresholds.

For a zero spin quantum system, each channel is characterized by two conserving quantum numbers, the magnetic quantum number $, m$, and the corresponding orbital angular

11

momentum quantum number, ℓ. The radial Schrodinger equation explicitly contains the quantum number, ℓ, after the separation of polar configuration variables into radial and angular part are performed [55].

The Laplacian operator in equation (2.19) , $\Delta_{\boldsymbol{r}}$, in polar coordinates, is defined in terms of the orbital angular momentum operator, $\hat{\boldsymbol{\ell}}$, by [55]:

$$\Delta_{\boldsymbol{r}} = \frac{1}{r^2}\partial_r\left(r^2\partial_r - \frac{\hat{\boldsymbol{\ell}}^2}{\hbar^2 r^2}\right). \tag{2.21}$$

The quantum numbers ℓ and m are related to the eigenvalues of the angular momentum operator , $\hat{\boldsymbol{\ell}} = \hat{\boldsymbol{r}} \times \hat{\boldsymbol{p}}$, for the two body system and the $z-$component, ℓ_z, of this operator in an arbitrary Cartesian coordinate system. The operators $\hat{\boldsymbol{\ell}}$ and $\hat{\ell}_z$ do not mutually commute whereas $\hat{\boldsymbol{\ell}}^2$ and $\hat{\ell}_z$ do commute hence they share the same eigenvectors, $|\ell m\rangle$. Their respective eigenvalues are:

$$\hat{\boldsymbol{\ell}}^2|\ell m\rangle = \ell(\ell+1)\hbar^2|\ell m\rangle \tag{2.22}$$

$$\hat{\ell}_z|\ell m\rangle = m\hbar|\ell m\rangle. \tag{2.23}$$

The position operator eigenvectors that describe a specific space-configuration in spherical coordinates are given by:

$$|\boldsymbol{r}\rangle = |r,\theta,\varphi\rangle. \tag{2.24}$$

The projection of, $|\ell m\rangle$, on the spherical-angle part of the configuration eigenvectors results in the well-known Spherical Harmonics [55]:

$$\langle\theta,\varphi|\ell m\rangle = Y_{\ell m}(\theta,\varphi), \tag{2.25}$$

which can be written in terms of the Associated Legendre polynomials, $P_{\ell m}(z)$[55]:

$$Y_{\ell m}(\theta,\varphi) = (-1)^m\sqrt{\frac{(2\ell+1)(\ell-m)!}{(4\pi)(\ell+m)!}}P_{\ell m}(\cos\theta)e^{im\varphi}. \tag{2.26}$$

It can be shown that the spherical harmonics are orthonormal:

$$\int Y_{\ell m}^* Y_{\ell'm'}d\Omega = \int_0^{2\pi}\int_0^\pi Y_{\ell m}^* Y_{\ell m}\sin\theta d\theta d\varphi = \delta_{\ell\ell'}\delta_{mm'}. \tag{2.27}$$

The eigenvalue equation and can now rewritten as follows:

$$\hat{\boldsymbol{\ell}}^2 Y_{\ell m}(\theta,\varphi) = \ell(\ell+1)Y_{\ell m}(\theta,\varphi), \tag{2.28}$$

$$\hat{\ell}_z Y_{\ell m}(\theta,\varphi) = mY_{\ell m}(\theta,\varphi). \tag{2.29}$$

The time-independent channel wave functions, $\psi_n(E,\boldsymbol{r})$, are set as projections of the time-independent wave vector on the basis of configuration vectors, $|\boldsymbol{r}\rangle$:

$$\langle\boldsymbol{r}|\psi_n\rangle = \psi_n(E,r,\theta,\varphi). \tag{2.30}$$

12

The channel wave-vectors are also eigenvectors of the operators $\hat{\ell}^2$ and $\hat{\ell}_z$, with their corresponding quantum numbers ℓ and m for each channel. Each channel wave-vector can be expanded over the orthonormal basis of eigenvectors, $|\ell_n m_n\rangle$, of each channel , n,

$$
\begin{aligned}
\psi_n(E,\boldsymbol{r}) &= \sum_{\ell_n m_n} \langle r,\theta,\varphi|\ell_n m_n\rangle\langle \ell_n m_n|\psi_n\rangle \\
&= \sum_{\ell_n m_n} \langle \theta,\varphi|\ell_n m_n\rangle\langle r,\ell_n m_n|\psi_n\rangle \\
&= \sum_{\ell_n m_n} Y_{\ell_n m_n}(\theta,\varphi)\langle r,\ell_n m_n|\psi_n\rangle
\end{aligned}
\tag{2.31}
$$

and each channel radial wave-function is now defined as:

$$
u_{\ell_n}(E,r) \equiv r\langle r,\ell_n m_n|\psi_n\rangle.
\tag{2.32}
$$

Using equation (2.31) together with equation (2.32) , we now get the time-independent channel wave-functions as an expansion of the product of a radial dependent part and the angular dependent spherical harmonics over $\ell_n m_n$:

$$
\psi_n(E,r,\theta,\varphi) = \sum_{\ell_n m_n} \frac{u_n(E,r)}{r} Y_{\ell_n m_n}(\theta,\varphi).
\tag{2.33}
$$

It is acceptable generally to further assume that the relative motion in each channel has a single value of ℓ_n and m_n. This simplifies the notation, hence the summation no longer required over all possible values of ℓ_n and m_n :

$$
\psi_n(E,r,\theta,\varphi) = \frac{u_n(E,r)}{r} Y_{\ell_n m_n}(\theta,\varphi).
\tag{2.34}
$$

The substitution of equations, (2.34 ,2.28 and 2.21) in the time-independent Schrodinger equation (2.19), yields the following equation:

$$
\begin{aligned}
\left[\partial_r^2 + k_n^2 - \frac{\ell_n(\ell_n+1)}{r^2}\right]&u_n(E,r)Y_{\ell_n m_n}(\theta,\varphi) \\
&= \sum_{n'=1}^{N} U_{nn'}(r)u_{n'}(E,r)Y_{\ell_{n'} m'_n}(\theta,\varphi),
\end{aligned}
\tag{2.35}
$$

where the channel wave-momenta k_n defined by:

$$
k_n^2 \equiv \frac{2\mu_n}{\hbar^2}(E-E_n).
\tag{2.36}
$$

if we multiply equation (2.35) by $Y^*_{\ell_n m_n}(\theta,\varphi)$, and integrate over spherical angles (θ,φ), using the orthonormal property of the spherical harmonics, (2.27), we get the following multi-channel radial Schrodinger equation:

$$
\left[\partial_r^2 + k_n^2 - \frac{\ell_n(\ell_n+1)}{r^2}\right]u_n(E,r) = \sum_{n'=1}^{N} V_{nn'}(r)u_{n'}(E,r),
\tag{2.37}
$$

13

which is a system of N coupled second-order differential equations, and where,

$$V_{nn'}(r) = \frac{2\mu_n}{\hbar^2} \int Y^*_{\ell_n m_n}(\theta, \varphi) U_{nn'}(r) Y_{\ell_{n'} m_{n'}}(\theta, \varphi) d\Omega, \qquad (2.38)$$

are the elements of the reduced coupling potential matrix.

2.2.1 Transformation of the Schrodinger equation

The system of N linear second-order differential equations (2.37) has $2N$ linearly-independent column solutions, and only half are regular at the origin [46]. These regular solutions are presented as $\phi_{nn'}(E, r)$, with,

$$\phi_{nn'}(E, r) \xrightarrow[r \to \infty]{} 0 \qquad \forall n, n'. \qquad (2.39)$$

The regular column solutions are presented as the fundamental matrix of regular solutions as:

$$\Phi(E, r) = \begin{pmatrix} \phi_{11}(E, r) & \phi_{12}(E, r) & \cdots & \phi_{1N}(E, r) \\ \phi_{21}(E, r) & \phi_{22}(E, r) & \cdots & \phi_{2N}(E, r) \\ \vdots & \vdots & \ddots & \vdots \\ \phi_{m1}(E, r) & \phi_{m2}(E, r) & \cdots & \phi_{NN}(E, r) \end{pmatrix} \qquad (2.40)$$

any other regular solution is a linear combination of the columns of the fundamental matrix, and any physical solution is a linear combination of the columns of the corresponding fundamental matrix [46]:

$$\begin{pmatrix} u_1 \\ u_2 \\ \vdots \\ u_N \end{pmatrix} = C_1 \begin{pmatrix} \phi_{11} \\ \phi_{21} \\ \vdots \\ \phi_{N1} \end{pmatrix} + C_2 \begin{pmatrix} \phi_{12} \\ \phi_{22} \\ \vdots \\ \phi_{N2} \end{pmatrix} + \cdots + C_N \begin{pmatrix} \phi_{1N} \\ \phi_{2N} \\ \vdots \\ \phi_{NN} \end{pmatrix}. \qquad (2.41)$$

We can compactly present equation (2.41), as summation over channels,

$$u_n = \sum_{n'=1}^{N} \phi_{nn'} C_n. \qquad (2.42)$$

The physical solution behaviour when $r \to 0$ is properly guaranteed, and with a proper choice of the combination coefficients C_n when $r \to \infty$, the correct asymptotic behaviour is also achieved.

When the particles are far apart from their interaction region (i.e $V_{nn'}(r \to \infty) \to 0$), Eq.(2.37) decouples to N second-order differential equations:

$$\left[\partial_r^2 + k_n^2 - \frac{\ell_n(\ell_n + 1)}{r^2} \right] u_n(E, r) \approx 0, \qquad r \to \infty, \qquad (2.43)$$

which are the Riccati-Bessel equations. For each of the N equation, Riccati-Hankel functions, $h_\ell^{(\pm)}(kr)$, are their corresponding two linearly-independent solutions from which

14

represent the incoming wave, $h_\ell^{(-)}(kr)$, and the out-going, $h_\ell^{(+)}(kr)$, physical spherical waves. Their asymptotic behaviour are given as:

$$h_\ell^{(\pm)}(kr) \xrightarrow[|kr|\to\infty]{} (\mp i)^{\ell+1} e^{\pm ikr} = e^{\pm i[kr - \frac{\pi}{2}(\ell+1)]}. \tag{2.44}$$

These are not unique solutions. Riccati-Bessel, $j_\ell(kr)$, and Riccati-Neumann, $y_\ell(kr)$, functions, are another pair of linearly independent solution that can be written as a linear combination of the Ricacati-Hankel functions that turns out to be both singular at point $r = 0$,

$$h_\ell^{(\pm)} = j_\ell(kr) \pm iy_\ell(kr) \xrightarrow[r\to 0]{} \pm iy_\ell(kr) \xrightarrow[r\to 0]{} \mp \frac{i(2\ell-1)!!}{(kr)^\ell}. \tag{2.45}$$

The Riccati-Bessel function is regular at the origin with the following behaviour,

$$j_\ell(kr) \xrightarrow[r\to 0]{} \frac{(kr)^{\ell+1}}{(2\ell+1)!!}. \tag{2.46}$$

There are $2N$ linearly-independent column solutions to the system of equations (2.43), which can be presented as square diagonal matrices where the matrix elements are the Riccati-Hankel functions:

$$W^{(\text{in})} = \begin{pmatrix} h_{\ell_1}^{(-)}(kr) & 0 & \cdots & 0 \\ 0 & h_{\ell_2}^{(-)}(kr) & \cdots & 0 \\ \vdots & \vdots & \ddots & \vdots \\ 0 & 0 & \cdots & h_{\ell_N}^{(-)}(kr) \end{pmatrix} \tag{2.47}$$

$$W^{(\text{out})} = \begin{pmatrix} h_{\ell_1}^{(+)}(kr) & 0 & \cdots & 0 \\ 0 & h_{\ell_2}^{(+)}(kr) & \cdots & 0 \\ \vdots & \vdots & \ddots & \vdots \\ 0 & 0 & \cdots & h_{\ell_N}^{(+)}(kr) \end{pmatrix} \tag{2.48}$$

that represent the incoming and outgoing spherical waves in all channels and forms a basis in the space of solutions. Any other column solution of equation (2.43) is a linear combination of these $2N$ columns.

The columns of the fundamental matrix of the regular solutions (2.40) at large distance $(r \to \infty)$ are solutions of (2.43) can be written as linear combination of (2.47) and (2.48):

$$\Phi(E, r) \xrightarrow[r\to\infty]{} W^{(\text{in})}(E, r) f^{(\text{in})}(E) + W^{(\text{out})}(E, r) f^{(\text{out})}(E), \tag{2.49}$$

where the "in" superscript notation only refer to the amplitude of incoming wave whereas the "out" notation refers to the amplitude for the outgoing wave. These amplitudes, $f^{(\text{in/out})}$, called the Jost matrices. The asymptotic behaviour of the physical radial

15

wave-functions (2.42) in terms of the energy dependent $N \times N$ Jost matrices is given by following equation in compact form:

$$U(E, r) \xrightarrow[r \to \infty]{} W^{(\text{in})}(E, r) f^{(\text{in})}(E)\mathcal{C} + W^{(\text{out})}(E, r) f^{(\text{out})}(E)\mathcal{C}, \qquad (2.50)$$

where,

$$\mathcal{C} = \begin{pmatrix} C_1 \\ C_2 \\ \vdots \\ C_N \end{pmatrix}, \qquad (2.51)$$

are unknown combination coefficients, and

$$U(E, r) = \begin{pmatrix} u_1(E, r) \\ u_2(E, r) \\ \vdots \\ u_N(E, r) \end{pmatrix}. \qquad (2.52)$$

For a single channel $(N = 1)$ case, these matrix reduces to the following equation,

$$\phi(E, r) \xrightarrow[r \to \infty]{} h_\ell^{(-)}(kr) f_\ell^{(\text{in})}(E) + h_\ell^{(+)}(kr) f_\ell^{(\text{out})}(E). \qquad (2.53)$$

The single-channel Jost functions are defined as the energy-dependent amplitudes of the incoming and outgoing spherical waves of the regular solution to the radial wave-equation. The Jost matrices entries can also be thought as an amplitudes of incoming and outgoing spherical waves for the corresponding channel.

The Jost function was first introduced by the Swiss physicist whose name was Res Jost in 1947 [56]. They completely describe the underlying physical system and thus determine the S-matrix,

$$S(E) = F^{(\text{out})}(E)[F^{(\text{in})}(E)]^{-1}. \qquad (2.54)$$

The fundamental regular matrix $\phi(E, r)$ at large distances is a linear combination (2.47) with the r-independent coefficients matrices $F^{(\text{in/out})}(E)$. We now look for $\phi(E, r)$ at any point r, in this case with the matrices coefficient depending on r :

$$\Phi(E, r) \equiv W^{(\text{in})}(E, r) F^{(\text{in})}(E, r) + W^{(\text{out})}(E, r) F^{(\text{out})}(E, r). \qquad (2.55)$$

The new unknown matrix functions $F^{(\text{in/out})}(E, r)$ becomes the Jost functions at large r :

$$f^{(\text{in/out})}(E) = \lim_{r \to \infty} F^{(\text{in/out})}(E, r). \qquad (2.56)$$

From Eq.(2.53) we have three unknown functions hence the functions in equation (2.54) cannot be independent of each other. We can impose any condition relating them, in this case the Lagrange condition within the variational parameters method [57]:

$$W^{(\text{in})}(E, r)\frac{\partial}{\partial r}F^{(\text{in})}(E, r) + W^{(\text{out})}(E, r)\frac{\partial}{\partial r}F^{(\text{out})}(E, r) = 0 \qquad (2.57)$$

16

which is standard in the theory of differential equations. The Lagrangian condition is also satisfied at large distances so we do not change the asymptotic behaviour of the solution. It has been shown using the Wronskian of the Riccati-Hankel functions $h_\ell^{(\pm)}(kr)$ (see Ref[56]) that:

$$W^{(\text{in})}(E,r)\big[\partial_r W^{(\text{out})}(E,r)\big] - \big[\partial_r W^{(\text{in})}(E,r)\big] W^{(\text{out})}(E,r) = 2iK, \tag{2.58}$$

where,

$$K = \begin{pmatrix} k_1 & 0 & \cdots & 0 \\ 0 & k_2 & \cdots & 0 \\ \vdots & \vdots & \ddots & \vdots \\ 0 & 0 & \cdots & k_N \end{pmatrix}. \tag{2.59}$$

Substituting Eq.(2.53) into the radial equation (2.37), apply the condition (2.55) and using Eq.(2.56) the following system of first-order differential equations:

$$\partial_r F^{(\text{in})} = -\frac{1}{2ik} W^{(\text{out})} V \big[W^{(\text{in})} F^{(\text{in})} + W^{(\text{out})} F^{(\text{out})} \big], \tag{2.60}$$

$$\partial_r F^{(\text{out})} = \frac{1}{2ik} W^{(\text{in})} V \big[W^{(\text{in})} F^{(\text{in})} + W^{(\text{out})} F^{(\text{out})} \big], \tag{2.61}$$

which are equivalent to the second-order Schrodinger equation (2.37) (See Refs.[46, 58]) for the full derivations. The boundary conditions for these equations (2.58 and 2.59) are only imposed at a single point. The demand for matrix (2.40) to be regular at the origin requires both Jost functions to converge to the same constant,

$$F_\ell^{(\text{in})}(E,0) = F_\ell^{(\text{out})}(E,0). \tag{2.62}$$

Because both , $h_\ell^{(\pm)}(kr)$, are singular at the origin, their singularities cancels each other in the combination,

$$h_\ell^{(-)}(kr) + h_\ell^{(+)}(kr) = 2j_\ell(kr). \tag{2.63}$$

The following boundary condition for N channel will now be chosen:

$$F^{(\text{in/out})}(E, r \to 0) = \frac{1}{2}I \tag{2.64}$$

where I is the $N \times N$ identity matrix [55]. If we introduce the following diagonal matrix J, whose elements are made up of the Riccati-Bessel functions,

$$J(E,r) = \begin{pmatrix} j_{\ell_1}(k_1 r) & 0 & \cdots & 0 \\ 0 & j_{\ell_2}(k_2 r) & \cdots & 0 \\ \vdots & \vdots & \ddots & \vdots \\ 0 & 0 & \cdots & j_{\ell_N}(k_N r) \end{pmatrix}. \tag{2.65}$$

Equation (2.45) can be re-written in the following way:

$$J(E,r) = \frac{1}{2} W^{(\text{in})} + \frac{1}{2} W^{(\text{out})}. \tag{2.66}$$

17

Implementing the boundary condition Eq.(2.55) near the origin, we obtain the following regular behaviour of the fundamental matrix :

$$\Phi(E, r \to 0) = J(E, r) \xrightarrow[r \to 0]{} \begin{pmatrix} \frac{(k_1 r)^{\ell_1+1}}{(2\ell_1+1)!!} & 0 & \cdots & 0 \\ 0 & \frac{(k_2 r)^{\ell_2+1}}{(2\ell_2+1)!!} & \cdots & 0 \\ \vdots & \vdots & \ddots & \vdots \\ 0 & 0 & \cdots & \frac{(k_N r)^{\ell_N+1}}{(2\ell_N+1)!!} \end{pmatrix}, \tag{2.67}$$

The physical radial solutions are now related to the regular solutions by Eq.(2.42) and that leads to the following system of equations:

$$u_n(E, r) = \sum_{n'=1}^{N} \left[h_{\ell_n}^{(-)}(k_n r) F_{nn'}^{(\text{in})}(E, r) C_n + h_{\ell_n}^{(+)}(k_n r) F_{nn'}^{(\text{out})}(E, r) C_n \right] \tag{2.68}$$

for each channel. Now, the time-independent wave-function for each channel is given by:

$$\psi_n(E, \boldsymbol{r}) = \frac{1}{r} \sum_{n'=1}^{N} \sum_{\ell_n m_n} \left[h_{\ell_n}^{(-)}(k_n r) F_{nn'}^{(\text{in})}(E, r) C_n + \right.$$
$$\left. h_{\ell_n}^{(+)}(k_n r) F_{nn'}^{(\text{out})}(E, r) C_n \right] Y_{\ell_n m_n}(\theta, \varphi). \tag{2.69}$$

The determined $F^{(\text{in/out})}(E, r)$ with the coupled system of first order differential equations (2.60 and 2.61) allows us to obtain the wave-function for each channel (2.69). The physical wave function should be normalized correctly to have the correct asymptotic behaviour.

Alternative form of the Schrodinger equation Transformation

This idea of alternative transformation is based on the relation between the two pairs of linearly independent solutions of the Riccati-Bessel equation, namely, between the Riccati-Hankel functions $h_\ell^{(\pm)}(kr)$ and the pair of Riccati-Bessel $j_\ell(kr)$ and Riccati-Neumann $y_\ell(kr)$ functions,

$$h_\ell^{(\pm)}(kr) = j_\ell(kr) \pm i y_\ell(kr). \tag{2.70}$$

Now by introducing these two diagonal matrices,

$$J = \frac{1}{2} \left[W^{(\text{in})} + W^{(\text{out})} \right] = \begin{pmatrix} j_{\ell_1}(k_1 r) & 0 & \cdots & 0 \\ 0 & j_{\ell_2}(k_2 r) & \cdots & 0 \\ \vdots & \vdots & \ddots & \vdots \\ 0 & 0 & \cdots & j_{\ell_N}(k_N r) \end{pmatrix}, \tag{2.71}$$

$$Y = \frac{1}{2}\left[W^{(\text{in})} - W^{(\text{out})}\right] = \begin{pmatrix} y_{\ell_1}(k_1 r) & 0 & \cdots & 0 \\ 0 & y_{\ell_2}(k_2 r) & \cdots & 0 \\ \vdots & \vdots & \ddots & \vdots \\ 0 & 0 & \cdots & y_{\ell_N}(k_N r) \end{pmatrix}, \tag{2.72}$$

as well as the new unknown matrices,

$$\mathcal{A}(E, r) = F^{(\text{in})}(E, r) + F^{(\text{out})}(E, r), \tag{2.73}$$

$$\mathcal{B}(E, r) = i\left[F^{(\text{in})}(E, r) - F^{(\text{out})}(E, r)\right], \tag{2.74}$$

we obtain equivalent representation of the fundamental matrix of the regular solutions[46],

$$\Phi(E, r) = J(E, r)\mathcal{A}(E, r) - Y(E, r)\mathcal{B}(E, r). \tag{2.75}$$

We obtain an equivalent system of differential equations for the new unknown matrices,

$$\partial_r \mathcal{A} = -K^{-1}YV(J\mathcal{A} - Y\mathcal{B}), \tag{2.76}$$

$$\partial_r \mathcal{B} = -K^{-1}YV(J\mathcal{A} - Y\mathcal{B}), \tag{2.77}$$

by combining Eqs.(2.60 and 2.61) with the boundary conditions

$$\mathcal{A}(E, 0) = I, \quad \mathcal{B}(E, 0) = 0. \tag{2.78}$$

These matrices should converge to their asymptotic values

$$\mathcal{A}(E, r) \xrightarrow[r \to \infty]{} A(E), \quad \mathcal{B}(E, r) \xrightarrow[r \to \infty]{} B(E), \tag{2.79}$$

and the Jost matrices can now be obtained,

$$F^{(\text{in})}(E) = \frac{1}{2}\left[A(E) - iB(E)\right], \quad F^{(\text{out})}(E) = \frac{1}{2}\left[A(E) + iB(E)\right]. \tag{2.80}$$

2.2.2 The boundary conditions

In order to numerically solve Eqs. (2.60 and 2.61) and/or Eqs.(2.76 and 2.77), we need to find the corresponding boundary conditions for the matrices $F^{(\text{in}/\text{out})}$ and A, B on their relevant intervals. Since the matrix $\phi(E, r)$ should be regular at $r \to 0$, we have

$$h_{\ell_n}^{(-)}(k_n r)F_{nn'}^{(\text{in})}(E, r) + h_{\ell_n}^{(+)}(k_n r)F_{nn'}^{(\text{out})}(E, r) \xrightarrow[r \to 0]{} 0, \tag{2.81}$$

using the Lagrange condition from Eq.(2.57),then the following condition is obtained,

$$h_{\ell_n}^{(-)}(k_n r)\partial_r F_{nn'}^{(\text{in})}(E, r) + h_{\ell_n}^{(+)}(k_n r)\partial_r F_{nn'}^{(\text{out})}(E, r) \equiv 0 \tag{2.82}$$

and,

$$\frac{h_\ell^{(+)}(kr)}{h_\ell^{(-)}(kr)} \equiv \frac{j_\ell(kr) + in_\ell(kr)}{j_\ell(kr) - in_\ell(kr)} \xrightarrow[r \to 0]{} -1. \tag{2.83}$$

19

Now the matrices $F^{(\text{in})}(E,r)$ and $F^{(\text{out})}(E,r)$ as well as their first derivative are identical, that is,

$$F^{(\text{in})}_{nn'}(E,r) \xrightarrow[r\to 0]{} F^{(\text{out})}_{nn'}(E,r), \tag{2.84}$$

$$\partial_r F^{(\text{in})}_{nn'}(E,r) \xrightarrow[r\to 0]{} \partial_r F^{(\text{out})}_{nn'}(E,r), \tag{2.85}$$

hence the boundary conditions for Eqs.(2.60 and 2.61) are obtained[59] and given by,

$$\lim_{r\to 0} \frac{j_{\ell_n}(k_n r) F^{(\text{in/out})}_{nn'}(E,r)}{j_{\ell_{n'}}(k_{n'}r)} = \delta_{nn'}. \tag{2.86}$$

From Eq.(2.73) both $F^{(\text{in})}$ and $F^{(\text{out})}$ tend to $A/2$ and thus

$$\phi_{nn'}(E,r) \xrightarrow[r\to 0]{} \frac{1}{2}\left[h_{\ell_n}{}^{(-)}(k_n r) + h_{\ell_n}{}^{(+)}(k_n r)\right] A_{nn'}(E,r) = j_{\ell_n}(k_n r) A_{nn'}(E,r) \quad (2.87)$$

such that the boundary conditions for Eqs.(2.76 and 2.77) is given by,

$$\lim_{r\to 0} \frac{j_{\ell_n}(k_n r) A_{nn'}(E,r)}{j_{\ell_{n'}}(k_{n'}r)} = \delta_{nn'}, \qquad \lim_{r\to 0} \frac{y_{\ell_n}(k_n r) B_{nn'}(E,r)}{j_{\ell_{n'}}(k_{n'}r)} = 0. \tag{2.88}$$

It is more convenient to work with Eqs.(2.75, 2.76 and 2.77) in the vicinity of $r = r_{min}$ near zero point then use Eqs.(2.55, 2.60 and 2.61) starting from $r = r_{int}$, up to infinity when doing numerical calculations. Near the point $r = 0$ the matrices $F^{(\text{in})}$ and $F^{(\text{out})}$ become identical then the cancellation of $h_\ell^{(+)}(kr)$ and $h_\ell^{(-)}(kr)$ singularities causes possible errors. The functions $h_\ell^{(\pm)}(kr)$ become more singular when increasing the angular momentum $,\ell$, hence the errors also increases. For larger ℓ the point $r = r_{min}$ must be shifted further away from the origin.

Therefore, in performing numerical calculations, we should solve Eqs.(2.76 and 2.77) from $r = r_{min}$ to an intermediate point $r = r_{int}$. Now at this point, using the calculated values of the matrices $A(E, r_{int})$ and $B(E, r_{int})$ in the relations,

$$F^{(\text{in/out})}(E,r) = \frac{1}{2}\left[A(E) \mp iB(E)\right]. \tag{2.89}$$

Then the initial matrices values $F^{(\text{in/out})}(E, r_{int})$ can be found for further integration of equations (2.60 and 2.61) up to a point $r = R$, where the matrices $F^{(\text{in/out})}$ reach their asymptotic values.

2.3 Multi-channel Riemann surface and the spectral points

The multi-channel Jost functions could be considered as the functions of the momentum or energy. Momentum is more preferable in contrast to the two-layered energy

20

surface[59]. For any fixed (including complex) value of energy E, each channel N momenta can have two different values,

$$k_n = \pm\sqrt{\frac{2\mu_n}{\hbar^2}(E - E_n)}, \quad n = 1, 2, ..., N \tag{2.90}$$

depending on the choice of the sign in front of the square root. These momenta appear as parameters in equations (2.60,2.61, 2.76 and 2.77). The solutions $\phi(E, r)$ and the Jost matrices depend on the choice of the signs in (2.81). That means the Jost matrices are not single-valued functions of E. At any specific energy E, they contain 2^N different values, for all possible combinations of the N channel momenta signs [46].

Multi-valued functions are treated as single valued functions defined on a multi-layered complex surface which is called the Riemann surface. Now, Jost matrices are defined on a Riemann surface of the energy consisting of 2^N layers. At the threshold energies , $E = E_n$, two sheets of the Riemann surface corresponding to $\pm k_n$, connect to each other. Therefore the layers of the Riemann surface are interconnected to form multi-
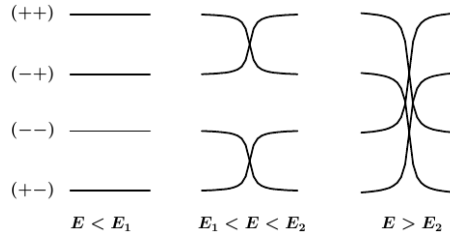
Figure 2.1: Layer of the Riemann surface for two-channel problem at three different energy intervals corresponding to different combinations of the signs of $\mathrm{Im}k_1$ and $\mathrm{Im}k_2$. Taken from Ref.[46]

layered manifold having threshold points $E_n(1, 2, ..., N)$ as branching points on this manifold. Any point on a circle centered at the threshold E_n, can be parameterized as $E = E_n + \rho\exp(i\theta)$, where ρ is the distance from E_n and θ is the polar angle. Now, the corresponding channel momentum given by,

$$k_n = \sqrt{\frac{2\mu_n\rho}{\hbar^2}}e^{i\theta/2}, \tag{2.91}$$

changes its sign after one full circle ($\theta = 2\pi$) and comes to its original point after two full circles ($\theta = 4\pi$). We can move around these points continuously to reach any of the 2^N layers. Riemann surface are constructed by making cuts and connects layers appropriately along the real energy axis. The cuts begins from the lowest threshold E_1, then goes to infinity in the positive direction.

21
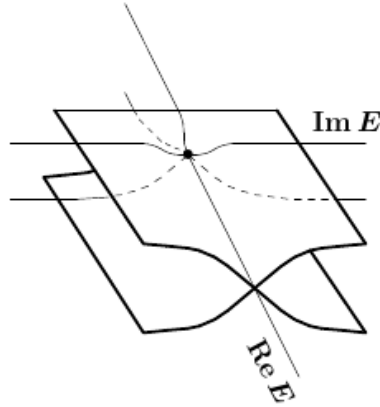
Figure 2.2: Riemann surface of the energy for a single-channel problem. The dot shows the branch point at $E = 0$. Taken from Ref.[46, 54]

The Spectral points

The points on the energy surface at which the physical wave function has only the outgoing wave asymptotic,

$$U(E_n, r) \underset{r \to \infty}{\sim} W^{(\text{out})}(E_n, r) f^{(\text{out})}(E_n)\mathcal{C}, \quad n = 1, 2, ... \tag{2.92}$$

are called the spectral points[59]. Depending on their locations on the Riemann surface, they may correspond to bound, resonance or virtual states solution to the Schrodinger equation. This is achieved by finding the combination coefficients C_n such that the contribution to the asymptotic behaviour from the first term of Eq.(2.50) is zero,

$$W^{(\text{in})}(E_n, r) f^{(\text{in})}(E_n)\mathcal{C} = 0, \tag{2.93}$$

and that implies that,

$$f^{(\text{in})}(E_n)\mathcal{C} = 0, \tag{2.94}$$

which is a system of homogeneous linear equations for the unknown variables C_n. It has a non-trivial solution if and only if the determinant of the matrix of its coefficients is zero,

$$\det f^{(\text{in})}(E_n) = 0. \tag{2.95}$$

The roots of Eq.(2.94) are the spectral points which are the discrete set of isolated energies $E_1, E_2, E_3, ...$ The energies E_n in general are complex numbers, and some how distributed on the Riemann surface. The next sections (2.3.1, 2.3.2 and 2.3.3) are based on how to find these spectral points.

22

2.3.1 Complex rotation

The numerical integration of Eqs.(2.60 and 2.61) works well when it is done for calculating the Jost matrices on the real energy and distance R axises. We encounter a technical problem when we do calculations on the complex energy plane along the same path, real R. The complex rotation technique is used to circumvent this problem to access the resonance states.

In general when the given potential asymptotically vanishes at large distances, we have [46]

$$F^{(\text{in/out})}(E, r) \xrightarrow[r \to \infty]{} f^{(\text{in/out})}(E). \qquad (2.96)$$

These Jost matrices limits are reached within required accuracy from $r = 0$ up to sufficiently large distance R using equations (2.60) and (2.61). The difficulty of finding resonances are caused by the asymptotic behaviour of the Riccati-Hankel functions[60],

$$h_\ell^{(\pm)}(kr) = \mp i \exp\left(\pm ikr \mp i\frac{\ell\pi}{2}\right). \qquad (2.97)$$

When momentum ,k, is complex, either $h_\ell^{(+)}(kr)$ or $h_\ell^{(-)}(kr)$ exponentially diverges, depending on the sign of Imk. Now neither the first or second of the equations (2.60) and (2.61) does give a numerically convergent solution. We circumvent the problem by following the path shown in figure (2.3), The integration of the differential equations no
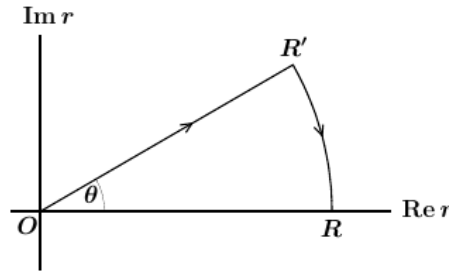
Figure 2.3: A deformed path for integrating the first order differential equations. Taken from Ref.[46]

longer happens along the real axis from $r = 0$ to $r = R$, but through the intermediate point $r = R'$ in the complex plane. The arc $R' \to R$ can be ignored since the potential is practically zero there. The divergence or convergence of the functions (2.602.61) is determined by the sign of Im(kr)[46]. If we have $k = |k|e^{i\varphi}$ the rotation via angle θ in $r = |r|e^{i\theta}$ such that the product

$$kr = |kr|e^{i(\theta + \varphi)} \qquad (2.98)$$

has either positive or negative (even zero) imaginary part. Further technical details of using complex rotation in calculating Jost matrices are exploited in Refs.[42, 43, 44, 46, 61, 62, 63, 64, 65, 66, 67].

© University of Pretoria

2.3.2 Bound states

Bound states are such states of the system that particles stay together and never leave their interaction region. The bound states spectral points are on the real negative axis, $\mathcal{E}_i < 0$, below all the thresholds,

$$\mathcal{E}_i < E_n, \quad \text{for all} \quad n = 1, 2, 3, \ldots, \tag{2.99}$$

on the physical Riemann sheet. All the thresholds energies are positive and since bound state energy is negative or possible zero, $\mathcal{E}_i \leq 0$, we can choose the lowest threshold to be zero.

In a two-body system the probability of finding one particle escaped from the interaction region with the other particle is zero, hence the system time-independent wave-functions for each channel, $\psi_n(E, r, \theta, \varphi)$, must also be zero for lager r. This implies that for each channel, $u_n(E, r) \xrightarrow[r \to \infty]{} 0$, and the same is true for the matrix of solutions: $U(E, r) \xrightarrow[r \to \infty]{} 0$.

The asymptotic behaviour of the physical solutions for bound states requires the Eq.(2.50) to converge to zero when r tends to infinity, i.e,

$$W^{(\text{in})}(\mathcal{E}_i, r \to \infty) f^{(\text{in})}(\mathcal{E}_i)\mathcal{C} + W^{(\text{out})}(\mathcal{E}_i, r \to \infty) f^{(\text{out})}(\mathcal{E}_i)\mathcal{C} \to 0. \tag{2.100}$$

Now since the corresponding channel momenta carries positive imaginary parts,

$$k_n = +\sqrt{2\mu\mathcal{E}_i/\hbar^2} = +i\kappa_n, \quad \kappa_n > 0. \tag{2.101}$$

then it is clear that,

$$h_{\ell_n}^{(+)}(i|k_n|r) \xrightarrow[r \to \infty]{} 0,$$
$$h_{\ell_n}^{(-)}(i|k_n|r) \xrightarrow[r \to \infty]{} \infty.$$

This implies that $W^{(\text{out})}(\mathcal{E}_i) = 0$ and $W^{(\text{in})}(\mathcal{E}_i)$ becomes an infinite diagonal matrix. It is then required that

$$f^{(\text{in})}(\mathcal{E}_i)\mathcal{C} = 0. \tag{2.102}$$

Since this is a system of linear homogeneous equations for the unknown combination coefficients, c_n, for a non-trivial solution, the column $\mathcal{C}$ matrix is non-zero, and Eq.(2.89) holds if and only if,

$$\det\left[f^{(\text{in})}(\mathcal{E}_i)\right] = 0. \tag{2.103}$$

on the physical sheet of the Riemann surface. For a single channel problem the Jost function tends to zero at a bound state energy [59], $\mathcal{E}_i$:

$$f^{(\text{in})}(\mathcal{E}_i) = 0. \tag{2.104}$$

24

Due to the symmetry relation between $f^{(\text{in})}(E)$ and $f^{(\text{out})}(E)$, for a negative choice of k_n, it can be shown that bound states also corresponds to the $\det\left[f^{(\text{out})}(\mathcal{E}_i)\right] = 0$, on the unphysical sheet of the Riemann surface. We will look at the resonance states in the next section.

2.3.3 Resonance states

Just like bound states, resonances are also spectral points. That means their corresponding physical solutions, $u(E_n, r)$, at larger distances are composed of only the outgoing spherical waves $W^{(\text{out})}(E_n, r)$. The asymptotic behaviour of the radial wave-functions at a resonance is given by:

$$U(\mathcal{E}_i, r) \xrightarrow[r \to \infty]{} W^{(\text{out})}(\mathcal{E}_i, r) f^{(\text{out})}(\mathcal{E}_i)\mathcal{C}$$

$$\xrightarrow[r \to \infty]{} \begin{pmatrix} -i^{\ell_1+1}e^{ik_1 r} & 0 & \cdots & 0 \\ 0 & -i^{\ell_2+1}e^{ik_2 r} & \cdots & 0 \\ \vdots & \vdots & \ddots & \vdots \\ 0 & 0 & \cdots & -i^{\ell_n+1}e^{ik_n r} \end{pmatrix} f^{(\text{out})}(\mathcal{E}_i)\mathcal{C}, \qquad (2.105)$$

where $k_n = \pm\sqrt{\frac{2\mu_n}{\hbar^2}(\mathcal{E}_i - E_n)}$, where the second term contribution is zero, i.e,

$$W^{(\text{in})}(\mathcal{E}_i, r) f^{(\text{in})}(\mathcal{E}_i)\mathcal{C} = 0 \qquad (2.106)$$

and by finding the same matrices and its determinant,

$$\det f^{(\text{in})}(\mathcal{E}_i) = 0, \qquad (2.107)$$

that determines the resonance energies. The resonance states are characterized by complex energies with positive real and negative imaginary parts,

$$\mathcal{E}_i = \mathcal{E}_r - \frac{i}{2}\Gamma, \quad \mathcal{E}_r > 0, \quad \Gamma > 0, \qquad (2.108)$$

where Γ is the total resonance width for the multi-channel resonance. Since the momentum is still given by $k_n = \pm\sqrt{\frac{2\mu_n}{\hbar^2}(E - E_n)}$, the positive choice for all n corresponds with the physical sheet and the negative momentum corresponds with the unphysical sheet of the Riemann surface. Therefore the resonance spectral points are located on the unphysical sheet of the Riemann surface. We use complex rotation technique when we are searching for resonances.

In the next section we will present how the spectral points (bound and resonance energies) including others (i.e virtual and sub-threshold energies) are distributed on the Riemann energy surface.

2.3.4 Distribution of the Spectral points on the Riemann surface

We have seen in the previous sections that the bound and resonance states energies can be located using the Jost matrices in a unified way. In this section we present the

25

distribution of the spectral points on the Riemann surface for single channel($N = 1$) case for short range potential interactions. The bound states discretely appear or distributed along the positive imaginary axis, see Figure(2.4). The resonances usually appear in
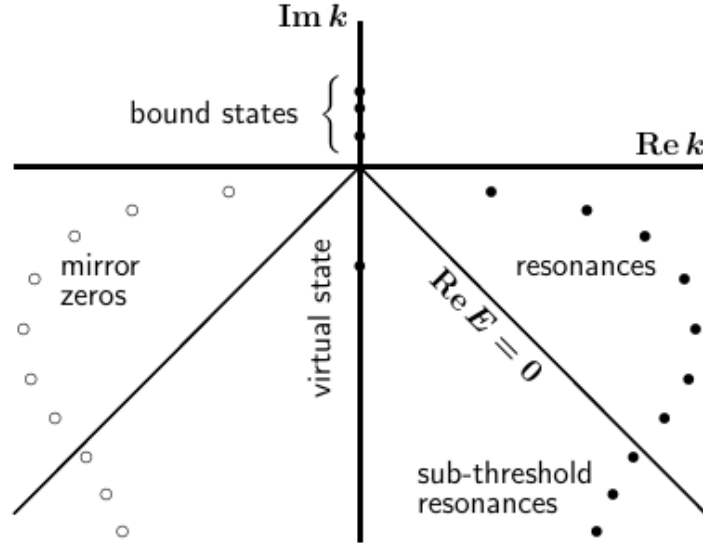
Figure 2.4: Distribution of the spectral points on the complex momentum plane.Taken from Ref.[46]

the form of a trajectory or a curve formed by discrete points in the complex k-plane. Furthermore there are infinitely many possible resonances[59], and their trajectory can curve is such way that corresponds with $E_r \to -\infty$ and $\Gamma \to \infty$. Such resonances with $E_r < 0$ are known as sub-threshold resonances and are not physically realizable. Now, the mirror zeros with negative $\text{Re}(k)$ are the mirror resonances due to the symmetries of the Jost matrices.

There are other spectral points that do not correspond to a physical realizable states [59]. They are real, negative energies located on the unphysical sheet of the Riemann energy surface. Therefore they correspond to the pure negative complex momenta:

$$k_n = -i\sqrt{2\mu_n |E_n|/\hbar^2}, \tag{2.109}$$

as they appear on Figure [2.4] on the negative imaginary axis,and also referred to as virtual states.

2.4 The Scattering states and the S-matrix

The scattering state is the transformation of an incoming wave into the outgoing wave at the real positive energies, when E is above the threshold.The scattering state wave function $\psi_{\boldsymbol{k}}(\boldsymbol{r}) = \langle \boldsymbol{r}|\psi_{\boldsymbol{k}}\rangle$ depends on two vectors ,$\boldsymbol{k}$ that indicates the direction where

26

the particles projectile come from and $\boldsymbol{r}$ that points in the direction of observation. The wave function is assumed to be normalized to the δ-function,

$$\langle \psi_{\boldsymbol{k}} | \psi_{\boldsymbol{k}'} \rangle = \delta(\boldsymbol{k} - \boldsymbol{k}'). \tag{2.110}$$

The wave function for N-channel scattering problem is the column matrix composed by these channel plane waves:

$$\Psi(E, r) = \begin{pmatrix} \psi_{\boldsymbol{k}_1(E, \boldsymbol{r})} \\ \psi_{\boldsymbol{k}_2(E, \boldsymbol{r})} \\ \vdots \\ \psi_{\boldsymbol{k}_N(E, \boldsymbol{r})} \end{pmatrix}. \tag{2.111}$$

When the potential is zero, the multichannel radial Schrodinger equation has the following solution:

$$U(E, r) = \frac{1}{2} W^{(\text{in})}(E, r)\mathcal{C} + \frac{1}{2} W^{(\text{out})}(E, r)\mathcal{C} = J(E, r)\mathcal{C}, \quad V = 0, \tag{2.112}$$

using the same boundary conditions:

$$f^{(\text{in}/\text{out})}(E) = F^{(\text{in}/\text{out})}(E) = \frac{1}{2} I \tag{2.113}$$

Now from Eq.(2.34), the time-independent partial wave-solutions for each channel is given by:

$$\psi_n(E, \boldsymbol{r}) = \frac{1}{r} j_{\ell_n}(k_n r) C_n Y_{\ell_n m_n}(\theta, \varphi), \quad V_{nn'} = 0. \tag{2.114}$$

Generally the channel plane wave in the partial wave expansion is given by:

$$\psi_{\boldsymbol{k}_n}(\boldsymbol{r}) = \sqrt{\frac{2}{\pi}} \frac{1}{k_n r} \sum_{\ell_n m_n} i^{\ell_n} j_{\ell_n}(k_n r_n) Y^*_{\ell_n m_n}(\hat{k}_n) Y^*_{\ell_n m_n}(\hat{r}) \tag{2.115}$$

where $\hat{k}_n = (\theta_{k_n}, \varphi_{k_n})$ and $\hat{r} = (\theta, \varphi)$ are unit vectors in the directions of $\boldsymbol{k}_n$ and $\boldsymbol{r}$. For a non-zero, short-ranged potential the general time-independent solution can be given by [59]:

$$\psi_n(E, \boldsymbol{r}) = \sqrt{\frac{2}{\pi}} \frac{1}{k_n r} \sum_{n'}^{N} \sum_{\ell_n m_n} i^{\ell_n} \big[h^{(-)}_{\ell_n}(k_n r) F^{(\text{in})}_{nn'}(E, r) +$$
$$h^{(+)}_{\ell_n}(k_n r) F^{(\text{out})}_{nn'}(E, r) \big] \frac{1}{2} [f^{(\text{in})}(E, r)]^{-1}_{nm'} Y^*_{\ell_n m_n}(\hat{k}_n) Y^*_{\ell_n m_n}(\hat{r}). \tag{2.116}$$

If the S-matrix is defined as:

$$S(E) = f^{(\text{out})}(E) [f^{(\text{in})}(E)]^{-1}, \tag{2.117}$$

then the asymptotic behaviour of Eq.(2.117) is obtained:

$$\psi_n(E, \boldsymbol{r}) \xrightarrow[r \to \infty]{} \frac{1}{2}\sqrt{\frac{2}{\pi}}\frac{1}{k_n r}\sum_{n'}^{N}\sum_{\ell_n m_n} i^{\ell_n}\big[h_{\ell_n}^{(-)}(k_n r)+$$

$$h_{\ell_n}^{(+)}(k_n r)S_{nn'}(E)\big]\frac{1}{2}[f^{(\mathrm{in})}(E, r)]_{nm'}^{-1}Y_{\ell_n m_n}^*(\hat{k}_n)Y_{\ell_n m_n}^*(\hat{r}), \tag{2.118}$$

where $S_{nn'}$ is the S-matrix elements. Now by subtracting and adding $h_\ell^{(+)}(kr)$ and using the relation $2j_\ell(kr) = h_\ell^{(-)}(kr) + h_\ell^{(+)}(kr)$ the expression becomes:

$$\psi_n(E, \boldsymbol{r}) \xrightarrow[r \to \infty]{} \frac{1}{2}\sqrt{\frac{2}{\pi}}\frac{1}{k_n r}\sum_{n'}^{N}\sum_{\ell_n m_n} i^{\ell_n}\big[2j_{\ell_n}(k_n r)+$$

$$h_{\ell_n}^{(+)}(k_n r)(S_{nn'}(E) - \delta_{nn'})\big]Y_{\ell_n m_n}^*(\hat{k}_n)Y_{\ell_n m_n}^*(\hat{r}), \tag{2.119}$$

and we obtain,

$$\psi_n(E, \boldsymbol{r}) \xrightarrow[r \to \infty]{} \frac{1}{2}\sqrt{\frac{2}{\pi}}\frac{1}{k_n r}\sum_{\ell_n m_n} i^{\ell_n} j_{\ell_n}(k_n r)Y_{\ell_n m_n}^*(\hat{k}_n)Y_{\ell_n m_n}^*(\hat{r})+$$

$$\frac{1}{2}\sqrt{\frac{2}{\pi}}\frac{1}{k_n r}\sum_{n'}^{N}\sum_{\ell_n m_n}\frac{i^{\ell_n}}{2}h_{\ell_n}^{(+)}(k_n r)(S_{nn'}(E) - \delta_{nn'})\big]Y_{\ell_n m_n}^*(\hat{k}_n)Y_{\ell_n m_n}^*(\hat{r}). \tag{2.120}$$

Eq.(2.120) can now be written as:

$$\psi_n(E, \boldsymbol{r}) \xrightarrow[r \to \infty]{} (2\pi)^{-3/2}e^{i\boldsymbol{k}_n \cdot \boldsymbol{r}}+$$

$$\frac{1}{2}\sqrt{\frac{2}{\pi}}\frac{1}{k_n r}\sum_{n'}^{N}\sum_{\ell_n m_n}\frac{i^{\ell_n}}{2}h_{\ell_n}^{(+)}(k_n r)(S_{nn'}(E) - \delta_{nn'})\big]Y_{\ell_n m_n}^*(\hat{k}_n)Y_{\ell_n m_n}^*(\hat{r}) \tag{2.121}$$

given the fact that the plane wave can be expanded as,

$$e^{i\boldsymbol{k}_n \cdot \boldsymbol{r}} = \frac{4\pi}{k_n r}\sum_{\ell_n m_n} i^{\ell_n} j_{\ell_n}(k_n r)Y_{\ell_n m_n}^*(\hat{k}_n)Y_{\ell_n m_n}^*(\hat{r}). \tag{2.122}$$

We can now extract matrix elements of the partial wave amplitude and define it as follows:

$$\mathrm{f}_{nm} \equiv \frac{1}{2ik_n}[(S_{nm})(E, r) - \delta_{nm}], \tag{2.123}$$

where now the full scattering amplitude is defined by:

$$\mathbf{f}_n(\hat{r} \leftarrow \hat{k}_n) = 4\pi \sum_{n'=1}^{N}\sum_{\ell_n m_n} \mathrm{f}_{nn'}(E)Y_{\ell_n m_n}^*(\hat{k}_n)Y_{\ell_n m_n}^*(\hat{r}). \tag{2.124}$$

Now the time-independent state wave-function of each channel is presented in this form:

$$\psi_n(E, \boldsymbol{r}) \xrightarrow[r \to \infty]{} (2\pi)^{-3/2}e^{i\boldsymbol{k}_n \cdot \boldsymbol{r}} + (2\pi)^{-3/2}\mathbf{f}_n(\hat{\boldsymbol{r}} \leftarrow \hat{\boldsymbol{k}}_n)\frac{e^{ik_n r}}{r} \tag{2.125}$$

28

2.5   S-matrix Residues

The S-matrix residues can also be calculated using the Jost matrices, it has been shown in [59]. Their relationship with the ANC and NVC is used to calculate these values for various range of single hypernuclei systems in Chapter 5.

The S-matrix elements are complex functions of energy and can be expanded in the Laurent series as:

$$S_{nm}(E) = \frac{R_{nm}}{E - \mathcal{E}_i} + D_{nm}^{(0)} + D_{nm}^{(1)}(E - \mathcal{E}_i) + D_{nm}^{(2)}(E - \mathcal{E}_i)^2 + \ldots\ldots, \qquad (2.126)$$

where $\mathcal{E}_i$ represented an isolated spectral energy point. The first term which is called the principal part dominates the expansion when energy E gets very close to $\mathcal{E}_i$ $(E \to \mathcal{E}_i,)$ so that:

$$S_{nm}(E) \xrightarrow[E \to \mathcal{E}_i]{} \frac{R_{nm}}{E - \mathcal{E}_i}. \qquad (2.127)$$

The residue is now defined as, $\text{Res}[S_{nm}, \mathcal{E}_i]$ for each matrix element at the spectral point and can be determined with:

$$\text{Res}[S_{nm}, \mathcal{E}_i] = \lim_{E \to \mathcal{E}_i} (E - \mathcal{E}_i) S_{nm}(E). \qquad (2.128)$$

Now using the Jost matrices and the S-matrix relationship we can derive the relation between Jost matrices and S-matrix residues. Near the spectral point the determinant of the Jost matrices, $\det\left[f^{(\text{in})}(E)\right]$ can be expanded using the Taylor series as [59],

$$\det\left[f^{(\text{in})}(E)\right] = \det\left[f^{(\text{in})}(E)\right] + (E - \mathcal{E}_i)\frac{d}{dE}\left[f^{(\text{in})}(E)\right]\Big|_{\mathcal{E}_i} + \cdots, \qquad (2.129)$$

where, $\det\left[f^{(\text{in})}(\mathcal{E}_i)\right] = 0$, at the spectral point and as $E \to \mathcal{E}_i$, all the higher-order terms are neglected. Thus:

$$\det\left[f^{(\text{in})}(E)\right] \approx (E - \mathcal{E}_i)\frac{d}{dE}\left[f^{(\text{in})}(E)\right]\Big|_{\mathcal{E}_i}. \qquad (2.130)$$

The S-matrix using Jost matrices determinant and its adjugate can now be written as follows:

$$S(E) = f^{(\text{out})}(E)\left[f^{(\text{in})}(E)\right]^{-1} = f^{(\text{out})}(E)\text{adj}\left[f^{(\text{in})}(E)\right]\frac{1}{\det\left[f^{(\text{in})}(E)\right]}. \qquad (2.131)$$

Eq.(2.131) above can now be re-written in the following form:

$$\lim_{E \to \mathcal{E}_i} (E - \mathcal{E}_i) S(E) = \lim_{E \to \mathcal{E}_i} f^{(\text{out})}(E) \text{adj}\left[f^{(\text{in})}(E)\right] \frac{1}{\frac{d}{dE} \det\left[f^{(\text{in})}(E)\right]_{\mathcal{E}_i}} \qquad (2.132)$$

The S-matrix residue is then given by:

$$\text{Res}[S, \mathcal{E}_i] = \lim_{E \to \mathcal{E}_i} f^{(\text{out})}(E) \text{adj}\left[f^{(\text{in})}(E)\right] \frac{1}{\frac{d}{dE} \det\left[f^{(\text{in})}(E)\right]_{\mathcal{E}_i}}. \qquad (2.133)$$

For single channel, this reduces to the following form:

$$\text{Res}[S, \mathcal{E}_i] = \frac{f^{(\text{out})}(\mathcal{E}_i)}{\dot{f}^{(\text{in})}(\mathcal{E}_i)} \qquad (2.134)$$

where the derivative $\dot{f}^{(\text{in})}(\mathcal{E}_i)$ can be calculated numerically using this equation:

$$\frac{d}{dE} \det\left[f^{(\text{in})}(E)\right] = \frac{\det\left[f^{(\text{in})}(E + \epsilon)\right] - \det\left[f^{(\text{in})}(E - \epsilon)\right]}{2\epsilon}, \qquad \epsilon \to 0 \qquad (2.135)$$

2.6 Asymptotic normalization constant and Nuclear vertex constant

The S-matrix is a meromorphic function of the energy with a well-known pattern of the poles distributed over the Riemann surface. These poles correspond to bound and resonant states. The residues of the S-matrix at the poles, determine the probabilities of the formation and decay of the corresponding bound and quasi-bound states. They therefore are among the important characteristics of such states.

In Appendix A it is shown that the so called Nuclear Vertex Constants (NVC), $G_{ab \to d}$ and $G_{d \to ab}$, describing the probabilities of virtual formation $(ab \to d)$ and decay $(d \to ab)$ of a discrete state d composed of the two fragments a and b, are related to the residue as follows:

$$G_{ab \to d} G_{d \to ab} = \frac{i\pi}{\mu \kappa_d} \text{Res}\left[S_\ell(z), \mathcal{E}_d\right] . \qquad (2.136)$$

It is also shown that, due to the time-reversal invariance, these two NVC's may only differ by sign (see Eq. (A.14)).

A residue of the S-matrix is also closely related to the corresponding Asymptotic Normalization Constant $\mathcal{A}_\ell$ (defined by Eq. (1.3)). This relation is usually derived in two different ways. It can be obtained by taking energy derivative of the Wronskian of the Jost and regular solutions of radial Schrödinger equation (see, for example, Sec. 6.5 of Ref. [68]). Alternatively, it can be found from the continuity equation (see, for example,

Sec. 15 of Ref. [69]). In the Appendix B, using the first of these two approaches, it is shown that at a bound-state energy $\mathcal{E}_d$

$$\text{Res}\left[S_\ell(E), \mathcal{E}_d\right] = (-1)^\ell \frac{\kappa_d}{\mu} \mathcal{A}_\ell^2 \ , \tag{2.137}$$

where $\kappa_d = |\sqrt{2\mu\mathcal{E}_d}|$ is the absolute value of the corresponding momentum. Taking into account Eq. (2.136), we see that the ANC can be factorized in terms of the NVC's.

Chapter 3

Expansion of the multi-channel Jost matrices

In this chapter we use the multi-channel Jost matrices presented in Chapter 2, to present the theoretical framework to be used for this study. The second part of the results of Ref.[54] are then presented. Section 3.2, the Jost matrix is constructed in such a way that their dependencies of its matrix elements on odd powers of the channel momenta are factorized explicitly. In Section 3.5, using the same ΛA-potential as in Ref.[54], the effective-range parameters were re-calculated for the same set of nuclear targets. In addition to the S-wave scattering lengths and effective radii reported in Ref.[54], the higher-order parameters were also calculated.

3.1   Introduction

Power-series expansions are commonly used in physics. An expansion of this kind that is most frequently used in quantum scattering theory, is known as the effective-range expansion[46, 67]. For a short-range potential that we are considering, this expansion reads,

$$k^{2\ell+1} \cot \delta_\ell(k) = \sum_{n=0}^{\infty} c_{\ell n} k^{2n} \tag{3.1}$$

where $\delta_\ell(k)$ is the scattering phase shift and the right-hand side is a sum of terms proportional to even powers of the collision momentum k. The $c_{\ell n}$ are energy independent expansion coefficients. This type of expansion has been suggested long time ago in nuclear physics for the S-wave type, nucleon-nucleon scattering in this form,

$$k^{2\ell+1} \cot \delta_0(k) = -\frac{1}{a_0} + \frac{\mathrm{r}_0}{2}k^2 - \mathrm{P}_0\mathrm{r}_0^3 k^4 + \mathrm{Q}_0\mathrm{r}_0^5 k^6 - \mathrm{L}_0\mathrm{r}_0^7 k^6 \tag{3.2}$$

where the first two parameters on the right-hand side, namely, a and r_0, were called the scattering length and the effective radius. The parameters in the higher order terms of this expansion (P_0 , Q_0, L_0 etc.) are known as the shape parameters. The limitation of this effective-range expansion is that it is only applicable near the point $k = 0$, when the energy is close to the threshold[46, 67].

In Refs.[46, 59, 67, 70] different approach in generalizing the effective-range expansion to multi-channel problems were developed, and will be presented in this chapter. Instead of considering the channel phase shifts and their cotangents, a more general approach is considered. A simple first-order differential equations were derived. By solving them one can easily calculate any number of coefficients in the series expansion 3.1, and not only for the S-wave state, but also for any angular momentum $\ell \neq 0$.

The structure of the Jost matrix is constructed in such a way that their dependencies of its matrix elements on odd powers of the channel momenta are factorized explicitly. These factors determine all the branching points of the Riemann surface of the energy, while the remaining factors are single-valued holomorphic functions defined on a simple energy plane. These functions are then expanded in power series of $(E - E_0)$, where E_0 is an arbitrary complex energy.

An expression for the Jost matrix such that each of its elements is a product of a nonanalytic "branching" factor and a power series, is obtained. In this way, we are not limited to the threshold points, but expand the Jost matrix practically anywhere on the Riemann surface. When the Jost matrix is obtained in such a semi-analytic form (the first several terms of the expansion), the S matrix and all the observables can be easily calculated. Although it is possible, there is no need in introducing the generalized scattering length and other parameters. The Jost matrix expansion coefficients are more simple and reliable for this purpose.

3.2   Factorization of the multi-channel Jost matrices

We consider the Riccati-Bessel and Riccati-Neumann functions which are represented by the absolutely convergent series, .,

$$j_\ell(kr) = \left(\frac{kr}{2}\right)^{\ell+1} \sum_{n=0}^{\infty} \frac{(-1)^n \sqrt{\pi}}{\Gamma(\ell + 3/2 + n)n!} \left(\frac{kr}{2}\right)^{2n} = k^{\ell+1} \tilde{j}_\ell(E, r), \qquad (3.3)$$

$$y_\ell(kr) = \left(\frac{2}{kr}\right)^{\ell} \sum_{n=0}^{\infty} \frac{(-1)^{n+\ell+1}}{\Gamma(-\ell + 1/2 + n)n!} \left(\frac{kr}{2}\right)^{2n} = k^{-\ell} \tilde{y}_\ell(E, r), \qquad (3.4)$$

which are factorized in terms of the odd and the even powers of k, hence the functions $\tilde{j}_\ell$ and $\tilde{y}_\ell$ are analytical single-valued functions of the energy E which do not depend on odd powers of k. This Eqs. (3.3 and 3.4) tells us that the matrices $\mathcal{A}(E, r)$ and $\mathcal{B}(E, r)$ including Jost matrices are multi-valued functions which can be defined on a complicated Riemann surface.

33

Now using the Equations.(3.3 and 3.4) each diagonal element of the matrices can be rewritten as the product of an integer power of a channel momentum and an entire function of the energy as [59],

$$
J = \begin{pmatrix} k_1^{\ell_1+1} & 0 & \cdots & 0 \\ 0 & k_2^{\ell_2+1} & \cdots & 0 \\ \vdots & \vdots & \ddots & \vdots \\ 0 & 0 & \cdots & k_N^{\ell_N+1} \end{pmatrix} \tilde{J}, \qquad Y = \begin{pmatrix} k_1^{-\ell_1} & 0 & \cdots & 0 \\ 0 & k_2^{-\ell_2} & \cdots & 0 \\ \vdots & \vdots & \ddots & \vdots \\ 0 & 0 & \cdots & k_N^{-\ell_N} \end{pmatrix} \tilde{Y}. \quad (3.5)
$$

where $\tilde{J}$ and $\tilde{Y}$ denote the diagonal matrices,

$$
\tilde{J} = \operatorname{diag}\left\{ \tilde{j}_{\ell_1}(E,r), \tilde{j}_{\ell_2}(E,r), ..., \tilde{j}_{\ell_N}(E,r) \right\}, \tag{3.6}
$$

$$
\tilde{Y} = \operatorname{diag}\left\{ \tilde{y}_{\ell_1}(E,r), \tilde{y}_{\ell_2}(E,r), ..., \tilde{y}_{\ell_N}(E,r) \right\}, \tag{3.7}
$$

with the tilted functions defined by Eqs.(3.3,3.4). All possible odd powers of the channel momenta are factorized and the remaining tilted functions are single-valued functions of the energy[59]. These factorized representations can be written in the compact form [59],

$$
J = D\tilde{J}, \qquad Y = KD^{-1}\tilde{Y}, \tag{3.8}
$$

where

$$
D = \operatorname{diag}\left\{ k_1^{\ell_1+1}, k_2^{\ell_2+1}, ..., k_N^{\ell_N+1} \right\}. \tag{3.9}
$$

Let us look for matrices $\mathcal{A}$ and $\mathcal{B}$ in the Eq. in the form,

$$
\mathcal{A} = D^{-1}\tilde{\mathcal{A}}D, \qquad \mathcal{B} = DK^{-1}\tilde{\mathcal{B}}D. \tag{3.10}
$$

Substituting them in the first order differential equations (2.76 and 2.77) the following equations were obtained,

$$
D^{-1}\partial_r \tilde{\mathcal{A}}D = -D^{-1}\tilde{Y}V(D\tilde{J}D^{-1}\tilde{\mathcal{A}}D - KD^{-1}\tilde{J}DK^{-1}\tilde{\mathcal{B}}D) \tag{3.11}
$$

$$
DK^{-1}\partial_r \tilde{\mathcal{B}}D = -K^{-1}D\tilde{J}V(D\tilde{J}D^{-1}\tilde{\mathcal{A}}D - KD^{-1}\tilde{J}DK^{-1}\tilde{\mathcal{B}}D). \tag{3.12}
$$

The first of these equations is multiplied by D from the left, the second by KD^{-1} also from the left, and both by D^{-1} from th right to eliminate all the momentum-dependent coefficients [59]. Since all the matrices K, D, $\tilde{J}$, and $\tilde{Y}$ are diagonal and commute, the following equations for tilted functions were obtained,

34

$$\partial_r \tilde{\mathcal{A}} = -\tilde{Y} V (\tilde{J}\tilde{\mathcal{A}} - Y\tilde{\mathcal{B}}), \tag{3.13}$$

$$\partial_r \tilde{\mathcal{B}} = -\tilde{J} V (\tilde{J}\tilde{\mathcal{A}} - Y\tilde{\mathcal{B}}). \tag{3.14}$$

The potential V depends on the radius r, while the other matrices are functions of both r and E. The boundary conditions for Eqs.(3.13 and 3.14) are given by:

$$\tilde{J}\tilde{\mathcal{A}}\tilde{J}^{-1} \xrightarrow[r\to 0]{} I, \qquad \tilde{Y}\tilde{\mathcal{B}}\tilde{J}^{-1} \xrightarrow[r\to 0]{} 0 \tag{3.15}$$

The coefficients in Eqs.(3.13 and 3.14) and their energy independent boundary conditions (3.15) do not involve odd powers of the momenta, which implies that $\tilde{\mathcal{A}}(E,r)$ and $\tilde{\mathcal{B}}(E,r)$ are single-valued functions of energy E, that is they are analytic and defined on a simple complex-energy plane without any branching points[59]. The matrices $\mathcal{A}(E,r)$ and $\mathcal{B}(E,r)$ are the ones carrying all difficulties associated with the multi-valuedness and Riemann surface which originate from the matrices D and K. Their matrices elements are given by,

$$\mathcal{A}_{mn}(E,r) = k_m^{-\ell_m-1}\tilde{\mathcal{A}}_{mn}(E,r)k_n^{\ell_n+1}, \quad \mathcal{B}_{mn}(E,r) = k_m^{\ell_m}\tilde{\mathcal{B}}_{mn}(E,r)k_n^{\ell_n+1}, \tag{3.16}$$

where $\tilde{\mathcal{A}}$ and $\tilde{\mathcal{B}}$ are real on the real axis, ImE, including Eqs. (3.13, 3.14 and 3.15).

When Eqs.(2.73 and 2.74) are combined the following expression obtained,

$$F^{(\text{in/out})} = \frac{1}{2}(\tilde{\mathcal{A}} \mp i\tilde{\mathcal{B}}) = \frac{1}{2}D^{-1}\left(\tilde{\mathcal{A}} \mp iD^2K^{-1}\tilde{\mathcal{B}}\right)D \tag{3.17}$$

or in the form,

$$F_{mn}^{(\text{in})} = \frac{k_n^{\ell_n+1}}{2k_m^{\ell_m+1}}\tilde{\mathcal{A}}_{mn} - \frac{ik_m^{\ell_m}k_n^{\ell_n+1}}{2}\tilde{\mathcal{B}}_{mn}, \tag{3.18}$$

$$F_{mn}^{(\text{out})} = \frac{k_n^{\ell_n+1}}{2k_m^{\ell_m+1}}\tilde{\mathcal{A}}_{mn} + \frac{ik_m^{\ell_m}k_n^{\ell_n+1}}{2}\tilde{\mathcal{B}}_{mn}. \tag{3.19}$$

Now considering Eq.(2.56) for the short range potential, the Jost matrices limits when $r \to \infty$ are,

$$f^{(\text{in/out})}(E) = D^{-1}a(E)D \mp iDK^{-1}b(E)D, \tag{3.20}$$

with the matrices $a(E)$ and $b(E)$ being the asymptotic values of the r-dependent functions of $\tilde{\mathcal{A}}(E,r)$ and $\tilde{\mathcal{B}}(E,r)$ i.e,

$$a(E) = \frac{1}{2}\lim_{r\to\infty}\tilde{\mathcal{A}}(E,r), \quad b(E) = \frac{1}{2}\lim_{r\to\infty}\tilde{\mathcal{B}}(E,r), \tag{3.21}$$

35

and the Jost matrices entries,

$$f_{mn}^{(\text{in/out})}(E) = \frac{k_n^{\ell_n+1}}{k_m^{\ell_m+1}} a_{mn}(E) \mp i k_m^{\ell_m} k_n^{\ell_n+1} b_{mn}(E), \tag{3.22}$$

where

$$a_{mn}(E) = \frac{1}{2}\tilde{\mathcal{A}}_{mn}(E,\infty), \quad b_{mn}(E) = \frac{1}{2}\tilde{\mathcal{B}}_{mn}(E,\infty). \tag{3.23}$$

Then we obtain the following $S-$matrix,

$$\begin{aligned} S(E) &= [D^{-1}a(E)D + iDK^{-1}b(E)D][D^{-1}a(E)D - iDK^{-1}b(E)D]^{-1} \\ &= [D^{-1}a(E) + iDK^{-1}b(E)][D^{-1}a(E) - iDK^{-1}b(E)]^{-1}, \end{aligned} \tag{3.24}$$

in terms of the holomorphic matrix-functions which depends on the variable E. The analytic matrix-functions $a(E)$ and $b(E)$ can be expanded using the Taylor series around any point E_0 :

$$a(E) = \sum_{n=0}^{\infty} \tilde{\alpha}_n(E_0)(E - E_0)^n, \quad b(E) = \sum_{n=0}^{\infty} \tilde{\beta}_n(E_0)(E - E_0)^n, \tag{3.25}$$

where the expansion coefficients, $\tilde{\alpha}_n$ and $\tilde{\beta}_n$, are the square matrices with the same dimensions as the matrices $a(E)$ and $b(E)$ and they also depend on the choice of the central point E_0.

3.3 Power series expansions near an arbitrary point

The matrices $\tilde{\mathcal{A}}(E,r)$ and $\tilde{\mathcal{B}}(E,r)$ are holomorphic functions of the parameter E for any finite value of radius r, hence they can be expanded in the power series around any point E_0 on the complex energy plane[46],

$$\tilde{\mathcal{A}}(E,r) = \sum_{n=0}^{\infty} (E - E_0)^n \alpha_n(E_0,r), \tag{3.26}$$

$$\tilde{\mathcal{B}}(E,r) = \sum_{n=0}^{\infty} (E - E_0)^n \beta_n(E_0,r), \tag{3.27}$$

where the unknown expansion coefficients α_n and β_n depend on the point E_0 and the variable radius r. The same kind of expansion is also done for the other matrices $\tilde{J}(E,r)$ and $\tilde{Y}(E,r)$ by using the known coefficients, η_n and γ_n,

$$\tilde{J}(E,r) = \sum_{n=0}^{\infty} (E - E_0)^n \gamma_n(E_0,r), \tag{3.28}$$

$$\tilde{Y}(E,r) = \sum_{n=0}^{\infty} (E - E_0)^n \eta_n(E_0,r). \tag{3.29}$$

where the diagonal matrices,

$$\eta_n(E_0, r) = \text{diag}\{\eta_n(\ell_1, E_0, r), \eta_n(\ell_2, E_0, r), ..., \eta_n(\ell_N, E_0, r)\} \tag{3.30}$$

and

$$\gamma_n(E_0, r) = \text{diag}\{\gamma_n(\ell_1, E_0, r), \gamma_n(\ell_2, E_0, r), ..., \gamma_n(\ell_N, E_0, r)\} \tag{3.31}$$

are made of the expansion coefficients given on Appendix.D. When all these series are substituted into the Eq.(3.13 and 3.14) and also replacing there the matrices $\tilde{J}$ and $\tilde{Y}$ with the corresponding series (3.28 and 3.29), the following set of differential equations were obtained [46, 59],

$$\partial_r \alpha_n = - \sum_{i+j+k=n} \eta_i V(\gamma_j \alpha_k - \eta_j \beta_k), \tag{3.32}$$

$$\partial_r \beta_n = - \sum_{i+j+k=n} \gamma_i V(\gamma_j \alpha_k - \eta_j \beta_k), \quad n = 0, 1, 2, ... \tag{3.33}$$

with the energy independent boundary conditions at $r = 0$,

$$\lim_{r \to 0} \tilde{J}(E, r) \alpha_n(E_0, r) [\tilde{J}(E, r)]^{-1} = \delta_{n0} I, \quad \beta_n(E_0, 0) = 0, \ \forall n. \tag{3.34}$$

The quantities α_n and β_n are functions of the square matrices, and their summation condition, $i + j + k = n$, decouples the first M pairs of the equations from any equations with $n > M$.

The expansion coefficients $\tilde{\alpha}$ and $\tilde{\beta}$ in the series (3.25) are the asymptotic values of the corresponding coefficients,

$$\tilde{\alpha}_n(E_0) = \frac{1}{2} \lim_{r \to \infty} \alpha_n(E_0, r), \quad \text{and} \quad \tilde{\beta}_n(E_0) = \frac{1}{2} \lim_{r \to \infty} \beta_n(E_0, r). \tag{3.35}$$

Therefore the coefficients $\tilde{\alpha}$ and $\tilde{\beta}$, can be obtained by numerically integrating Eqs.(3.32,3.33) from the boundary values (3.34) up to a faraway point where the potential vanishes and the limits(3.35) are reached within acceptable accuracy.

Now for a single channel case using short range potential, we obtain the following Jost functions factorized structure,

$$f_\ell^{(\text{in}/\text{out})}(E) = a_\ell(E) \mp k^{2\ell+1} b_\ell(E), \tag{3.36}$$

where the factor $k^{2\ell+1}$ is responsible for the branching of the Riemann surface with the unknown single valued analytic functions $a_\ell(E)$ and $b_\ell(E)$. These functions can be expanded in the Taylor series around an arbitrary point E_0 on the complex energy pane,

$$a(E) = \sum_{n=0}^{\infty} \tilde{\alpha}_n(\ell, E_0)(E - E_0)^n, \quad b(E) = \sum_{n=0}^{\infty} \tilde{\beta}_n(\ell, E_0)(E - E_0)^n, \tag{3.37}$$

37

then S-matrix can also be obtained with the following ratio,

$$S_\ell(E) = \frac{f_\ell^{(\text{out})}(E)}{f_\ell^{(\text{in})}(E)} = \frac{\sum\limits_{n=0}^{\infty} (\tilde{\alpha}_n + k^{2\ell+1}\tilde{\beta}_n)(E - E_0)^n}{\sum\limits_{n=0}^{\infty} (\tilde{\alpha}_n - k^{2\ell+1}\tilde{\beta}_n)(E - E_0)^n} \tag{3.38}$$

3.4   Effective range parameters

We consider the expansions (3.25) around the real energies, in this case around the threshold energy $E_0 = 0$. The S-matrix (3.38) then takes the following form,

$$S_\ell(E) = \frac{f_\ell^{(\text{out})}(E)}{f_\ell^{(\text{in})}(E)} = \frac{\sum\limits_{n=0}^{\infty} (\tilde{\alpha}_n + ik^{2\ell+1}\tilde{\beta}_n)E^n}{\sum\limits_{n=0}^{\infty} (\tilde{\alpha}_n - ik^{2\ell+1}\tilde{\beta}_n)E^n} \tag{3.39}$$

It was shown that for the real scattering energies, the functions $a_\ell(E)$ and $b_\ell(E)$ are real, therefore for real E_0 all the expansion coefficients are real as well [59]. That also makes the Jost functions, the numerator and denominator in Eq.(3.39) to be complex conjugates of each other at real energies, i.e,

$$f_\ell^{(\text{out})}(E) = f_\ell^{(\text{in})*}(E), \quad \text{Im} E = 0. \tag{3.40}$$

The functions can be expressed in terms of the scattering phase shifts as,

$$f_\ell^{(\text{out/in})}e^{\pm i\delta_\ell} = \sum_{n=0}^{\infty} \tilde{\alpha}_n E^n \pm ik^{2\ell+1}\sum_{n=0}^{\infty} \tilde{\beta}_n E^n, \tag{3.41}$$

then,

$$\sum_{n=0}^{\infty} \tilde{\alpha}_n E^n = |f_\ell^{(\text{out})}|\cos\delta_\ell \tag{3.42}$$

$$ik^{2\ell+1}\sum_{n=0}^{\infty} \tilde{\beta}_n E^n = |f_\ell^{(\text{out})}|\sin\delta_\ell. \tag{3.43}$$

When these two equations are divided, the following expression is obtained

$$k^{2\ell+1}\cot\delta_\ell = \frac{\tilde{\alpha}_0 + \tilde{\alpha}_1 E + \tilde{\alpha}_2 E^2 + ...}{\tilde{\beta}_0 + \tilde{\beta}_1 E + \tilde{\beta}_2 E^2 + ...}. \tag{3.44}$$

Now the division on the right hand side of Eq.(3.44),

$$\mathcal{K}(E) = \frac{\tilde{\alpha}_0 + \tilde{\alpha}_1 E + \tilde{\alpha}_2 E^2 + ...}{\tilde{\beta}_0 + \tilde{\beta}_1 E + \tilde{\beta}_2 E^2 + ...}. \tag{3.45}$$

38

can be performed and expressed in the Maclaurin series(see AppendixC),

$$\mathcal{K}(E) = \mathcal{K}(0) + \mathcal{K}'(0)E + \mathcal{K}''(0)\frac{E^2}{2} + \mathcal{K}'''(0)\frac{E^3}{6} + \mathcal{K}^{(4)}(0)\frac{E^4}{24}. \qquad (3.46)$$

This expression is well known in the following form,

$$k^{2\ell+1}\cot\delta_\ell = -\frac{1}{a_\ell} + \frac{r_\ell}{2}k^2 - P_\ell r_\ell^3 k^4 + Q_\ell r_\ell^5 k^6 - L_\ell r_\ell^7 k^6 \qquad (3.47)$$

Once the the expansion coefficients $\tilde{\alpha}_n$ and $\tilde{\beta}_n$ in Eqs.(3.44 and 3.45) are calculated, then using the relation $E = (\hbar k)^2/2\mu$, and doing simple algebra the following parameters can be obtained,

$$a_\ell = -1/\mathcal{K}(0), \qquad r_\ell = \mathcal{K}'(0)\hbar^2/\mu \qquad (3.48)$$

$$P_\ell = -\frac{\mu\mathcal{K}''(0)}{8\hbar^2[\mathcal{K}'(0)]^3}, \quad Q_\ell = -\frac{\mu^2\mathcal{K}'''(0)}{48\hbar^2[\mathcal{K}'(0)]^5}, \quad L_\ell = -\frac{\mu^3\mathcal{K}^{(4)}(0)}{384\hbar^6[\mathcal{K}'(0)]^7}, \qquad (3.49)$$

hence any number of effective-range parameters can also be calculated in Eq.3.47

3.5 Results and discussion

In this section we now use the method presented in the previous sections using the same ΛA-potential as in Ref.[54] to calculate the effective-range parameters for the same set of nuclear targets. In addition to the S-wave scattering lengths and effective radii reported in Ref.[54], the higher-order parameters were also calculated.

In order to obtain the effective-range parameters, we numerically integrated the system of differential equations (3.32,3.33) with max(n) = 4, from $r_{min} = 10^{-5}$ fm to $r_{max} = 30$ fm. This integration gave us the sets of five coefficients $a_0,\dots,a_4$ and $b_0,\dots,b_4$, of the expansions (3.26,3.27) around the threshold energy $E_0 = 0$, for each of the hypernuclei listed in Table 5.1. This was done for three values of the angular momentum, namely, $\ell = 0, 1, 2$. Using these coefficients, we calculated the effective range parameters as is described in Sec. 3.4 and in Appendix C. The results of these calculations are given in Tables 3.1, 3.2,3.3, 3.4. For comparison, these tables also include the corresponding scattering lengths and effective radii obtained in Ref. [53, 71] for $\ell = 0$.

As is seen from the tables, our values of a_0 and r_0 in most cases are different from those reported in Ref. [53]. The reason for that is the following. The calculation of these parameters in Ref. [53] involves two steps. At the first step, the authors of this paper accurately calculate the energy $\mathcal{E}$ of the bound state and the corresponding ANC. At the second step, they approximate the scattering amplitude using the effective-range expansion and choose such values for a_0 and r_0 that make this amplitude singular at the exact value of the energy $E = \mathcal{E}$ and give the exact value of the ANC. The problem stems from the fact that the effective-range expansion is only accurate within a circle around the point $k = 0$ on the complex k-plane. If the bound-state point is too far from $k = 0$, then the exact $\mathcal{E}$ and ANC cannot correspond to exact a_0 and r_0. Ignoring

this fact, i.e. using such a correspondence, the authors of Ref. [53] inevitably obtained wrong values for the scattering length and effective radius. The deeper the bound state is (longer distance from $k = 0$), the greater is the error. This can indeed be seen from our Tables 3.1, 3.2, 3.3, 3.4. The most obviously these errors are visible in the cases of the

$^{A+1}_{\Lambda}Z$	ℓ	a_ℓ (fm$^{2\ell+1}$)	r_ℓ (fm$^{1-2\ell}$)	$P_\ell r_\ell^3$ (fm$^{3-2\ell}$)	$Q_\ell r_\ell^5$ (fm$^{5-2\ell}$)	$L_\ell r_\ell^7$ (fm$^{7-2\ell}$)
$^{7}_{\Lambda}$Li	0	3.2367318 3.23 Ref. [53] 3.233 Ref. [71]	1.5479933 1.55 Ref. [53] 1.528 Ref. [71]	0.0305817	−0.0470130	−0.0541120
	1	−11.8890107	−0.4454250	−0.7367272	0.0373076	0.0199897
	2	−3.5980580	1.4895451	−0.1114456	0.6823769	−0.0412388
$^{7}_{\Lambda}$Be	0	3.3370310 3.32 Ref. [53] 3.333 Ref. [71]	1.5954418 1.58 Ref. [53] 1.584 Ref. [71]	0.0201644	−0.0567890	−0.0537531
	1	−11.0842228	−0.4105994	−0.7524937	0.0422563	0.0203875
	2	−3.4693398	1.5548120	−0.1454417	0.6965474	−0.0440340
$^{8}_{\Lambda}$He	0	2.9083436 2.94 Ref. [53] 2.913 Ref. [71]	1.3781134 1.44 Ref. [53] 1.351 Ref. [71]	0.0669379	−0.0114131	−0.0591511
	1	−18.5495216	−0.5948328	−0.6851782	0.0250095	0.0217978
	2	−4.6199137	1.1229734	0.0544659	0.6355698	−0.0357335

Table 3.1: Effective-range parameters calculated with the potential (5.10) for a set of the ΛA-hypernuclei at three values of the angular momentum $\ell = 0, 1, 2$.

hypernuclei $^{40}_{\Lambda}$Ca, $^{89}_{\Lambda}$Zr, and $^{208}_{\Lambda}$Pb, where several different values for the same scattering lengths and effective radii are obtained in Ref. [53] for each of these ΛA systems. The different effective range parameters resulted from fitting different bound states, $1s$, $2s$, or $3s$.

Its was stated in Ref. [53] that to check the accuracy of the calculated values of the low energy parameters a_ℓ and r_ℓ the continuous states of the Λ-core system for the same potentials will be considered through calculation of the scattering amplitude at low positive energies. Hence, the a_ℓ and r_ℓ were obtained by solving the Schrodinger equation in the continuum. This was done in Ref. [71] and their results are also presented

$^{A+1}_{\Lambda}Z$	ℓ	a_ℓ (fm$^{2\ell+1}$)	r_ℓ (fm$^{1-2\ell}$)	$P_\ell r_\ell^3$ (fm$^{3-2\ell}$)	$Q_\ell r_\ell^5$ (fm$^{5-2\ell}$)	$L_\ell r_\ell^7$ (fm$^{7-2\ell}$)
$^{8}_{\Lambda}$Li	0	2.9776372 3.00 Ref. [53] 2.98 Ref. [71]	1.4179011 1.46 Ref. [53] 1.39 Ref. [71]	0.0612997	-0.0222939	-0.0627927
	1	-17.2944438	-0.5715822	-0.6964672	0.0288635	0.0222372
	2	-4.4914834	1.1627380	0.0330627	0.6451820	-0.0378284
$^{8}_{\Lambda}$Be	0	2.9696895 2.99 Ref. [53] 2.973 Ref. [71]	1.4133919 1.46 Ref. [53] 1.387 Ref. [71]	0.0619893	-0.0210722	-0.0624442
	1	-17.4302322	-0.5742543	-0.6951727	0.0284209	0.0221893
	2	-4.5059661	1.1581426	0.0355338	0.6440746	-0.0375875
$^{9}_{\Lambda}$Li	0	2.6601704 2.75 Ref. [53] 2.66 Ref. [71]	1.2233537 1.36 Ref. [53] 1.16 Ref. [71]	0.0872264	0.0344588	-0.0447297
	1	-30.2816174	-0.6995040	-0.6472675	0.0141482	0.0233884
	2	-5.7360210	0.8719319	0.1680681	0.6032644	-0.0314505

Table 3.2: Continuation of Table 3.1.

in Tables 3.1, 3.2, 3.3, 3.4. The new parameters from Ref. [71] correspond very well with our scattering length values. However, there is a slight deviation with the effective radius values. For the lighter hypernuclei our values are slightly higher, for heavy hypernuclei our values are slightly lower.

3.6 Conclusion

Using the power-series expansion method developed, we calculated the effective-range parameters for a set of hypernuclear systems. These parameters were obtained for the expansion of the effective-range function up to the order of $\sim k^8$ and for three values of the angular momentum, $\ell = 0, 1, 2$. The S-wave scattering lengths and effective radii reported in Ref. [53], agree with our results only for the hypernuclear systems with weak Λ-core binding. We explained and discussed where the errors in Ref. [53] stemmed from.

The set of parameters we report here, could be used for doing quick and simple estimations of various low-energy Λ-nucleus scattering and radiative processes in nuclear

$^{A+1}_{\Lambda}Z$	ℓ	a_ℓ (fm$^{2\ell+1}$)	r_ℓ (fm$^{1-2\ell}$)	$P_\ell r_\ell^3$ (fm$^{3-2\ell}$)	$Q_\ell r_\ell^5$ (fm$^{5-2\ell}$)	$L_\ell r_\ell^7$ (fm$^{7-2\ell}$)
$^{9}_{\Lambda}$Be	0	2.9949610 3.01 Ref. [53] 2.99 Ref. [71]	1.4295702 1.47 Ref. [53] 1.40 Ref. [71]	0.0676614	-0.0301867	-0.0789783
	1	-19.9324375	-0.5944134	-0.7009987	0.0338693	0.0257979
	2	-4.9944344	1.0403790	0.0749026	0.6476081	-0.0419002
$^{9}_{\Lambda}$B	0	2.6954527 2.78 Ref. [53]	1.2459502 1.36 Ref. [53]	0.0867934	0.0274860	-0.0507608
	1	-28.7670176	-0.6887342	-0.6528373	0.0161647	0.0237073
	2	-5.6531369	0.8886130	0.1587855	0.6077361	-0.0325131
$^{10}_{\Lambda}$Be	0	2.5418377 2.67 Ref. [53] 2.54 Ref. [71]	1.1389516 1.32 Ref. [53] 1.10 Ref. [71]	0.0940851	0.0666536	-0.0282953
	1	-45.9686609	-0.7514965	-0.6315538	0.0094229	0.0257815
	2	-6.6953629	0.7268421	0.2292201	0.5904672	-0.0306455
$^{10}_{\Lambda}$B	0	2.5806786 2.70 Ref. [53]	1.1647722 1.34 Ref. [53]	0.0958299	0.0584115	-0.0389325
	1	-42.6407535	-0.7406425	-0.6374433	0.0116790	0.0261801
	2	-6.5910600	0.7424771	0.2202733	0.5950236	-0.0318070

Table 3.3: Continuation of Tables 3.1 and 3.2.

astrophysics.

© University of Pretoria

$^{A+1}_{\Lambda}Z$	ℓ	a_ℓ (fm$^{2\ell+1}$)	r_ℓ (fm$^{1-2\ell}$)	$P_\ell r_\ell^3$ (fm$^{3-2\ell}$)	$Q_\ell r_\ell^5$ (fm$^{5-2\ell}$)	$L_\ell r_\ell^7$ (fm$^{7-2\ell}$)
$^{11}_{\Lambda}$B	0	2.3147558 2.55 Ref. [53]	0.9787536 1.27 Ref. [53]	0.0727682	0.1184816	0.0548001
	1	-118.8978026	-0.8221524	-0.6018303	-0.0020250	0.0266744
	2	-8.0761179	0.5735226	0.3000920	0.5683354	-0.0265776
$^{12}_{\Lambda}$B	0	2.0571138 2.55 Ref. [53]	0.8188044 1.27 Ref. [53]	-0.0038234	0.1109938	0.1697086
	1	330.0349120	-0.8857725	-0.5721756	-0.0146351	0.0265256
	2	-9.6971038	0.4483233	0.3591966	0.5482936	-0.0221406
$^{12}_{\Lambda}$C	0	2.1873420 2.50 Ref. [53] 2.18 Ref. [71]	0.8870320 1.24 Ref. [53] 0.87 Ref. [71]	0.0425647	0.1403582	0.1295937
	1	-1053.1827267	-0.8583324	-0.5885167	-0.0081525	0.0285572
	2	-9.2778856	0.4801945	0.3397185	0.5594619	-0.0253774
$^{13}_{\Lambda}$C	0	1.9422817 2.42 Ref. [53]	0.7595789 1.20 Ref. [53]	-0.0584755	0.0686700	0.2026431
	1	120.1688352	-0.9107199	-0.5629724	-0.0200066	0.0283618
	2	-10.9669098	0.3798920	0.3870105	0.5432989	-0.0214692
$^{15}_{\Lambda}$N	0	1.2437603 2.27 Ref. [53] 1.24 Ref. [71]	1.7907520 1.13 Ref. [53] 1.67 Ref. [71]	1.4652316	4.8109104	15.6207199
	1	40.3050008	-1.0126792	-0.5058925	-0.0471947	0.0223077
	2	-15.3407597	0.2204808	0.4653529	0.5123503	-0.0121394
$^{16}_{\Lambda}$O	0	1.5307321 2.36 Ref. [53] 1.53 Ref. [71]	0.8736759 1.18 Ref. [53] 0.94 Ref. [71]	-0.1261722	-0.2782570	-0.5461116
	1	48.7623418	-0.9717814	-0.5355508	-0.0389966	0.0324707
	2	-15.4742106	0.2274335	0.4494018	0.5311126	-0.0185748

Table 3.4: Continuation of Tables 3.1, 3.2, and 3.3 .

$^{A+1}_{\Lambda}Z$	ℓ	a_ℓ (fm$^{2\ell+1}$)	r_ℓ (fm$^{1-2\ell}$)	$P_\ell r_\ell^3$ (fm$^{3-2\ell}$)	$Q_\ell r_\ell^5$ (fm$^{5-2\ell}$)	$L_\ell r_\ell^7$ (fm$^{7-2\ell}$)
	0	6.5920480 1.90 Ref. [53] 5.85 Ref. [53] 6.59 Ref. [71]	3.7823570 0.95 Ref. [53] 2.88 Ref. [53] 3.97 Ref. [71]	-3.1674773	6.4512113	-13.0581977
$^{40}_{\Lambda}$Ca	1	-3.3401800	4.4214286	-14.5509496	63.5512029	-284.9201300
	2	139.6342309	-0.2476025	0.7496207	0.2861516	0.1431451
	0	4.2587252 1.75 Ref. [53] 2.99 Ref. [53] 4.26 Ref. [71]	2.4738256 0.88 Ref. [53] 1.49 Ref. [53] 2.55 Ref. [71]	-0.6830432	0.3916780	-1.1890961
$^{89}_{\Lambda}$Zr	1	182.0488652	-0.5351246	-1.2474277	1.0674631	-1.1429785
	2	-53.3804347	0.1579840	0.0821054	1.5135949	-1.4317562
	0	7.6146983 1.61 Ref. [53] 2.07 Ref. [53] 4.05 Ref. [53] 7.61 Ref. [71]	4.8695342 0.81 Ref. [53] 1.03 Ref. [53] 2.25 Ref. [53] 5.44 Ref. [71]	-7.9426465	34.5899671	-153.5075775
$^{208}_{\Lambda}$Pb	1	-118.5362295	-0.1132765	-2.8121229	9.5035524	-40.8388895
	2	376.4672323	-0.0830591	0.4487441	0.7200042	-0.0258889

Table 3.5: Continuation of Tables 3.1, 3.2, 3.3, and 3.4

44

Chapter 4

Jost matrices for non-zero spin systems using the hyperspherical approach

In this Chapter we present the background material to solve the many-body Schrodinger equation using the hyperspherical approach for non zero spin particles. In Section4.2 we introduce the hyperspherical variables and the hyperspherical harmonics. Section 4.3 present the infinite system of coupled hyper-radial Schrodinger equation and it's transformation into the first-order differential equations of the Jost matrices. Section 4.3.1 up to 4.3.3 explains how the spectral points can be obtained using the Jost matrices. Section 4.4 present the minimal approximation method that can be use to truncate the infinite system of coupled hyperradial Schrodinger equations for numerical calculations purpose.

4.1 Introduction

The study of the many body problem composed of N particles have led to the construction of the hyperspherical harmonics, which are harmonic polynomials in $3(N-1)$ dimensional space. A configuration of those particles can now be specified by a set of $(N-1)$ Jacobi vectors, $\boldsymbol{r} = \{\boldsymbol{r}_1, \boldsymbol{r}_2, ..., \boldsymbol{r}_{N-1}\}$.

Within the hyperspherical coordinate framework, the configuration of a system made up of $N \geq 3$ particles is represented as a point in a $(3N-3)$-dimensional hyperspace, after the separation of the center-of-mass motion, and its kinematics is equivalent to that of one body of mass M (the total mass of the system) on the $(3N-4)$-dimensional surface[72]. The hypersphere size depends on the hyperradius, in this case denoted $r = |\boldsymbol{r}|$. the other key relevant quantity is the so-called grand angular momentum ,

45

denoted as Λ. The corresponding grand angular momentum correspond to the operator Λ^2 appears in the kinetic energy part $\hat{T}$ of the quantum Hamiltonian operator written in terms of hyperspherical coordinates. The operator $\hat{T}$ is split into two parts, a hyperradial operator $\hat{T}_r$ and a grand angular momentum operator $\hat{T}_\Lambda$, as follows:

$$\hat{T} = -\frac{1}{2M}\left(\frac{\hbar^2}{r^{3N-4}}\frac{\partial}{\partial r}r^{3N-4}\frac{\partial}{\partial r} - \frac{\hat{\Lambda}^2}{r^2}\right) = \hat{T}_\rho + \hat{T}_\Lambda, \tag{4.1}$$

in terms of hyperspherical coordinates. The reduced mass of the system,

$$\mu = \left(\frac{m_1 m_2 m_3 .... m_N}{m_1 + m_2 + m_3 + ... + m_N}\right)^{1/(N-1)} \tag{4.2}$$

is usually used instead of the total mass,

$$M = m_1 + m_2 + m_3 + ... + m_N \tag{4.3}$$

$(m_1, m_2, ..., m_N$ being the masses of individual particles); the presence of μ in Eq.4.1 requires just another mass scaling of r. The potential energy function $V = V(r, \Omega)$ of the hyperspherical coordinates, in general depends on the hyperradius r and the complete set of hyperangles, collectively denoted as Ω. The total Hamiltonian can be written,

$$\hat{H} = \hat{T} + \hat{V} = -\frac{1}{2M}\left(\frac{\hbar^2}{r^{3N-4}}\frac{\partial}{\partial r}r^{3N-4}\frac{\partial}{\partial r} - \frac{\hat{\Lambda}^2}{r^2}\right) + V(r, \Omega), \tag{4.4}$$

which act on the total wave function Ψ^{JM} that must be an eigenfunction of the total angular momentum J and its projections. We look at the simple wave function of a many-body system which does not form any bound clusters. Any bound state of the whole system is characterized by the wave function that vanishes at large distance in all directions.At complex energies the resonance wave function exponentially grow in all directions.Such a simplification of the asymptotic wave function is actually an approximation. The Jost matrices will be defined by considering the asymptotic behaviour of the N-body wave function when the variable r goes to infinity in this Chapter. The Jost functions (i.e the Jost matrices elements) are the coefficients in the superposition of the incoming and outgoing waves(in each channels) in the asymptotic behaviour of the wave function[59].

4.2   HyperSpherical variables and Harmonics expansion

We consider a system of A particles of mass m_i each. The system is described using $N = A - 1$ relative vectors and one center of mass vector. Let's choose the relative vectors to be Jacobi vectors, $\boldsymbol{\rho} = \{\boldsymbol{\rho}_1, \boldsymbol{\rho}_2, ..., \boldsymbol{\rho}_{N-1}\}$, specifying the space configuration of the system. The total kinetic energy operator of the internal motion for such system is,

$$H_0 = -\frac{\hbar^2}{2\mu_1}\Delta_{\boldsymbol{\rho}_1} - \frac{\hbar^2}{2\mu_2}\Delta_{\boldsymbol{\rho}_2} - \frac{\hbar^2}{2\mu_3}\Delta_{\boldsymbol{\rho}_3} - .... - \frac{\hbar^2}{2\mu_{N-1}}\Delta_{\boldsymbol{\rho}_{N-1}} \tag{4.5}$$

where μ_i is the reduced mass associated with the motion along the i-th Jacobi coordinates. The same space configuration can be described by the set $\boldsymbol{r} = \{\boldsymbol{r}_1, \boldsymbol{r}_2, ..., \boldsymbol{r}_{N-1}\}$, of the scaled vectors defined by[59],

$$\boldsymbol{r}_i = \sqrt{\frac{\mu_i}{\mu}}\,\boldsymbol{\rho}_i, \quad i = 1, 2, ..., N-1, \tag{4.6}$$

where the μ is the reduced mass of the whole system. Now, the total kinetic operator can be re-defined as,

$$H_0 = -\frac{\hbar^2}{2\mu}\left(\Delta_{\boldsymbol{r}_1} + \Delta_{\boldsymbol{r}_2} + ... + \Delta_{\boldsymbol{r}_{N-1}}\right) = -\frac{\hbar^2}{2\mu}\sum_{i=1}^{N-1}\Delta_{\boldsymbol{r}_i} = -\frac{\hbar^2}{2\mu}\Delta, \tag{4.7}$$

where Δ is the Laplacian in the space configuration of the dimension $D = 3(N-1)$[59]. The hyperradius can be as follows,

$$r = \sqrt{r_1^2 + r_2^2 + r_3^2 + ... + r_{N-1}^2}. \tag{4.8}$$

The set of $(3N - 1)$ hyperangles consisting of $2N$ ordinary spherical polar angles of the N Jacobi vectors $[(\vartheta_i, \varphi_i), i = 1, ..., N]$ and $(N - 1)$ angles $(\phi_2, ..., \phi_N)$ defining the lengths of N Jacobi vectors are introduced through,

$$r_N = r\cos\phi_N$$
$$r_{N-1} = r\sin\phi_N\cos\phi_{N-1}$$
$$r_{N-2} = r\sin\phi_N\sin\phi_{N-1}\cos\phi_{N-2}$$
$$r_{N-3} = r\sin\phi_N\sin\phi_{N-1}\sin\phi_{N-2}\cos\phi_{N-3}$$
$$\vdots$$
$$r_2 = r\sin\phi_N\sin\phi_{N-1}\cdots\cdots\cdots\sin\phi_3\cos\phi_2$$
$$r_1 = r\sin\phi_N\sin\phi_{N-1}\cdots\cdots\cdots\sin\phi_3\cos\phi_2\cos\phi_1 \tag{4.9}$$

where $\phi_1 = 0$. Each angle ϕ_i lie in the interval $[0, \pi/2]$. The collection of all specified angles above will be denoted by the symbol Ω, hence $\boldsymbol{r} = \{r, \Omega\}$. It can be shown that the Laplace operator,

$$\Delta = \sum_{i=1}^{N-1}\Delta_{\boldsymbol{r}_i} \tag{4.10}$$

in terms of the hypershperical variables , $\boldsymbol{r} = \{r, \Omega\}$, is,

$$\sum_{i=1}^{N-1}\Delta_{\boldsymbol{r}_i} = \left(\frac{\partial^2}{\partial r^2} + \frac{3N-1}{r}\frac{\partial}{\partial r} - \frac{\Lambda^2(\Omega)}{r^2}\right), \tag{4.11}$$

47

where

$$\Lambda^2 = -\sum_{i=1}^{N-1} \left(\prod_{j=i+1}^{N-1} \sin^2 \phi_j \right)^{-1}$$
$$\times \left[\frac{\partial^2}{\partial \phi_i^2} + ((3i-4)\cot\phi_i - 2\tan\phi_i)\frac{\partial}{\partial\phi_i} - \frac{\hat{\ell}_i^2(\vartheta_i, \varphi_i)}{\cos^2\phi_i} \right]. \tag{4.12}$$

The eigenfunctions , $Y_{[\mathcal{L}]}$, of this operator are called the hyperspherical harmonics. They are also solutions of the equation

$$\Lambda^2 Y_{[\mathcal{L}]} = \hbar^2 L(L + 3(N-1) - 2)Y_{[\mathcal{L}]}. \tag{4.13}$$

$\mathcal{L}$ is called the hyperangular momentum quantum number and the symbol $[\mathcal{L}]$ denotes the full set of $3(N-1) - 1$ quantum numbers for a fixed $\mathcal{L}$. These numbers include the following[59],

- The orbital angular momentum ℓ_i and its third component m_i for each Jacobi coordinate, $i = 1, 2, ..., N - 1$;

- The partial grand orbital numbers , L_i, for the subsystems of the particles, and the grand orbital number, L, for the whole system:

$$L_i = L_{i-1} + \ell_i + 2n_i, \quad i = 1, 2, ..., N - 1, \quad n_i = 0, 1, 2, ..., \tag{4.14}$$

where $L_1 = \ell_1$ and $L_{N-1} = L$ is a grand orbital number.

The hyperspherical harmonics constitute an orthonormal basis in the space of the hyperspherical angles, which implies

$$\int Y_{[\mathcal{L}']}^*(\Omega)Y_{[\mathcal{L}]}(\Omega)d\Omega = \delta_{[\mathcal{L}'][\mathcal{L}]}. \tag{4.15}$$

The J and M numbers are the remaining two conserving part of the full set of numbers. Now, it is more suitable to use the basis elements which correspond to the states with definite values of the conserving total angular momentum. The linear combination of the hyperspherical harmonics, denoted $\mathcal{Y}_{\mathcal{L}}^{JM}(\Omega)$, can be constructed such that they describe the states with total angular momentum J (including spin) and its third component M using the Clebsch-Gordan coefficients. The multi-index $[\mathcal{L}]$ constitutes the $[L]$ quantum numbers plus the two conserving numbers.

Since the functions $\mathcal{Y}_{\mathcal{L}}^{JM}$ constitute a basis in the space of hyperangles including the space of the spins, the N-body wave function, $\Psi^{JM}(E, \boldsymbol{r})$, can be expanded over this basis with unknown coefficients, $u_L^J(E, r)$,

$$\Psi^{JM}(E, \boldsymbol{r}) = r^{2-3N/2} \sum_{[L]=[L_{min}]}^{\infty} \mathcal{Y}_{\mathcal{L}}^{JM}(\Omega)u_L^J(E, r). \tag{4.16}$$

48

The summation generally begins from non-zero L_{min}, hence the minimal value of grand orbital number is determined by chosen value of J and by the permutation symmetry of the considered system. When the calculations are done we can find some physical reasons to truncate the summation in Eq.4.16.The factor $r^{2-3N/2}$ in front is included to remove the first derivative term in the radial Schrodinger equation.

4.3   Hyper-radial Schrodinger equation and the Jost matrices

The $N-$body wave function obeys the following Schrodinger equation,

$$\left(-\frac{\hbar^2}{2\mu}\Delta + U - E \right)\Psi^{JM}(E, \boldsymbol{r}) = 0, \tag{4.17}$$

where,

$$U(\boldsymbol{r}) = \sum_{i<j} U_{ij}(\boldsymbol{r}) \tag{4.18}$$

is the sum of all the two-body potentials that describe the interactions between the particles i and j. When one substitutes the expansion (4.16) into the Schrodinger equation(4.17), one arrives at the following infinite system of coupled hyperradial equations,

$$\left[\partial_r^2 + k^2 - \frac{\lambda(\lambda+1)}{r^2} \right] u_{[L]}^J(E, r) = \sum_{[L']} V_{[L][L']}^J(r) u_{[L']}^J(E, r), \tag{4.19}$$

where the parameter $k = \sqrt{2\mu E/\hbar^2}$ can be called hypermomentum, the parameter

$$\lambda = L + \frac{3}{2}(N - 2), \tag{4.20}$$

which is the integer for an even number of particles and half-integer for an odd N, is the generalization of the orbital angular momentum [59]. The potential-matrix elements are obtained by integrating $U(\boldsymbol{r})$ with the hyperharmonics over all the hyperangles:

$$V_{[L][L']}^J(r) = \frac{2\mu}{\hbar^2}\langle Y_L^{JM}|U(\boldsymbol{r})|Y_{L'}^{JM}\rangle. \tag{4.21}$$

The required boundary conditions for the differential equations (4.19) are,

$$u_{[L]}^J(E, r) \to 0 \qquad r \to 0, \tag{4.22}$$

and the solutions must be regular at the origin.

The summations in (4.16) and (4.19) runs up to infinity, hence, the equations are truncated at some $[L_{max}]$, then the number $\mathcal{N}$ of equations in the system (4.19) are finite and each of its solutions becomes a column matrix of a finite length $\mathcal{N}$.

The only considered solutions are regular column-solutions. There are $(\mathcal{N})$ linearly independent regular columns that can be combined in the form of a square $(\mathcal{N} \times \mathcal{N})$ matrix. This square matrix ϕ asymptotically behaves as a superposition of the incoming and outgoing waves,

$$W^{(\text{in/out})} = \begin{pmatrix} h_{\lambda_1}^{(\mp)}(kr) & 0 & \cdots & 0 \\ 0 & h_{\lambda_2}^{(\mp)}(kr) & \cdots & 0 \\ \vdots & \vdots & \ddots & \vdots \\ 0 & 0 & \cdots & h_{\lambda_{\mathcal{N}}}^{(\mp)}(kr) \end{pmatrix} \tag{4.23}$$

i.e,

$$\phi^J(E,r) \xrightarrow[r\to\infty]{} W^{(\text{in})}(E,r)f^{(\text{in})J}(E) + W^{(\text{out})}(E,r)f^{(\text{out})J}(E), \tag{4.24}$$

where now $f^{(\text{in/out})J}(E)$ are the N-body Jost matrices for the states with the total angular momentum J. They are found as the asymptotic values,

$$f^{(\text{in/out})J}(E) = \lim_{r\to\infty} F^{(\text{in/out})J}(E,r), \tag{4.25}$$

of the functions $F^{(\text{in/out})J}(E,r)$, that are in this way,

$$\phi^J(E,r) = W^{(\text{in})}(E,r)F^{(\text{in})J}(E,r) + W^{(\text{out})}(E,r)F^{(\text{out})J}(E,r), \tag{4.26}$$

and obey the same system of differential equations,

$$\partial_r F^{(\text{in})J} = -\frac{1}{2ik}W^{(\text{out})}V^J\left[W^{(\text{in})}F^{(\text{in})J} + W^{(\text{out})}F^{(\text{out})J}\right], \tag{4.27}$$

$$\partial_r F^{(\text{out})J} = \frac{1}{2ik}W^{(\text{in})}V^J\left[W^{(\text{in})}F^{(\text{in})J} + W^{(\text{out})}F^{(\text{out})J}\right], \tag{4.28}$$

with the boundary conditions

$$\lim_{r\to 0} \frac{j_\lambda(kr)F_{[L][L']}^{(\text{in/out})J}(E,r)}{j_{\lambda'}(kr)} = \frac{1}{2}\delta_{[L][L']}. \tag{4.29}$$

The physical wave function can now be constructed using fundamental matrix 4.26,

$$\begin{aligned} u_{[L]}^J(E,r) &= W^{(\text{in})}(E,r)F^{(\text{in})J}(E,r)C + W^{(\text{out})}(E,r)F^{(\text{out})J}(E,r)C \\ &= \phi^J(E,r)C \\ &= \sum_{[L']} \phi_{[L][L']}^J(E,r)C_{[L']} \end{aligned} \tag{4.30}$$

The alternative form of differential equations can be used to calculate the Jost matrices the same way as it mentioned in Chapter.2. We introduce the linear combination of the matrices (4.23)

$$j = \text{diag}\{j_{\lambda_1}(kr), j_{\lambda_2}(kr), ..., j_{\lambda_{\mathcal{N}}}(kr)\} \tag{4.31}$$

$$n = \text{diag}\{n_{\lambda_1}(kr), n_{\lambda_2}(kr), ..., n_{\lambda_{\mathcal{N}}}(kr)\} \tag{4.32}$$

50

as well as the combinations of the unknown matrices,

$$A^J(E, r) = F^{(\mathrm{in})J}(E, r) + F^{(\mathrm{out})J}(E, r), \tag{4.33}$$

$$B^J(E, r) = i[F^{(\mathrm{in})J}(E, r) - F^{(\mathrm{out})J}(E, r)], \tag{4.34}$$

which obey the alternative system of differential equations,

$$\partial_r A^J = -\frac{1}{k} n V^J \left(j A^J - n B^J \right) \tag{4.35}$$

$$\partial_r B^J = -\frac{1}{k} j V^J \left(j A^J - n B^J \right) \tag{4.36}$$

with the boundary conditions,

$$\lim_{r \to 0} \frac{j_\lambda(kr) A^J_{[L][L']}(E, r)}{j_{\lambda'}(kr)} = \frac{1}{2} \delta_{[L][L']}, \quad \lim_{r \to 0} \frac{j_\lambda(kr) B^J_{[L][L']}(E, r)}{j_{\lambda'}(kr)} = 0. \tag{4.37}$$

4.3.1 Bound states and Resonance states

It is already mentioned in Chapter 2 section 2.3 that the spectral points E_n (bound and resonant states) are those at which the physical solution has only outgoing waves in its asymptotic, hence,

$$W^{(\mathrm{in})}(E_n, r) f^{(\mathrm{in})J}(E_n, r) C = 0. \tag{4.38}$$

This condition also implies that,

$$\sum_{[L']} f^J_{[L][L']}(E_n) C_{[L']} = 0, \tag{4.39}$$

and this condition has non-trivial solution if and only if,

$$\det f^{(\mathrm{in})J}(E_n) = 0. \tag{4.40}$$

The roots of Eq.4.40 are the discreet spectral points. The negative real energies , $E_n < 0$, which lie on the physical Riemann sheet are associated with the bound states and corresponds with the positive imaginary momentum,

$$k_n = \sqrt{2\mu E_n / \hbar^2} = i\kappa_n.$$

The resonance states energies are complex with positive real and negative imaginary,

$$E_n = E_r - \frac{i}{2} \Gamma, \quad E_r > 0, \quad \Gamma > 0,$$

located on the unphysical sheet of the Riemann surface.

4.3.2 Virtual and sub-threshold resonances

51

The virtual states, at times referred to as anti-bound states, are the other spectral points located at real negative energies $,E_n < 0$, on the unphysical sheet on the Riemann surface [59]. The corresponds to the pure imaginary negative momenta,

$$k_n = -i\sqrt{(2\mu/\hbar^2)|E_n|}, \tag{4.41}$$

opposite to the bound states on the complex momentum plane. They are only possible for zero angular momentum, $\ell = 0$.

Mathematically, virtual states and resonance states corresponds to a wave function with the same exponential growing asymptotic, hence they no difference between them theoretically. Physically there is a difference between the virtual states and resonance states. A virtual state happens at a negative collision energy, $E_r < 0$, with a zero width, Γ, compare to resonance states. The resonances spectral points in most cases bends towards the imaginary axis and continues toward infinity with $E_r \to -\infty$ and $\Gamma \to \infty$. We call this type of points with the negative E_r the sub-threshold resonances. This spectral points were briefly discussed on Chapter2 Section2.3.4 and shown on Figure2.4.

4.3.3 Complex rotation

It is known from Chapter2 that starting with a two-body radial Schrodinger equation in its ordinary form, the Jost function for a long-range potential can be defined for only $\mathrm{Im}\{p\} \geq 0$[44]. Without repeating the reasons given in Section2.3.1, the limits of equations (4.25) can be obtained. We can state that if the integration of the differential equations(4.27 and 4.28) is done along the real r-axis and the real energy axis, the bound states energies are obtained without a problem.

At complex energies, these limits(4.25) along the real r-axis do no exists simultaneously.The complex rotation of the coordinate r is employed to circumvent the difficulty caused by this Riccatti-Hankel functions,

$$h_\lambda^\pm(kr) \xrightarrow[|kr|\to\infty]{} \mp\exp[\pm i(kr - \lambda\pi/2)]. \tag{4.42}$$

In equations (4.27 and 4.28) we replace the real hyperradius with a complex one,$i.e,$

$$r' = r\exp^{i\theta}, \qquad r \geq 0, \qquad 0 \leq \theta \leq \frac{\pi}{2},$$

hence we have the following system of first-order differential equations matrix elements,

$$\partial_r F^{\mathrm{in}}_{[L][L']}(E, r') = -\frac{h_\lambda^+(kr')}{2ik}\sum_{[L'']} V^J_{[L][L'']}(kr')$$
$$\times \left[h^{(-)}_{\lambda''}(kr')F^{\mathrm{in}}_{[L''][L']}(E, r') + h^{(+)}_{\lambda''}(kr')F^{\mathrm{out}}_{[L''][L']}(E, r') \right],$$
$$\partial_r F^{\mathrm{out}}_{[L][L']}(E, r') = +\frac{h_\lambda^-(kr')}{2ik}\sum_{[L'']} V^J_{[L][L'']}(kr')$$
$$\times \left[h^{(-)}_{\lambda''}(kr')F^{\mathrm{in}}_{[L''][L']}(E, r') + h^{(+)}_{\lambda''}(kr')F^{\mathrm{out}}_{[L''][L']}(E, r') \right]. \tag{4.43}$$

52

Thus, we are able to access the resonance states energies on the fourth quadrant of the complex momentum p-plane.

4.4 The minimal Approximation

The system 4.19 consists of an infinite number of equations and in order to use it in numerical calculations, we have to truncate it somewhere. In order to achieve this, the minimal approximation method can be used. This corresponds to the minimal $(n = 0)$ value of the grand orbital number and is called the hypercentral approximation, $[L] = [L_{min}]$.

The total potential can be expanded in terms of the Hyperspherical harmonics basis,

$$V(\boldsymbol{r}) = \sum_{[L]=[L_{min}]} U_{[L]}(\boldsymbol{r})\mathcal{Y}_{[\mathcal{L}]}(\Omega). \tag{4.44}$$

In general, realistic or phenomelogical nuclear potentials are not hypercentral. An important property of hypercentral potentials is that in the ground state the grand orbital L takes its minimal value. Hence,the minimal value of L is obtained when the particles fill the lowest shells.

Chapter 5

The Lambda-nucleus systems

This chapter presents the first part of the results of Ref.[54], which is the first of the two articles that this thesis is based on. The two-body multichannel Jost matrices method described in chapter 3 is used in this study.

The single channel Jost matrices are used to calculate the spectral points (bound states and resonance states) for various ΛA-hypernucleus systems. The calculated bound states were also used to calculate the S-matrix residues as well as their corresponding asymptotic normalization and nuclear vertex values.

5.1 The single channel Jost method

The single channel radial part, $u_\ell(E, r)$, of the ΛA-wave function, $\psi_{\ell m}(\vec{r}) = u_\ell(E, r) Y_{\ell m}(\hat{\vec{r}})/r$, obeys the Schrödinger equation,

$$\left[\partial_r^2 + k^2 - \frac{\ell(\ell+1)}{r^2} - U(r)\right] u_\ell(E, r) = 0 , \tag{5.1}$$

where $k = \sqrt{2\mu E}$, $U(r) = 2\mu V(r)$, and μ is the Λ-nucleus reduced mass. This second-order equation is equivalent to the system of two first-order equations (see, for example, Refs.[42, 43]),

$$\partial_r F_\ell^{(\text{in})} = -\frac{h_\ell^{(+)}(kr)}{2ik} U \left[h_\ell^{(-)}(kr) F_\ell^{(\text{in})} + h_\ell^{(+)}(kr) F_\ell^{(\text{out})}\right] , \tag{5.2}$$

$$\partial_r F_\ell^{(\text{out})} = \frac{h_\ell^{(-)}(kr)}{2ik} U \left[h_\ell^{(-)}(kr) F_\ell^{(\text{in})} + h_\ell^{(+)}(kr) F_\ell^{(\text{out})}\right] , \tag{5.3}$$

where $h_\ell^{(\pm)}(kr)$ are the Riccati-Hankel functions, and the solution of Eq. (5.1) is obtained

from $F_\ell^{(\text{in/out})}(E, r)$ as follows:

$$u_\ell(E, r) = h_\ell^{(-)}(kr) F_\ell^{(\text{in})}(E, r) + h_\ell^{(+)}(kr) F_\ell^{(\text{out})}(E, r) \ . \tag{5.4}$$

Simple boundary conditions,

$$F_\ell^{(\text{in})}(E, 0) = F_\ell^{(\text{out})}(E, 0) = \frac{1}{2} \ , \tag{5.5}$$

guarantee that the wave function, $u_\ell(E, r) \xrightarrow[r \to 0]{} j_\ell(kr)$, is regular at $r = 0$. Here $j_\ell = [h_\ell^{(-)} + h_\ell^{(+)}]/2$ is the Riccati-Bessel function. Asymptotically, the functions $F_\ell^{(\text{in/out})}(E, r)$ converge to the Jost functions $f_\ell^{(\text{in/out})}(E)$,

$$F_\ell^{(\text{in/out})}(E, r) \xrightarrow[r \to \infty]{} f_\ell^{(\text{in/out})}(E) \ , \tag{5.6}$$

which gives

$$u_\ell(E, r) \xrightarrow[r \to \infty]{} h_\ell^{(-)}(kr) f_\ell^{(\text{in})}(E) + h_\ell^{(+)}(kr) f_\ell^{(\text{out})}(E) \ . \tag{5.7}$$

The discrete states and the corresponding energies $\mathcal{E}_d$ (spectral points) are found under the condition that only the outgoing wave remains in the asymptotic form (5.7),

$$f_\ell^{(\text{in})}(\mathcal{E}_d) = 0 \ . \tag{5.8}$$

For any given energy E the Jost functions $f_\ell^{(\text{in/out})}(E)$ are obtained by numerically solving Eqs. (5.2,5.3), starting at $r = 0$ with the values (5.5), up to a distance where the potential vanishes (which makes the right hand sides of these equations zero). In this way the spectral points $\mathcal{E}_d$ can be easily located

The partial wave S-matrix is the ratio

$$s_\ell(z) = f_\ell^{(\text{out})}(z) \left[f_\ell^{(\text{in})}(z) \right]^{-1} \tag{5.9}$$

and therefore is singular at each $\mathcal{E}_d$.

The Jost functions $f_\ell^{(\text{in/out})}(E)$ depend on the energy via the momentum k. Since in the momentum-energy relation, $k = \pm\sqrt{2\mu E}$, there are two possibilities for choosing the sign, the Jost functions are double valued and thus are defined on a two layer Riemann surface. This surface has a branch point at $E = 0$ and a cut along the positive real axis where the two sheets are connected (as is illustrated in Fig. 2.2).

5.2 Lambda-nucleus potential model

As we said before, there are too few experimental data for constructing a sophisticated ΛN or ΛA potential. For the purposes of doing some estimates that would be useful in nuclear astrophysics, it is sufficient to take into account the most general features of the Λ-nucleus interaction. Apparently, the potential should be attractive (because the hypernuclei exist) and proportional to the density and size of the nucleus. The strength of such a potential can be adjusted to reproduce experimentally known (see Refs. [73] and [53]) binding energies of the ground states of the hypernuclei. All possible spin effects in the interaction are smaller than the uncertainties in the shape and in the parameters of the central part of the potential. We therefore ignore such effects and, following Ref. [53], use the interaction of the Woods-Saxon type:

$$V(r) = \frac{V_0}{1 + \exp\left(\dfrac{r - R}{d}\right)} , \qquad (5.10)$$

where $R = r_0 A^{1/3}$ with $r_0 = 1.1\,\text{fm}$, and $d = 0.6\,\text{fm}$. The values of the strength parameter V_0 obtained in Ref. [53], which fit the ground-state ΛA energies for a set of core-nuclei ($6 \leqslant A \leqslant 207$), are given in Table 5.1. In our calculations, we used the same parameters.

5.3   Results and discussions

In this study, several ΛA-hypernucleus systems presented on Table 5.2 were studied in order to obtain their respective spectral points.

The first-order system of coupled-differential equation for Jost functions with the potential (5.10) were solved numerically from $r_{\min} = 10^{-5}\,\text{fm}$ to $r_{\max} = 30\,\text{fm}$. The Jost functions solutions for a given value E of energy were obtained, whereby they converges to a constant values at $r_{\max}$. For each of the hypernuclei listed in Table 5.1, varying E and using the Newton's method (see, for example, Ref. [74]), we located the spectral points $\mathcal{E}$ (bound states and resonance states), where $f_\ell^{(\text{in})}(\mathcal{E}) = 0$. These spectral energies(bound states) are given in the second columns of Tables 5.2,5.3,5.4. The resonance states energies were also calculated and presented on the third and fourth columns of Table 5.5,5.6.

For the given hypernuclei, we found all possible bound states within the two-body (Λ-core) model with the potential (5.10). In order to check if no bound state is missing, we used the Chew-Frautschi plots [75] (spectral points on the $E - \ell$ plane). An example of such a plot for the heaviest hypernucleus in our list, $^{208}_{\Lambda}\text{Pb}$, is shown in Fig. 5.1. Each curve begins at an S-wave state. Actually, each Chew-Frautschi curve corresponds to a separate Regge trajectory on the complex ℓ-plane. The thick dots shown in Fig. 5.1, are the bound states. Each curve continues into the domain of positive energies, where the

56

$^{A+1}_{\Lambda}Z$	V_0 (MeV)	$|\mathcal{E}|$ (MeV)
$^{7}_{\Lambda}$Li	29.65	5.58
$^{7}_{\Lambda}$Be	28.73	5.16
$^{8}_{\Lambda}$He	30.66	7.16
$^{8}_{\Lambda}$Li	29.96	6.80
$^{8}_{\Lambda}$Be	30.04	6.84
$^{9}_{\Lambda}$Li	31.31	8.50
$^{9}_{\Lambda}$Be	28.01	6.71
$^{9}_{\Lambda}$B	30.95	8.30
$^{10}_{\Lambda}$Be	30.81	9.11
$^{10}_{\Lambda}$B	30.44	8.90
$^{11}_{\Lambda}$B	31.36	10.24
$^{12}_{\Lambda}$B	31.97	11.37
$^{12}_{\Lambda}$C	31.00	10.75
$^{13}_{\Lambda}$C	31.42	11.69
$^{15}_{\Lambda}$N	32.45	13.59
$^{16}_{\Lambda}$O	30.15	12.51
$^{40}_{\Lambda}$Ca	31.40	20.01
$^{89}_{\Lambda}$Zr	30.07	22.99
$^{208}_{\Lambda}$Pb	31.20	27.00

Table 5.1: Strength parameters V_0 of the potential(5.10) and the corresponding energies of the ground states for a set of the ΛA-hypernuclei. In the nuclear notation, the superscript is the total number of baryons (including the Λ-particle).

plot includes the resonance spectral points. As is seen, the pattern of the dots includes any additional bound states for the hypernucleus $^{208}_{\Lambda}$Pb.

It should be noted, however, that the two-body model is a simplification. In actual physical systems the core nucleus can be in any of its excited states. If these excitations are taken into account, then each of the dots shown in Fig. 5.1, is split into several states (above this dot).This means that there are more parallel Chew-Frautschi lines, than are plotted. Such a description, however, is outside of our model.

After finding the bound states, we calculated the residue of the S-matrix at each of them and the corresponding NVC's and ANC's. The residue was obtained as the ratio

$$\operatorname{Res}\left[s_{\ell}(E), \mathcal{E}\right] = \frac{f_{\ell}^{(\text{out})}(\mathcal{E})}{\left[\dfrac{d}{dE}f_{\ell}^{(\text{in})}(E)\right]_{E=\mathcal{E}}} \approx \frac{2\epsilon f_{\ell}^{(\text{out})}(\mathcal{E})}{f_{\ell}^{(\text{in})}(\mathcal{E}+\epsilon) - f_{\ell}^{(\text{in})}(\mathcal{E}-\epsilon)} , \qquad (5.11)$$

with $\epsilon = 10^{-9}$ MeV. Then the squares of the NVC's and ANC's were found using the

57
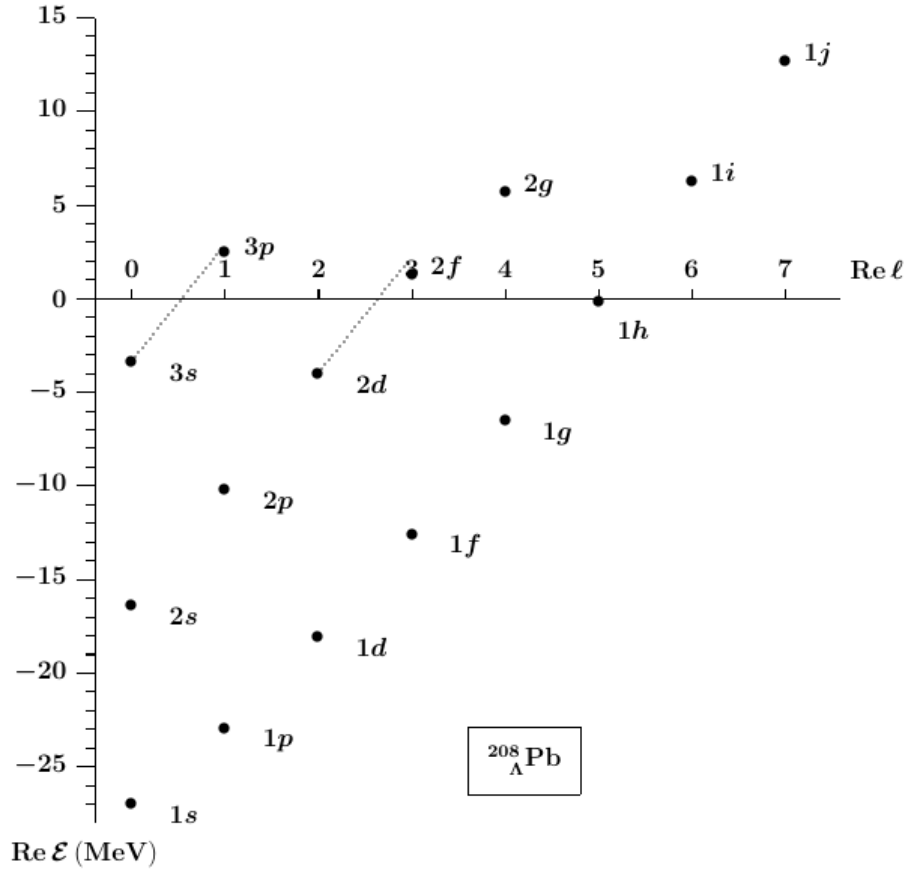
Figure 5.1: Chew-Frautschi plot of the two-body bound states generated by the potential (5.10) for the hypernucleus $^{208}_{\Lambda}$Pb.

relations (5.12,5.13).

$$G_{ab\to d}G_{d\to ab} = \frac{i\pi}{\mu\kappa_d}\mathrm{Res}\left[s_\ell(z),\mathcal{E}_d\right] \tag{5.12}$$

and,

$$\mathrm{Res}\left[s_\ell(E),\mathcal{E}_d\right] = (-1)^\ell\frac{\kappa_d}{\mu}\mathcal{A}_\ell^2 \ . \tag{5.13}$$

Thus obtained results are given in Tables 5.2,5.3,5.4. For the ANC's, we give the absolute values. Actually, the $\mathcal{A}_\ell$ can be multiplied by any complex number z, such that $|z| = 1$, without changing the wave function normalization. It is a matter of convention that ANC is real and for the ground state the wave function (having no nodes) approaches zero at large distances from above ($\mathcal{A}_\ell > 0$). Then for the first excited state (with one node) it approaches zero from below ($\mathcal{A}_\ell < 0$), etc.

For the sake of comparison, Tables 5.2,5.3,5.4 also include (where available) the NVC's

58

and ANC's obtained in Ref. [53]. It is seen that the differences are minor.

5.4   Conclusions

In this work, we calculated the S-matrix residues as well as the corresponding Nuclear-Vertex and Asymptotic-Normalization constants (NVC's and ANC's) for the bound states of a wide range of hypernuclei within a two-body (Λ plus nuclear core) model. This was done via a direct numerical evaluation of the Jost functions.The ANC's and the so called vertex constants within our method are found via calculating the residues of the S-matrix at the bound-state poles. It turned out that for the ΛA-systems with relatively large binding energies, our scattering lengths and the effective radii are significantly different from those reported in Ref. [53]. Our results reasonably well agree with the NVC's and ANC's obtained in Ref. [53] within a completely different approach.

59

$^{A+1}_{\Lambda}Z$ (level)	$|\mathcal{E}|$ (MeV)	$\mathrm{Res}\,[s_\ell, \mathcal{E}]$ (fm^{-1})	G^2 (fm)	$|\mathcal{A}_\ell|$ (fm$^{-1/2}$)
$^{7}_{\Lambda}\mathrm{Li}\,(1s)$	5.57509	0.56811	0.73338 0.73 Ref. [53]	2.2780 2.28 Ref. [53]
$^{7}_{\Lambda}\mathrm{Be}\,(1s)$	5.15684	0.49406	0.66303 0.66 Ref. [53]	2.1663 2.16 Ref. [53]
$^{8}_{\Lambda}\mathrm{He}\,(1s)$	7.15486	0.97455	1.0709 1.07 Ref. [53]	2.8203 2.82 Ref. [53]
$^{8}_{\Lambda}\mathrm{Li}\,(1s)$	6.79456	0.88114	0.99394 0.99 Ref. [53]	2.7164 2.72 Ref. [53]
$^{8}_{\Lambda}\mathrm{Be}\,(1s)$	6.83532	0.89140	1.0025 1.00 Ref. [53]	2.7281 2.73 Ref. [53]
$^{9}_{\Lambda}\mathrm{Li}\,(1s)$	8.49712	1.4812	1.4533 1.45 Ref. [53]	3.3459 3.35 Ref. [53]
$^{9}_{\Lambda}\mathrm{Be}\,(1s)$	6.70592	0.91699	1.0132 1.01 Ref. [53]	2.7929 2.80 Ref. [53]
$^{9}_{\Lambda}\mathrm{B}\,(1s)$	8.29738	1.4097	1.3996 1.40 Ref. [53]	3.2836 3.29 Ref. [53]
$^{10}_{\Lambda}\mathrm{Be}\,(1s)$	9.10317	1.8388	1.7058 1.71 Ref. [53]	3.6774 3.68 Ref. [53]
$^{10}_{\Lambda}\mathrm{B}\,(1s)$	8.88801	1.7462	1.6394 1.64 Ref. [53]	3.6052 3.61 Ref. [53]
$^{11}_{\Lambda}\mathrm{B}\,(1s)$	10.23707	2.5560	2.1969 2.20 Ref. [53]	4.2228 4.23 Ref. [53]

Table 5.2: The S-matrix residues, nuclear vertex-constants, and asymptotic normalization constants, calculated with the potential (5.10) for a set of the lowest levels of ΛA-hypernuclei. In the calculations, the energies and masses are measured in the units of fm^{-1}. In order to obtain the residues in MeV, the values given in the third column should be multiplied by the factor $\hbar c = 197.327054\,\mathrm{MeV}\cdot\mathrm{fm}$.

$^{A+1}_{\Lambda}Z$ (level)	$|\mathcal{E}|$ (MeV)	$\mathrm{Res}\,[s_\ell, \mathcal{E}]\,(\mathrm{fm}^{-1})$	G^2 (fm)	$|\mathcal{A}_\ell|\,(\mathrm{fm}^{-1/2})$
$^{12}_{\Lambda}\mathrm{B}\,(1s)$	11.36230	3.4912	2.8069 2.81 Ref. [53]	4.8198 4.83 Ref. [53]
$^{12}_{\Lambda}\mathrm{B}\,(1p)$	0.16495	-0.00049	0.00327	0.16461
$^{12}_{\Lambda}\mathrm{C}\,(1s)$	10.74421	3.0575	2.5279 2.53 Ref. [53]	4.5741 4.58 Ref. [53]
$^{13}_{\Lambda}\mathrm{C}\,(1s)$	11.68269	3.9924	3.1272 3.13 Ref. [53]	5.1289 5.14 Ref. [53]
$^{13}_{\Lambda}\mathrm{C}\,(1p)$	0.52243	-0.00366	0.01356	0.33777
$^{15}_{\Lambda}\mathrm{N}\,(1s)$	13.58176	6.6788	4.7577 4.77 Ref. [53]	6.4095 6.42 Ref. [53]
$^{15}_{\Lambda}\mathrm{N}\,(1p)$	1.99497	-0.05144	0.09561	0.90861
$^{16}_{\Lambda}\mathrm{O}\,(1s)$	12.50272	5.7165	4.2109 4.22 Ref. [53]	6.0618 6.07 Ref. [53]
$^{16}_{\Lambda}\mathrm{O}\,(1p)$	1.61479	-0.03438	0.07047	0.78418
$^{40}_{\Lambda}\mathrm{Ca}\,(1s)$	20.00100	86.354	46.900 47.00 Ref. [53]	21.194 21.23 Ref. [53]
$^{40}_{\Lambda}\mathrm{Ca}\,(1p)$	10.84196	-10.719	7.9072 7.93 Ref. [53]	8.7024 8.72 Ref. [53]
$^{40}_{\Lambda}\mathrm{Ca}\,(2s)$	1.63748	0.25670	0.48725 0.48 Ref. [53]	2.1603 2.16 Ref. [53]
$^{40}_{\Lambda}\mathrm{Ca}\,(1d)$	1.57505	0.00822	0.01591	0.39036

Table 5.3: Continuation of Table 5.2.

$^{A+1}_{\Lambda}Z$ (level)	$|\mathcal{E}|$ (MeV)	Res $[s_\ell, \mathcal{E}]$ (fm^{-1})	G^2 (fm)	$|\mathcal{A}_\ell|$ (fm$^{-1/2}$)
$^{89}_{\Lambda}$Zr $(1s)$	22.99126	990.29	489.21 490.47 Ref. [53]	69.606 69.73 Ref. [53]
$^{89}_{\Lambda}$Zr $(1p)$	16.61716	-279.00	162.12 162.36 Ref. [53]	40.070 40.12 Ref. [53]
$^{89}_{\Lambda}$Zr $(1d)$	9.40883	13.107	10.122	10.012
$^{89}_{\Lambda}$Zr $(2s)$	7.86607	36.870	31.139 31.27 Ref. [53]	17.561 17.61 Ref. [53]
$^{89}_{\Lambda}$Zr $(1f)$	1.80713	-0.00312	0.00550	0.23345
$^{89}_{\Lambda}$Zr $(2p)$	1.00149	-0.05696	0.13482	1.15550
$^{208}_{\Lambda}$Pb $(1s)$	27.00085	53546.56	24126.79 24213.63 Ref. [53]	492.63 493.74 Ref. [53]
$^{208}_{\Lambda}$Pb $(1p)$	22.93632	-27435.30	13412.34 13465.11 Ref. [53]	367.30 368.19 Ref. [53]
$^{208}_{\Lambda}$Pb $(1d)$	18.08386	5058.43	2785.01 2797.61 Ref. [53]	167.37 167.83 Ref. [53]
$^{208}_{\Lambda}$Pb $(2s)$	16.42311	8903.42	5143.82 5165.33 Ref. [53]	227.47 228.04 Ref. [53]
$^{208}_{\Lambda}$Pb $(1f)$	12.578	-262.95	173.59	41.786
$^{208}_{\Lambda}$Pb $(2p)$	10.24455	-631.96	462.27 463.64 Ref. [53]	68.190 68.32 Ref. [53]
$^{208}_{\Lambda}$Pb $(1g)$	6.5487	1.3719	1.2551	3.5532
$^{208}_{\Lambda}$Pb $(2d)$	4.0609	4.0345	4.6874	6.8666
$^{208}_{\Lambda}$Pb $(3s)$	3.40020	10.965	13.922 13.17 Ref. [53]	11.834 11.52 Ref. [53]
$^{208}_{\Lambda}$Pb $(1h)$	0.16549	-9.2635×10^{-11}	5.3314×10^{-10}	7.3231×10^{-5}

Table 5.4: Continuation of Tables 5.2 and 5.3.

$^{A+1}_{\Lambda}Z$(level)	ℓ	E_r(MeV)	Γ(MeV)
$^{7}_{\Lambda}$Li	1	1.9178231921814795	5.1163908538293432
	2	7.0606069276069174	28.999157801053936
	3	11.638163884102228	65.384919028938256
$^{7}_{\Lambda}$Be	1	1.9424168036962184	5.5310221529539474
	2	6.8876676481683310	29.692084985143108
	3	11.235793655528200	66.278091007635979
$^{8}_{\Lambda}$He	1	1.5603396764374713	3.0006274799314485
	2	7.4052821915060356	23.769983469363900
	3	13.127339204934087	56.556649680832756
$^{8}_{\Lambda}$Li	1	1.6146122599667934	3.2781366305488095
	2	7.3254019119191964	24.300966531998231
	3	12.891474174341820	57.269866969899567
$^{8}_{\Lambda}$Be	1	1.6087350045020326	3.2462549389647255
	2	7.3349820201906200	24.240952881812046
	3	12.919007493881827	57.189906299890843
$^{9}_{\Lambda}$Li	1	1.1296122447854291	1.5881894726830055
	2	7.4083040016184789	19.735357762597690
	3	13.890120072541530	49.549412020791138
$^{9}_{\Lambda}$Be	1	1.4643014823738187	2.7673557115979812
	2	7.1464617631276690	22.187071910849159
	3	12.934644893267391	52.879919475183407
$^{9}_{\Lambda}$B	1	1.1707491071361265	1.7037782298665096
	2	7.3868199993355530	19.992415559953702
	3	13.795908610626590	49.900280123098064
$^{10}_{\Lambda}$Be	1	0.81332083913457320	0.90332727979106042
	2	7.2125657126831291	17.174399016510481
	3	14.040393191605983	44.727926666720293

Table 5.5: Spectral points calculated with the potential (5.10) for a set of the ΛA-hypernuclei at the angular momentum of $\ell = 0, 1, 2, 3....$

$^{A+1}_{\Lambda}Z$(level)	ℓ	E_r(MeV)	Γ(MeV)
$^{10}_{\Lambda}$B	1	0.86380616880177519	1.0051058555609897
	2	7.2022340122567501	17.435417523377023
	3	13.959240813965808	45.090955260065954
$^{11}_{\Lambda}$B	1	0.35103303774348327	0.23181785818254996
	2	6.9662726857148893	14.365125723837570
	3	14.215548364046471	39.680833911850392
$^{12}_{\Lambda}$B	1	-0.16494636120783870	0.000000000
	2	6.6376036013406612	11.931411929450753
	3	14.218160705758168	35.234035112327142
$^{12}_{\Lambda}$C	1	4.2182463906099997E-002	9.1926667163653875E-003
	2	6.6804876801390538	12.558492403629060
	3	14.099259355095148	36.149877868537963
$^{13}_{\Lambda}$C	1	-0.52242817461742730	0.0000000000000000
	2	6.3372032114166528	10.551024022151582
	3	13.992086052501529	32.391861643802812
$^{15}_{\Lambda}$N	1	-1.9949704200772127	0.0000000000000000
	2	5.5305200837084731	7.1970616263067066
	3	13.532085549801309	25.924404137252708
$^{16}_{\Lambda}$O	1	-1.6147854310054131	0.0000000000000000
	2	5.4668210517256810	7.3733350515213125
	3	13.194559959641195	25.654169517172718
$^{40}_{\Lambda}$Ca	3	6.0935063784045589	3.2578318586341943
	4	14.334652426741114	12.947291050277592
$^{89}_{\Lambda}$Zr	4	5.2892158537898641	0.99592825926590989
	5	12.563777690050783	5.5544678023091389
$^{208}_{\Lambda}$Pb	6	6.2170118138641133	0.28201932368002602
	7	12.667829307282350	2.0339774898641125

Table 5.6: Continuation of Tables 5.5

64

Chapter 6

The multi-Λ Systems

6.1 Introduction

An understanding of how the hyperons interact with nucleons and with each other is crucial for developing adequate models in nuclear astrophysics. In particular, the equation of state and the models describing the neutron stars strongly depend on the presence of the hyperon component in these celectial bodies (see, for example, Ref. [76]). The present work is focused on one particular aspect of the the $\Lambda\Lambda$-interaction. A simple question can be asked: if many Λ-particles are placed close to each other, is it possible for them to form a bound state? Of course, we cannot answer such a question in full. We can only do some estimate calculations for a limited number of Λ-particles in the system.

It is well known (see Ref. [77]) that for a two-body system the S-matrix pole, corresponding to a bound state, continuously moves on the Riemann surface of the energy, when the strength of the interaction is changing. When its strength is decreasing, the pole moves along the negative real axis, passes through zero energy (the threshold), and becomes either a virtual state (if the angular momentum is zero), or a resonance. It is logical to expect that the poles of a multi-particle S-matrix behave in a similar way. This becomes obvious, if we desribe the multi-particle system within the hyperspherical theory, because the set of the hyperradial equations is formally the same as for the coupled partial waves in a two-body problem.

In order to get an idea how far a multi-Λ system is from being bound, the $\Lambda\Lambda$-potential is multiplied by a numerical factor $g > 1$, and gradually increasing it, trace the movement of the corresponding resonance pole until it reaches the threshold energy. Thus found critical value of g (with which a bound state just appears) characterises the "readiness" of

the system to be bound. When such a multi-Λ system is placed in an external attractive field (inside a nucleus or a neutron star, for example), it can form a cluster there, if that external attraction is strong enough to effectively provide the same increase of the potential as with the critical g. In other words, the critical value of the factor g gives us an indication to the ability of a particular multi-Λ system to form clusters inside some bigger systems.

6.2 Theoretical framework

The multi-hyperon systems $\Lambda\Lambda$, $\Lambda\Lambda\Lambda$, and $\Lambda\Lambda\Lambda\Lambda$ will be considered in this study. The main feature of them is that none of their subsystems can form a bound state. Sometimes the systems with such properties are called "democratic" [78, 79, 80, 81]. This feature simplifies the asymptotic behaviour of the corresponding wave functions that describe possible resonances. Since there is only one decay-channel, such a wave function has the same behaviour, when any of the Jacobi coordinates tends to infinity, namely, it behaves as the exponential, $\sim \exp(ik\rho)$, where ρ is the hyperradius and k is the momentum associated with the total energy. In other words, for a "democratic" system the asymptotic behaviour of a resonance wave function has the same simplicity as for a bound state. The only difference is that k is complex.

The simplicity of the long-range asymptotics makes it possible to introduce a many-body analog of the Jost function. Therefore, the spectral points (either bound or resonant states) can be located in a unified way, as zeros of the many-body Jost function (on different sheets of the Riemann surface, of course).

The method we use here, was suggested and described in detail in Chapter 4 and Ref.[44], where the multi-neutron systems nn, nnn, and $nnnn$ were considered in Ref.[44]. Since neutron and Λ-particle both are neutral and both have the same spin $1/2$, all the formulae from Ref. [44] can be used here without modifications.

In essence, the method is based on the expansion of the N-body wave function (for a given total angular momentum J) over the hyper-spherical harmonics, $Y_{[L]}^J(\Omega)$,

$$\Psi^J(\rho, \Omega) = \rho^{2-3N/2} \sum_{L=L_{\min}}^{\infty} Y_{[L]}^J(\Omega) u_{[L]}^J(\rho) , \qquad (6.1)$$

where we retain only the first term with minimal value of the grand orbital quantum number, $L = L_{\min}$. With such "minimal" approximation, the hyperradial part of this wave function obeys the Schrödinger equation

$$\left[\partial_\rho^2 + k^2 - \lambda(\lambda+1)/\rho^2 \right] u_{[L]}^J(\rho) = W_{[L][L]}^J(\rho) u_{[L]}^J(\rho) , \qquad (6.2)$$

where $k^2 = 2mE$ (m is the Λ-particle mass), λ is an analog of the orbital angular

momentum, (which assumes half-integer values when N is uneven),

$$\lambda \equiv L + \frac{3}{2}(N-2) \ , \tag{6.3}$$

the matrix W is given by

$$W^J_{[L][L']}(\rho) \equiv 2m\langle Y^J_{[L]}|\sum_{i<j}V_{ij}|Y^J_{[L']}\rangle \ , \tag{6.4}$$

where the integration runs over all the hyperangles and V_{ij} are the two-body $\Lambda\Lambda$-potentials.

Formally, Eq. (6.2) looks exactly like the corresponding two-body radial equation. We therefore can introduce the Jost functions, $f^{J(\text{in/out})}_{[L]}(E)$, as the amplitudes of the incoming and outgoing hyperspherical waves in the asymptotic behaviour of the regular solution of Eq. (6.2),

$$u^J_{[L]}(\rho) \xrightarrow[\rho\to\infty]{} h^{(-)}_\lambda(k\rho)f^{J(\text{in})}_{[L]}(E) + h^{(+)}_\lambda(k\rho)f^{J(\text{out})}_{[L]}(E) \ , \tag{6.5}$$

where $h^{(\pm)}_\lambda$ are the Riccati-hankel functions. By definition, the spectral points are those (complex) values of the energy E, where the asymptotics (6.5) includes only the outgoing waves. These points can be located by finding the roots of the equation

$$f^{J(\text{in})}_{[L]}(E) = 0 \ . \tag{6.6}$$

When searching these spectral points, an appropriate sign should be chosen in front of the square root $k = \pm\sqrt{2mE}$ in order to look for them at the physical ($\text{Im } k > 0$) or non-physical ($\text{Im } k < 0$) sheet of the Riemann surface.

In order to calculate $f^{J(\text{in/out})}_{[L]}(E)$ for any given E, we transform Eq. (6.2) into an equivalent system of first order differential equations, whose solutions asymptotically tend to the Jost functions (the derivation can be found in Refs. [42, 43, 44]). To this end, we look for the hyperradial wave function in the form

$$u^J_{[L]}(\rho) = h^{(-)}_\lambda(k\rho)F^{J(\text{in})}_{[L]}(E,\rho) + h^{(+)}_\lambda(k\rho)F^{J(\text{out})}_{[L]}(E,\rho) \ , \tag{6.7}$$

and for the unknown functions $F^{J(\text{in/out})}_{[L]}(E,\rho)$ obtain the system of equations

$$\partial_\rho F^{J(\text{in})}_{[L]} = -\frac{h^{(+)}_\lambda(k\rho)}{2ik}W^J_{[L][L]}\left[h^{(-)}_\lambda(k\rho)F^{J(\text{in})}_{[L]} + h^{(+)}_\lambda(k\rho)F^{J(\text{out})}_{[L]}\right] \ , \tag{6.8}$$

$$\partial_\rho F^{J(\text{out})}_{[L]} = \frac{h^{(-)}_\lambda(k\rho)}{2ik}W^J_{[L][L]}\left[h^{(-)}_\lambda(k\rho)F^{J(\text{in})}_{[L]} + h^{(+)}_\lambda(k\rho)F^{J(\text{out})}_{[L]}\right] \ , \tag{6.9}$$

67

with the following simple boundary conditions:

$$F_{[L]}^{J(\text{in/out})}(E, \rho) \xrightarrow[\rho \to 0]{} \frac{1}{2} \ . \tag{6.10}$$

It can be shown [42, 43, 44] that

$$f_{[L]}^{J(\text{in/out})}(E) = \lim_{\rho \to \infty} F_{[L]}^{J(\text{in/out})}(E, \rho) \ . \tag{6.11}$$

This means that to obtain the Jost functions for a given energy E, we need to (numerically) solve the differential equations (6.8,6.9) from the boundary values (6.10) at short distances up to a large hyperradius where the right-hand sides of these equations vanish (because $W_{[L][L]}^{J}(\rho) \xrightarrow[\rho \to \infty]{} 0$) and the limits (6.11) are reached. As it is shown in Refs. [42, 43, 44], to find these limits for complex values of the energy, equations (6.8,6.9) must be integrated along a path in the complex plane of ρ.

Apparently, all the above equations are also applicable for a two-body system ($N = 2$). In such a case we obtain the ordinary expansion over the spherical harmonics. If the potential is spherically symmetric, then the partial waves are not coupled to each other, and the "minimal" (S-wave) approximation becomes exact with $L_{\text{min}} = 0$.

6.3 ΛΛ-Potential model

It is clear that there are no (and most probably cannot be) experimental data on the ΛΛ-scattering. The corresponding interaction potential is therefore deduced from the quark-theories. Its validity can only be checked indirectly, via the calculations of the properties of the double-Λ hypernuclei.

The present calculations made here can only be viewed as just a rough estimate, a simple $^1S_0$ ΛΛ-potential of this kind proposed in Ref. [82] is also used here. It allowed the authors of that paper to rather well reproduce experimental binding energies of the light double-Λ hypernuclei. The potential is made of the two gaussian terms:

$$V_{\Lambda\Lambda}(r) = Ae^{-ar^2} - Be^{-br^2} \ , \tag{6.12}$$

with $A = 200.0 \, \text{MeV}$, $B = 130.8 \, \text{MeV}$, $a = 2.776 \, \text{fm}^{-2}$, and $b = 1.062 \, \text{fm}^{-2}$.

This potential describes a weak attraction between the Λ particles at the intermediate distances (few fm). This attraction is, however, insufficient to bind the particles. The ΛΛ potentials can only generate the virtual state, which is given in the Table 6.1.

In order to artificially increase the attractive force, we multiply the potential by a factor $g > 1$:

$$V_{\Lambda\Lambda}(r) \ \to \ gV_{\Lambda\Lambda}(r) \ . \tag{6.13}$$

By increasing and decreasing g, we can move the spectral points on the Riemann surface.

68

6.4 $\Lambda\Lambda\Lambda$ and $\Lambda\Lambda\Lambda\Lambda$ Potential model matrices

As was already mentioned, the quantum numbers of possible multi-Λ systems are exactly the same as for the corresponding multi-neutron ones considered in Ref. [44]. Based on that analysis, we conclude that the lowest possible multi-Λ states are: $\Lambda\Lambda(0^+)$ with $\lambda = 0$; $\Lambda\Lambda\Lambda(\frac{1}{2}^-)$ with $\lambda = 5/2$; $\Lambda\Lambda\Lambda\Lambda(0^+, 1^+, 2^+)$ with $\lambda = 5$. The corresponding matrix elements, $W_{[L][L]}^{J}(\rho)$, of the collective potential can be obtained using the same formulae that are given in Sec. 3 of Ref. [44]. The general form of the matrix elements for three and four Lambda (Λ) systems will then be given by,

$$W_{[L_{min}][L_{min}]}^{(\Lambda\Lambda\Lambda,1/2^-)}(r) = \frac{48}{\pi} \int_0^{\pi/2} \sin^4\theta \cos^2\theta V_{\Lambda\Lambda}(\sqrt{2}r\cos\theta)d\theta \tag{6.14}$$

$$W_{[L_{min}][L_{min}]}^{(\Lambda\Lambda\Lambda\Lambda,0^+)}(r) = \frac{105 \times 33}{8 \times 16} \int_0^{\pi/2} \sin^5\theta \cos^2\theta \left(4\cos^4\theta - 4\cos^2\theta \sin^2\theta \right.$$
$$\left. + \frac{13}{4} \sin^4\theta \right) \times V_{\Lambda\Lambda}(\sqrt{2}r\cos\theta)d\theta \tag{6.15}$$

$$W_{[L_{min}][L_{min}]}^{(\Lambda\Lambda\Lambda\Lambda,1^+)}(r) = \frac{105 \times 33}{64} \int_0^{\pi/2} \sin^9\theta \cos^2\theta V_{\Lambda\Lambda}(\sqrt{2}r\cos\theta)d\theta \tag{6.16}$$

$$W_{[L_{min}][L_{min}]}^{(\Lambda\Lambda\Lambda\Lambda,2^+)}(r) = \frac{105 \times 33}{80} \int_0^{\pi/2} \sin^5\theta \cos^2\theta \left(\cos^4\theta + \frac{25}{16} \sin^4\theta \right)$$
$$\times V_{\Lambda\Lambda}(\sqrt{2}r\cos\theta)d\theta. \tag{6.17}$$

6.5   Results and discussion

The spectral points, nearest to the threshold energy, found for the two-,three-, and four-Λ systems, are given in Table 6.1. In the case of two Λ-particles, it is a virtual state. When $N > 2$, the effective angular momentum λ in Eq. (6.2) is non-zero and therefore the virtual states are not possible. Instead of them, we found the near-threshold resonances with very large widths.   Of course the "minimal" approximation, $L = L_{\min}$, diminishes the predictive power of our results. In other words, the actual positions of the resonances on the Riemann surface of the energy may be different from those given in Table6.1. However, it should be mentioned that in hyperspherical calculations of the light nuclei the "minimal" approximation always underestimates their binding (see, for example, Ref. [79]). As was pointed out in Ref. [81], for a resonance, the decay in the states with $L > L_{\min}$ is suppressed due to the large centrifugal barrier, $\lambda(\lambda + 1)/\rho^2$. Besides this, the contribution from all higher hyperharmonics can effectively be taken into account by an additional term in $W_{[L_{\min}][L_{\min}]}^{J}(\rho)$. This means that such an effective potential should be more attractive. As we see, an increase of the attraction drives the resonances up (i.e. reduces their widths). Based on this,we conclude that the widths given in Table 6.1, should be considered as the upper bounds for them.

69

state	E (MeV) for $g = 1$	g for $E = 0$
$\Lambda\Lambda(0^+)$	-2.361 (virtual)	1.461
$\Lambda\Lambda\Lambda(\frac{1}{2}^-)$	$0.219 - \frac{i}{2}22.128$	3.449
$\Lambda\Lambda\Lambda\Lambda(0^+)$	$2.378 - \frac{i}{2}31.173$	3.018
$\Lambda\Lambda\Lambda\Lambda(1^+)$	$0.708 - \frac{i}{2}46.515$	4.360
$\Lambda\Lambda\Lambda\Lambda(2^+)$	$0.973 - \frac{i}{2}47.123$	3.419

Table 6.1: Virtual and resonant states of the multi-Λ systems, generated by the potential (6.12), as well as the critical values of the echancing factor g in (6.13) with which a bound state just appears ($E = 0$).

6.6 Conclusion

Gradually increasing the enhancing factor g from its physical value, $g = 1$, we found the critical values of g at which the spectral points pass the threshold and become bound states. These values are listed in the last column of Table 6.1. The corresponding trajectories of the resonance spectral points for the considered multi-Λ states are shown in Figs.6.1, 6.2, 6.3, and 6.4. The sequences of the points in these figures are shown for a uniform increase of g by 0.1, $g = 1.0$(lowest point), $1.1, 1.2, ...$ etc. Using the same reasoning as for the widths, it can be said that the critical values of g found, are the upper limits for them.

As is seen, one can move from the system $\Lambda\Lambda\Lambda$ to the system $\Lambda\Lambda\Lambda\Lambda$, the minimal critical value of g is decreasing. This fact may be (speculatively) interpreted as a tendency and an indication that a large enough system of Λ-particles could be bound.
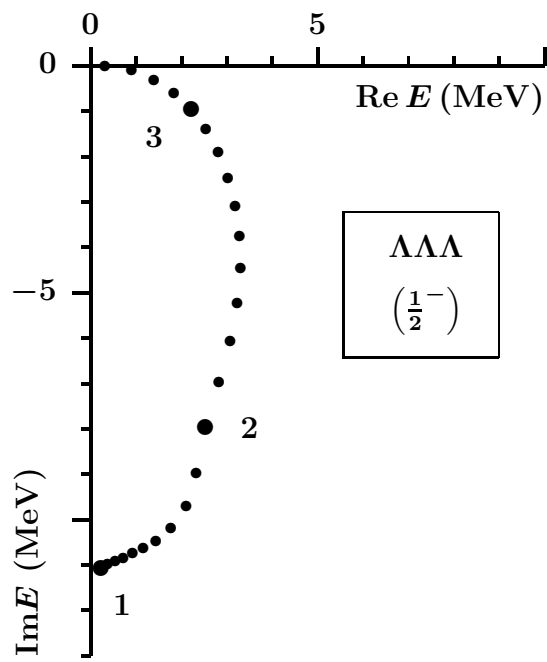
Figure 6.1: Movement of the 3Λ resonance when the enhancing factor g in (6.13) is increased from 1 to 3.4 with the uniform step 0.1. The points corresponding to integer values of g (1,2, and 3) are shown in a bigger size.
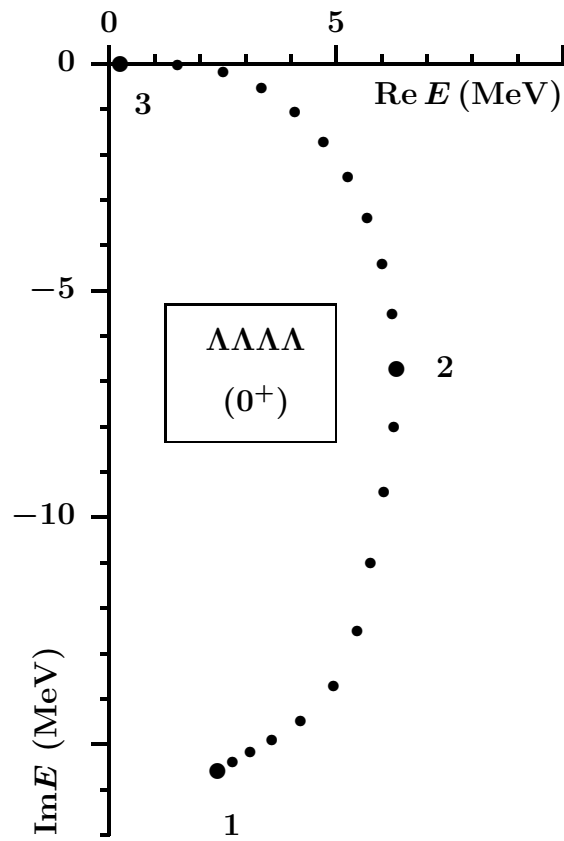
Figure 6.2: Movement of the 4Λ resonance 0^+ when the enhancing factor g in (6.13) is increased from 1 to 3 with the uniform step 0.1. The points corresponding to integer values of g (1,2, and 3) are shown in a bigger size.
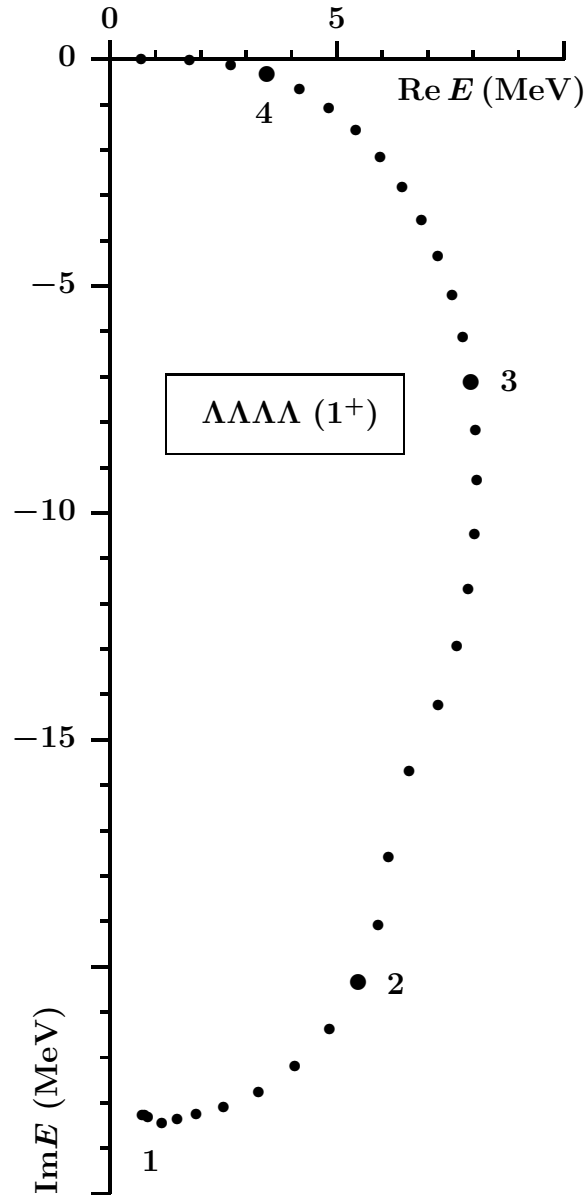
Figure 6.3: Movement of the 4Λ resonance 1^+ when the enhancing factor g in (6.13) is increased from 1 to 4.3 with the uniform step 0.1. The points corresponding to integer values of g (1,2,3, and 4) are shown in a bigger size.
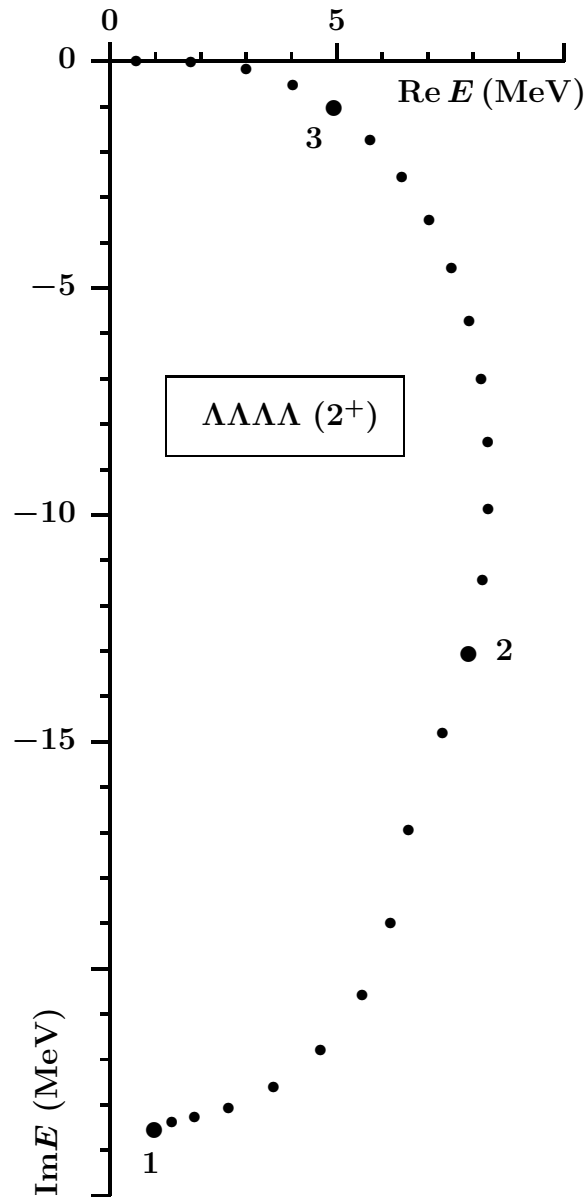
Figure 6.4: Movement of the 4Λ resonance 2^+ when the enhancing factor g in (6.13) is increased from 1 to 3.4 with the uniform step 0.1. The points corresponding to integer values of g (1,2, and 3) are shown in a bigger size.

74

Chapter 7

Recovery of the two-body Potential from a given wavefunction

7.1   Introduction

In many publications dealing with the few-body problems, it is a commonplace to say that a three-body system can reveal some additional information about the two-body subsystems involved. It is however difficult to find any practical implementation of such a statement. At the most, the few-body calculations are used to test how good the guess of the unknown two-body forces is. In contrast to this, in the present paper, we suggest a way to directly obtain the two-body potential, using available information on a three-body system where the two bodies in question are included.

What kind of the three-body information are we speaking about? Suppose we want to find out how the particles A and B interact with each other. However for some reason it is not possible to study the AB-scattering. At the same time we know the potentials that describe the interactions of these particles with a third particle, C, and they form a bound state (ABC) whose energy can be determined experimentally. As we will show shortly, in such a situation, in order to obtain the AB-potential, we need to know the three-body wave function. Of course, one cannot calculate the (ABC) wave function if all the two-body forces keeping this system together, are not known. Very often, however, one can make a reasonable assumptions as to the size of the system and its density distribution. Guessing the wave function in this way, one then can obtain a reasonable guess for the two-body potential.

In some cases, when the AB scattering data are not available this might be the only way to "derive" the AB-potential from the corresponding three body experimental data. In the present paper, as an example, we look for the singlet $\Lambda\Lambda$ potential.

The advantage of such an approach is that thus constructed potential generates the bound state at exactly the given experimental energy. At this point it should be emphasized that the method we are proposing here is not intended to compete with the sophisticated approaches developed in the inverse scattering theory. Our goal is much more modest. What we are trying to do is to roughly find the shape of the potential when very little is known about it. We therefore cannot hope to deduce the correct angular dependence of the potential if it is non-central, i.e. we assume that the potential is spherically symmetric, $V(\vec{r}) \equiv V(r)$. Due to the same reason it is logical to approximate the wave function by its dominant component.

7.2   Two-body Model

To begin with, let us obtain the potential V that binds a two-body system with the reduced mass μ, assuming that we know the bound-state wave function, $\psi(\vec{r}) = \langle \vec{r} | \psi \rangle$, and the corresponding energy E. The state vector $|\psi\rangle$ obeys the Schrödinger equation,

$$V|\psi\rangle = (E - H_0)|\psi\rangle \ , \tag{7.1}$$

where H_0 is the free-motion hamiltonian. Writing this equation in the coordinate representation, we immediately find the potential,

$$V(\vec{r}) = \frac{1}{\psi(\vec{r})} \left(E - \frac{\hbar^2}{2\mu} \Delta \right) \psi(\vec{r}) \ . \tag{7.2}$$

In principle, Eq. (7.2) gives us a recipe to deduce a non-central potential, if we know E and the corresponding complete wave function depending on the three-dimensional vector $\vec{r}$. However, as was mentioned above, we are only intended to look for the general properties of an unknown potential using an approximate wave function and therefore will ignore various fine details of it. This means that among all possible partial-wave components of ψ we only use the dominant one,

$$\psi(\vec{r}) = \sum_{[\ell']} R_{[\ell']}(r) \mathcal{Y}_{[\ell']}(\hat{\vec{r}}) \approx R_{[\ell]}(r) \mathcal{Y}_{[\ell]}(\hat{\vec{r}}) \ , \tag{7.3}$$

where $R_{[\ell]}$ is the radial wave function; the multi-index $[\ell] \equiv \{\ell, s, J, M\}$ includes the orbital angular momentum ℓ, the two-body spin s, the total angular momentum J, and its third component M; the symbol $\hat{\vec{r}}$ represents the spherical angles of vector $\vec{r}$; and $\mathcal{Y}_{[\ell]}(\hat{\vec{r}})$ is the spin-angular part of the wave function in a single partial wave,

$$\mathcal{Y}_{[\ell]}(\hat{\vec{r}}) = \sum_{ms_z} C_{\ell m s s_z}^{JM} Y_{\ell m}(\hat{\vec{r}}) \chi_{s s_z} \ . \tag{7.4}$$

76

Here $C^{JM}_{\ell m s s_z}$ and $\chi_{s s_z}$ are the Clebsch-Gordan coefficients and the two-body spin function, respectively. Just to simplify notation, we furtherdown omit where possible the quantum numbers J and M. For the same reason, in some places we omit even the multiindex $[\ell]$. This should not cause confusion since $R(r)$ is supposed to describe the motion in a single partial wave for which we are constructing a spherically symmetric potential, $V(r)$, acting in that state $[\ell]$.

Formally, we can get rid of the angular dependence by projecting Eq. (7.1) onto a particular spin-angular state,

$$\langle \mathcal{Y}_{[\ell]} | V | \psi \rangle = \langle \mathcal{Y}_{[\ell]} | (E - H_0) | \psi \rangle \ , \tag{7.5}$$

which replaces Eq. (7.2) with

$$V(r) = E - \frac{\hbar^2 \ell(\ell+1)}{2\mu r^2} + \frac{\hbar^2}{2\mu R(r)} \left[\frac{2}{r} R'(r) + R''(r) \right] \ , \tag{7.6}$$

where all unnecessary subscripts are omitted and the prime means the derivative with respect to r.

It should be noted that since the bound-state wave function $R(r)$ is a factor in both the numerator and denominator of Eq. (7.6), the normalization of this function can be arbitrary.

7.2.1 Example of recovering Coulombic potential

Let us check if we can recover the Coulomb potential with the help of Eq. (7.6), starting with exactly known wave function of the ground state of the hydrogen atom,

$$\psi_{100}(\vec{r}) = \frac{2}{a_0^{3/2}} \exp\left(-\frac{r}{a_0}\right) Y_{00}(\hat{r}) \ , \tag{7.7}$$

where

$$a_0 = \frac{\hbar^2}{\mu e^2} \ .$$

The function ψ_{100} describes the state with $\ell = 0$ and the energy

$$E = -\frac{\mu e^4}{2\hbar^2} = -\frac{e^2}{2a_0} \ .$$

When evaluating the derivatives in Eq. (7.6), we can use non-normalized radial part of the function (7.7),

$$R(r) = e^{-r/a_0} \ . \tag{7.8}$$

Performing the differentiations, we obtain:

$$V(r) = -\frac{e^2}{2a_0} - \frac{\hbar^2}{\mu a_0 r} + \frac{\hbar^2}{2\mu a_0^2} = -\frac{e^2}{r} \ , \tag{7.9}$$

as was expected.

7.2.2 Numerical example to recover the triplet $NN-$potential

In Sec. 7.2.1 it has been demonstrated how Eq. (7.6) works in the simplest case when all the derivations can be done analytically, which allows us to trace all the steps and to see mutual cancellations of some extra terms. How would this work if analytic derivations were not possible? Can the potential be accurately recovered if the derivatives are evaluated numerically? Do the extra terms still cancel each other? To answer these questions, we consider here another example, namely, the triplet NN-potential that generates the proton-neutron bound state, i.e. the deuteron.
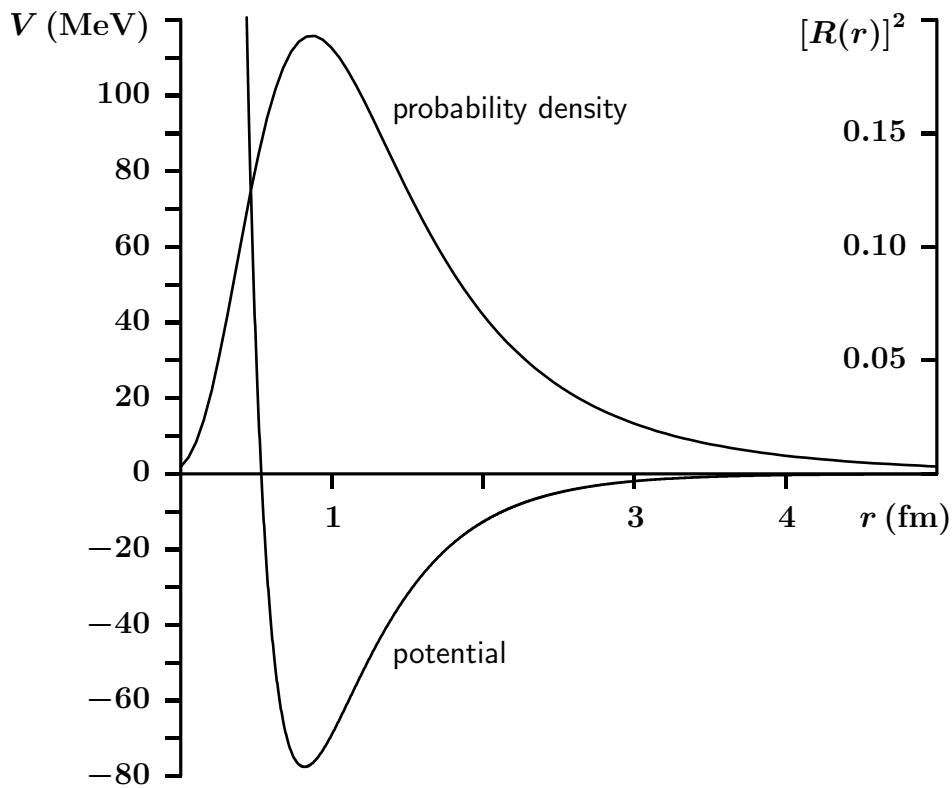
Figure 7.1: Triplet Malflied-Tjon potential (7.10) and the radial probability density, $R^2(r)$ [fm^{-3}], for the S-wave bound state generated by this potential.

Let us consider the system consisting of a proton and a neutron. When their spins are parallel and the total spin is 1 (the triplet state), the attaraction between these two nucleons is sufficient to bind them in a stable nucleus, the deuteron, with experimentally known binding energy 2.224566 MeV [83] and the RMS-radius 2.128 fm [84].

It is not our intention to accurately describe the deuteron. Its energy and size for us

are merely the reference characteristics of a quantum state for which we are going to artificially construct a wave function and then to generate the corresponding two-body potential.

In order to do the test, we choose a simple NN-potential, numerically obtain the deuteron wave function, and using this wave function try to numerically recover the NN-potential from which we started. As such a potential, we use the triplet NN-potential proposed by R. A. Malfliet and J. A. Tjon in Ref. [85] (its slightly modified parameters, which we use, are given in Ref. [86]). It is a combination of two Yukawa terms,

$$V(r) = -\lambda_A \frac{e^{-\mu_A r}}{r} + \lambda_R \frac{e^{-\mu_R r}}{r} \ , \qquad (7.10)$$

where $\lambda_A = 626.885\,\text{MeV}$, $\lambda_R = 1438.72\,\text{MeV}$, $\mu_A = 1.55\,\text{fm}^{-1}$, $\mu_R = 3.11\,\text{fm}^{-1}$, and it is assumed that $\hbar^2/m_N = 41.47\,\text{MeV}\cdot\text{fm}^2$ with m_N being the nucleon mass.

This potential supports an S-wave bound state with $E = -2.2307\,\text{MeV}$ and the RMS-radius $1.985\,\text{fm}$. The Malflied-Tjon potential and the radial dependence of the probability density for the bound state, are shown in Fig. 7.1. For locating the bound state and calculating its wave function, we used the Jost-function method described in Refs. [42, 43].

Numerically obtained radial wave function $R(r)$ was used then in Eq. (7.6) to re-construct the potential. Thus recovered potential turned out to be practically indistinguishable from the one shown in Fig. 7.1.

In the examples that we used so far the wave function was known or calculated exactly. The main idea of the method we propose here is to uncover general features of a completely unknown potential, when the bound state energy is known and one can guess the space distribution of the probability density. Therefore a question arises: how stable is the method to unavoidable deviations of the guessed wave function from the unknown exact one? To shed some light on this, let us examine how significant would be the changes in the potential if we slightly distort the wave function of the deuteron.

As a distorted radial wave function, we use the following parametrization (this function is not normalized):

$$R(r) = \frac{r}{r_0} \arctan\left[4(r/r_0)^2\right] e^{-3r/r_0} + \frac{6r_0}{\pi r} \arctan\left[(r/r_0)^2\right] \exp\left(-\sqrt{\frac{2\mu|E|}{\hbar^2}}r\right) \ , \quad (7.11)$$

where $r_0 = 1\,\text{fm}$ and $E = -2.2307\,\text{MeV}$ is the same as for the Malfliet-Tjon potential. Since $\varkappa = \sqrt{2\mu|E|/\hbar^2} = 0.2319\,\text{fm}^{-1} \ll 3\,\text{fm}^{-1}$, the first term in Eq. (7.11) vanishes much faster when $r \to \infty$, and thus this function has the correct asymptotic behaviour determined by the second term.

The radial probability distributions, $[R(r)]^2$, for the Malflied-Tjon deuteron model and
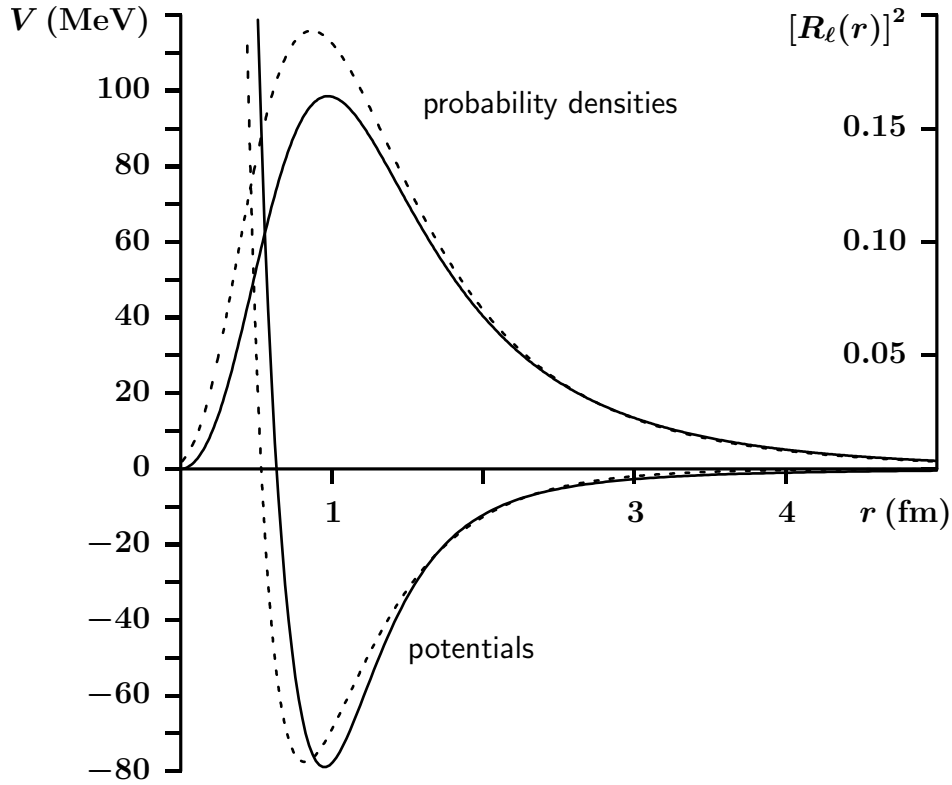
Figure 7.2: Triplet Malflied-Tjon potential (7.10) and the corresponding probability density for the deuteron (dashed curves) are compared with a "hand-made" density (solid curve) and the corresponding potential that was obtained from it (solid curve).

for the normalized distorted function, are shown in Fig. 7.2. The distorted function (7.11) near the origin vanishes faster, but is slightly above the Malflied-Tjon one at large distances (the latter is not visible in the figure). As a result the distorted probability is shifted to the right, and the RMS-radius is a bit larger, namely, $2.071\,\mathrm{fm}$ (which is a bit closer to the experimental value, $2.128\,\mathrm{fm}$ [84], by the way).

If we denote

$$A(r) = \frac{r}{r_0} \arctan\left[4(r/r_0)^2\right] \tag{7.12}$$

and

$$B(r) = \frac{6r_0}{\pi r} \arctan\left[(r/r_0)^2\right]\ , \tag{7.13}$$

then

$$R(r) = A(r)e^{-3r/r_0} + B(r)e^{-\varkappa r}\ , \tag{7.14}$$

$$R'(r) = \left[A'(r) - \frac{3}{r_0}A(r)\right]e^{-3r/r_0} + \left[B'(r) - \varkappa B(r)\right]e^{-\varkappa r}\ , \tag{7.15}$$

80

and

$$R''(r) = \left[A''(r) - \frac{6}{r_0} A'(r) + \frac{9}{r_0^2} A(r) \right] e^{-3r/r_0} + \qquad (7.16)$$

$$+ \left[B''(r) - 2\varkappa B'(r) + \varkappa^2 B(r) \right] e^{-\varkappa r} ,$$

where the derivatives of the auxiliary functions are:

$$A'(r) = \frac{1}{r} A(r) + \frac{8r_0 r^2}{r_0^4 + 16r^4} , \qquad (7.17)$$

$$A''(r) = \frac{1}{r} A'(r) - \frac{1}{r^2} A(r) + 16 r_0 r \frac{r_0^4 - 16r^4}{(r_0^4 + 16r^4)^2} , \qquad (7.18)$$

$$B'(r) = -\frac{1}{r} B(r) + \frac{12 r_0^3}{\pi(r_0^4 + r^4)} , \qquad (7.19)$$

$$B''(r) = \frac{1}{r^2} B(r) - \frac{1}{r} B'(r) - \frac{48 r_0^3 r^3}{\pi(r_0^4 + r^4)^2} . \qquad (7.20)$$

Substituting the above R, R', and R'' in Eq. (7.6), we obtain the potential, $V(r)$, for which the function (7.11) is an exact solution of the radial Schrödinger equation with the binding energy $|E|$. For the sake of comparison, we choose $|E| = 2.2307\,\mathrm{MeV}$, i.e. the same as for the potential (7.10), but in principle we can use any other value for it.

The Malflied-Tjon potential and the potential reconstructed from the distorted function (7.11) are compared in the same Fig. 7.2. As we see, the suppression of the probability near the origin results in a larger repulsive core (as one would expect). Despite the fact that the analytic expression for the reconstructed potential is very complicated, there are no drastic changes in the general features of the potential when we change the wave function. In other words, the reconstruction procedure based on Eq. (7.6) is rather stable against variations (errors) of the wave function.

7.3 Three-body Model

In the case of three interacting particles, the Schrödinger equation formally looks exactly the same as Eq. (7.1), but now the operator V is the sum of three two-body potentials,

$$V = V_{12} + V_{13} + V_{23} , \qquad (7.21)$$

81

where the subscripts are the particle labels. Let the potentials V_{13} and V_{23} be known while the potential acting between the particles 1 and 2, unknown. It is convenient to re-write the Schrödinger equation in the form,

$$V_{12}|\psi\rangle = (E - V_{13} - V_{23} - H_0)|\psi\rangle \, , \tag{7.22}$$

where the unknown potential is separated.
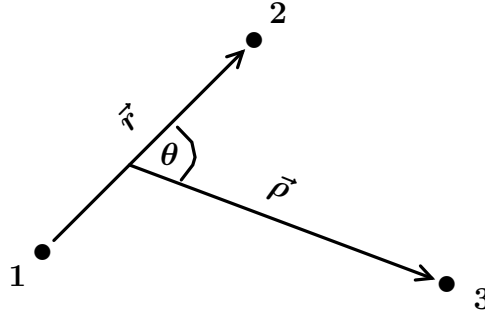
Figure 7.3: Jacobi coordinates $(\vec{r}, \vec{\rho})$ for the three particles 1, 2, and 3.

Let $|\vec{r}, \vec{\rho}\rangle$ be the state with definite values of the Jacobi coordinates shown in Fig. 7.3. Multiplying Eq. (7.22) by $\langle \vec{r}, \vec{\rho}|$ from the left and assuming that all the potentials are local and spherically symmetric, we obtain

$$V_{12}(r)\psi(\vec{r}, \vec{\rho}) = \left[E - V_{13}(r_{13}) - V_{23}(r_{23}) + \frac{\hbar^2}{2\mu_r}\Delta_{\vec{r}} + \frac{\hbar^2}{2\mu_\rho}\Delta_{\vec{\rho}} \right] \psi(\vec{r}, \vec{\rho}) \, , \tag{7.23}$$

where $\psi(\vec{r}, \vec{\rho}) = \langle \vec{r}, \vec{\rho}|\psi\rangle$ is the wave function of the three-body bound state, μ_r and μ_ρ are the reduced masses associated with the motion along the corresponding Jacobi coordinates, and the radial variables r_{13} and r_{23},

$$r_{13} = \left| \frac{m_2}{m_1 + m_2}\vec{r} + \vec{\rho} \right| = \sqrt{\left(\frac{m_2}{m_1 + m_2} \right)^2 r^2 + \rho^2 + \frac{m_2}{m_1 + m_2} r\rho \cos\theta} \, , \tag{7.24}$$

$$r_{23} = \left| \frac{m_1}{m_1 + m_2}\vec{r} - \vec{\rho} \right| = \sqrt{\left(\frac{m_1}{m_1 + m_2} \right)^2 r^2 + \rho^2 - \frac{m_1}{m_1 + m_2} r\rho \cos\theta} \, , \tag{7.25}$$

are the inter-particle distances in the particle pairs (1,3) and (2,3). Here m_1 and m_2 are the particle masses and θ is the angle between vectors $\vec{r}$ and $\vec{\rho}$.

Perhaps it should be reiterated once more that the method we propose here is intended for just a very rough estimating of the unknown potential that describes the interaction between the particles 1 and 2. When doing this we know exactly the energy, E, of the bound state but need to guess (i.e. to construct "by hand") the corresponding wave function, $\psi(\vec{r}, \vec{\rho})$. Of course we can hope to make a reasonable guess only for the ground

82

state and only for the main component of such a function. Similarly to Eq. (7.3), we therefore take it as

$$\psi(\vec{r}, \vec{\rho}) \approx R(r, \rho) Y_{00}(\hat{\vec{r}}) Y_{00}(\hat{\vec{\rho}}) \chi , \qquad (7.26)$$

where it is assumed that all orbital angular momenta are zero and the total angular momentum, J, is built from the particle spins,

$$\chi = |((s_1 s_2) s_{12} s_3) J J^z\rangle . \qquad (7.27)$$

In order to leave in Eq. (7.23) only one "free" variable, r, which the potential V_{12} depends on, we multiply this equation by $\psi^\dagger(\vec{r}, \vec{\rho})$ from the left and integrate over $\vec{\rho}$ as well as over the spherical angles $\hat{\vec{r}}$. When integrating over $\hat{\vec{\rho}}$, we choose the z-component of $\vec{\rho}$ along vector $\vec{r}$. This makes the polar angle of $\vec{\rho}$ coinciding with θ. As a result, we obtain:

$$V_{12}(r) = E - \frac{1}{2D(r)} \int_0^\infty d\rho \int_0^\pi d\theta \, \rho^2 \sin(\theta) R^2(r, \rho) \big[\langle V_{13}(r_{13}) \rangle + \langle V_{23}(r_{23}) \rangle \big] +$$

$$+ \frac{\hbar^2}{2D(r)} \int_0^\infty d\rho \, \rho^2 R(r, \rho) \left[\frac{1}{\mu_r r^2} \partial_r (r^2 \partial_r) + \frac{1}{\mu_\rho \rho^2} \partial_\rho (\rho^2 \partial_\rho) \right] R(r, \rho) , \quad (7.28)$$

where

$$D(r) = \int_0^\infty R^2(r, \rho) \rho^2 \, d\rho \qquad (7.29)$$

is the two-body density of the particles 1 and 2; the symbols $\langle V_{13} \rangle$ and $\langle V_{23} \rangle$ denote the averages of the corresponding potentials in the spin space, i.e.

$$\langle V_{13} \rangle = \chi^\dagger V_{13} \chi \qquad \text{and} \qquad \langle V_{23} \rangle = \chi^\dagger V_{23} \chi . \qquad (7.30)$$

For calculating these averages, it is convenient to represent the potentials in terms of the operators $P(s_{ij})$ projecting onto the states with certain values of the two-body spin, s_{ij}, of the particles i and j,

$$V_{13}(r_{13}) = \sum_{s_{13}} \mathscr{V}_{13}^{[s_{13}]}(r_{13}) P(s_{13}) \qquad \text{and} \qquad V_{23}(r_{23}) = \sum_{s_{23}} \mathscr{V}_{23}^{[s_{23}]}(r_{23}) P(s_{23}) . \quad (7.31)$$

Writing the projection operators in the form

$$P(s_{13}) = |((s_1 s_3) s_{13} s_2) J J^z\rangle \langle((s_1 s_3) s_{13} s_2) J J^z| \qquad (7.32)$$

and

$$P(s_{23}) = |((s_2 s_3) s_{23} s_1) J J^z\rangle \langle((s_2 s_3) s_{23} s_1) J J^z| , \qquad (7.33)$$

we can express the spin-averaging via the $6j$-symbols (see Ref. [87]) as follows:

$$\langle V_{13}(r_{13}) \rangle = \sum_{s_{13}} \mathscr{V}_{13}^{[s_{13}]}(r_{13})(2s_{12} + 1)(2s_{13} + 1) \left\{ \begin{array}{ccc} s_3 & s_1 & s_{13} \\ s_2 & J & s_{12} \end{array} \right\}^2 , \qquad (7.34)$$

83

$$\langle V_{23}(r_{23})\rangle = \sum_{s_{23}} \mathscr{V}_{23}^{[s_{23}]}(r_{23})(2s_{12}+1)(2s_{23}+1) \left\{ \begin{array}{ccc} s_3 & s_2 & s_{23} \\ s_1 & J & s_{12} \end{array} \right\}^2 . \tag{7.35}$$

As is seen the square of the radial wave function is present in both the numerator and denominator of Eq. (7.28) and therefore it is not necessary to use it with the proper normalization.

7.3.1 Recovering $nn-$potential from triton data

In order to test how accurately an unknown potential can be recovered with the help of the procedure described in the preceding section, we consider the three-body bound system nnp (triton), where all the potentials are actually known. However, we pretend that the neutron-neutron potential is unknown and try to recover it using Eq. (7.28) and the properties of triton.

Referring to Fig. 7.3, the proton is particle number 3 and the neutrons are particles 1 and 2. Neutron can interact with proton either in the singlet or triplet spin-state via the potentials $\mathscr{V}_{NN}^s$ and $\mathscr{V}_{NN}^t$, respectively. Due to the Pauli principle, the nn system with $\ell = 0$ can only be in the singlet state. Therefore, if our method works, then as a result of the recovering we should obtain the singlet NN-potential for the "unknown"nn-interaction.

In the sums (7.34, 7.35), we have $s_{12} = 0$ (nn-spin) and $J = 1/2$ (triton spin). The summation involves only two terms and gives:

$$\langle V_{13}(r_{13})\rangle = \frac{1}{4}\mathscr{V}_{NN}^s(r_{13}) + \frac{3}{4}\mathscr{V}_{NN}^t(r_{13}) , \tag{7.36}$$

$$\langle V_{23}(r_{23})\rangle = \frac{1}{4}\mathscr{V}_{NN}^s(r_{23}) + \frac{3}{4}\mathscr{V}_{NN}^t(r_{23}) . \tag{7.37}$$

As the triplet NN-potential, $\mathscr{V}_{NN}^t$, we take the Malflied-Tjon one given by Eq. (7.10) with the parameters listed just after that equation. The singlet potential, $\mathscr{V}_{NN}^s$, has exactly the same functional form and almost all the same parameters except the first one, namely, $\lambda_A = 513.968\,\mathrm{MeV}$ for the singlet state [86].

The main question in the proposed procedure of the unknown potential recovering is how to make a reasonable guess of the three-body wave function. We assume that we can only know the binding energy and perhaps (but not for sure and not always) the RMS-radius of the three-body state.

The knowledge of the energy gives us the asymptotic behaviour of the wave function at large distances. Indeed, it is known (see, for example,Ref. [88]) that the main contribution to the asymptotics of a three-body bound-state wave function comes from the

out-going hyper-spherical wave, namely,

$$R(r, \rho) \xrightarrow[\zeta \to \infty]{} \sim \frac{e^{-\varkappa\zeta}}{\zeta^{5/2}} \,, \tag{7.38}$$

where ζ is the hyperradius,

$$\zeta = \sqrt{\frac{\mu_{12}}{\mu} r^2 + \rho^2} \,, \tag{7.39}$$

and $\varkappa$ is the imaginary part of the momentum corresponding to the negative energy of the bound state,

$$\varkappa = \sqrt{\frac{2\mu|E|}{\hbar^2}} \,. \tag{7.40}$$

It is clear that the hyper-spherical wave (7.38) cannot be used as the function R at all distances. Indeed, the right hand side of Eq. (7.38) becomes singular when $\zeta \to 0$, which is unphysical. This problem can be circumvented by introducing a positive parameter α in the denominator,

$$R(r, \rho) \sim \frac{e^{-\varkappa\zeta}}{\alpha + \zeta^{5/2}} \,, \tag{7.41}$$

which removes the singularity and keeps the behaviour (7.38) when $\alpha \ll \zeta^{5/2}$.

The expression (7.41) is still not a satisfactory choice even as a very rough approximation of the wave function because it is monotonically decreasing while a realistic wave function should have a maximum somewhere at the distances corresponding to the size (RMS-radius) of the system. Such a maximum can appear if we introduce a factor suppressing the probability of finding the particles at short distances. The physical reason for such a factor is the strong repulsion of the particles at distances ~ 1 fm (the hard or soft core in the two-body potentials). In nuclear theory such factors are known as Jastrow factors (see, for example, chapter 3 of the book [89]).

Of course the Jastrow factor can be constructed in many different ways. We found that for our problem of triton a good choice is the following (please take note that this function is not normalized):

$$R(r, \rho) = \frac{1}{r} \arctan\left(\gamma r^{3/2}\right) \frac{e^{-\varkappa\zeta}}{\alpha + \zeta^{5/2}} \,. \tag{7.42}$$

With the parameters $\gamma = 0.81 \, \text{fm}^{-3/2}$ and $\alpha = 29.0 \, \text{fm}^{5/2}$ this wave function gives the RMS-radius of triton 1.745 fm, which is within the uncertainty interval of its experimental value (1.7591 ± 0.0363) fm [90]. As the binding energy of triton, we used the experimental value, $|E| = 8.481798$ MeV, [91].

Two things should be explained concerning the approximate wave function (7.42). Firstly, it does not involve explicit Jastrow factors that would suppress approaching of the first and the second neutrons to the proton. In fact, such factors are not needed because the

85

Figure 7.4: The neutron-neutron potential (solid curve) numerically recovered using Eq. (7.28) with the approximate (guessed) wave function (7.42) of triton and with its experimentally known ground-state energy $E = -8.481798$ MeV. For the sake of comparison, the singlet and triplet Malfliet-Tjon NN-potentials are shown by the upper and lower dashed curves, respectively.

motion along both Jacobi coordinates is in the S-wave states. Therefore the proton can approach any of the two neutrons only at the centre of mass where all three particles meet. Such a configuration is already suppressed by the factor depending on r, and thus no additional Jastrow factors are needed. Secondly, the function (7.42) is symmetric only with respect to the permutations of the neutrons. This fact might be seen as violation of the Pauli principle. However, protons and neutrons, in fact, are not identical. The isotopic invariance is an approximate symmetry. We therefore are not obliged to construct a completely symmetric wave function.

Eq. (7.28) involves the first and second derivatives with respect to the radial variables r and ρ. In principle, all necessary differentiation of the function (7.42) can be done explicitly. However, to avoid cumbersome derivations and to reserve the possibility of changing the functional form of the wave function, we calculated all the derivatives numerically using simple finite difference formulae,

$$f'(x) = \frac{f(x+h) - f(x-h)}{2h} \ , \qquad f''(x) = \frac{f(x+h) + f(x-h) - 2f(x)}{h^2} \ , \qquad (7.43)$$

which give stable results with the step $h = 10^{-5}$ fm.

The neutron-neutron potential obtained in this way using Eq. (7.28) is shown in Fig. 7.4 by the solid curve. For the sake of comparison the singlet and triplet Malfliet-Tjon NN-potentials are shown in that figure by the dashed curves. As is seen, the recovered potential is almost correct, i.e. it almost reproduces the singlet potential. This successful test allows us to hope that the proposed method can indeed give a reliable estimate of a truly unknown potential in any other physical system even if its wave function is constructed on the basis of general reasoning and intuition.

7.3.2   Recovering the $\Lambda\Lambda-$potential

Due to the obvious reasons it is not possible to study the $\Lambda\Lambda$-interaction in the direct collisions of these two particles. The only experimental information from which one can deduce some general features of the forces acting between them, is the information on the double-Λ hypernuclei. Therefore various $\Lambda\Lambda$-potentials can only be constructed on the basis of either the quark or boson-exchange theories. Validity of such potentials is tested in the calculations of the properties of various double hypernuclei whose characteristics are known experimentally.

Examples of the soft-core boson-exchange $\Lambda\Lambda$-potentials can be found in Ref. [92]. They are known as the Nijmegen Soft-Core (NSC97) potentials. Since there are some ambiguities in the constructing of them, several versions of such potentials are available. For the purposes of the few-body calculations these potentials are usually simulated in the coordinate representation by a simple functional form, $V_{\Lambda\Lambda}(r)$, (see, for example, Refs. [93, 94, 95]) with the parameters adjusted to make $V_{\Lambda\Lambda}(r)$ either phase-equivalent to the corresponding Nijmegen potentials or to exactly reproduce the measured binding energy of the hypernucleus $^{6}_{\Lambda\Lambda}$He. The observation of this hypernucleus was so important that nowadays it is known as the NAGARA event[96].

The method we are developing in the present work may also make a contribution to the constructing of such a $V_{\Lambda\Lambda}(r)$. Of course we do not expect to propose a very reliable $\Lambda\Lambda$-potential. As it was emphasized from the very beginning, our method can only deduce some general features of a potential, such as, for example, its approximate depth, range,etc. However, in the case of the $\Lambda\Lambda$-interaction even this limited information can be helpful in choosing the most adequate one among many available potentials.

Following the same line of reasoning as in Sec. 7.3.1, we construct the following (not normalized) wave function of the hypernucleus $^{6}_{\Lambda\Lambda}$He in the three-body model $\Lambda\Lambda\alpha$:

$$R(r,\rho) = \arctan\left(\gamma r^{5/2}\right) \frac{e^{-\varkappa\zeta}}{\alpha + \zeta^{5/2}} \ . \tag{7.44}$$

Here r and ρ are the Jacobi distances shown in Fig. 7.3,where ^{4}He is the particle number 3, and ζ is the hyperradius (7.39). The momentum parameter (7.40) corresponds to the binding energy of the three-body system ($\Lambda\Lambda\alpha$), $|E| = 7.25\,$MeV determined in the

87

NAGARA experiment [96]. The other two parameters, $\alpha = 35\,\mathrm{fm}^{5/2}$ and $\gamma = 2.5\,\mathrm{fm}^{-5/2}$, were chosen such that the function (7.44) gives the following geometric sizes:

$$\sqrt{\langle r^2 \rangle} = 3.80\,\mathrm{fm} \ , \qquad \sqrt{\langle \rho^2 \rangle} = 2.35\,\mathrm{fm} \ . \tag{7.45}$$

These RMS-distances are within the corresponding intervals obtained in Refs. [94, 97] for various $\Lambda\Lambda$-potentials, namely,

$$3.09\,\mathrm{fm} \leqslant \sqrt{\langle r^2 \rangle} \leqslant 4.09\,\mathrm{fm} \ , \qquad 2.11\,\mathrm{fm} \leqslant \sqrt{\langle \rho^2 \rangle} \leqslant 2.35\,\mathrm{fm} \ . \tag{7.46}$$

We assume that the $\Lambda\alpha$ potential is known. We take it the same as in Ref. [94], namely, as

$$V_{\Lambda\alpha}(r) = \Lambda_1 \exp\left(-r^2/\beta_1^2\right) - \Lambda_2 \exp\left(-r^2/\beta_2^2\right) \ , \tag{7.47}$$

where $\Lambda_1 = 450.4\,\mathrm{MeV}$, $\beta_1 = 1.25\,\mathrm{fm}$, $\Lambda_2 = 404.9\,\mathrm{MeV}$, $\beta_2 = 1.41\,\mathrm{fm}$. Since the spin of the α-particle is zero, there is only one spin state in the $\Lambda\alpha$-system and therefore the spin-averaging prescribed by Eqs. (7.34, 7.35) is trivial, i.e.

$$\langle V_{13}(r_{13}) \rangle = V_{\Lambda\alpha}(r_{13}) \ , \qquad \langle V_{23}(r_{23}) \rangle = V_{\Lambda\alpha}(r_{23}) \ .$$

The $\Lambda\Lambda$-subsystem in $_{\Lambda\Lambda}^{6}\mathrm{He}$ is assumed to be in the S-wave state and therefore in the singlet spin state. This means that we can only obtain the information on the $^1S_0$ potential $V_{\Lambda\Lambda}$.

7.4 Conclusion

In this study, we suggested a simple and efficient method for relating a given wave function of a three-body bound state to the corresponding two-body potential acting in a chosen pair of particles, while the potentials in the other two pairs are assumed to be given. The most interesting feature of the presented method is that (thanks to the formal construction) any given wave function becomes an exact solution of the three-body Schrödinger equation for a given binding energy and with the corresponding (numerically obtained) two-body potential in a chosen pair of particles. The method works for a two-body bound state as well. The accuracy of the method is demonstrated using the examples of the bound systems ep,np, nnp, and $\Lambda\Lambda\alpha$.

Two possible applications of the presented method are envisaged. Firstly, we can deduce an unknown two-body potential from an approximate (guessed) wave function. This may be helpful when very little is known about such a potential and there is no possibility of doing the scattering experiments. Secondly, if the two-body potential is known, we can construct the corresponding three-body wave function. In doing this we can postulate a wave function in a reasonable functional form with some free parameters and then can fix these parameters by minimizing the deviations of the deduced potential from the known (exact) one. The wave function obtained in this way is always a solution of the Schrödinger equation with a given binding energy.
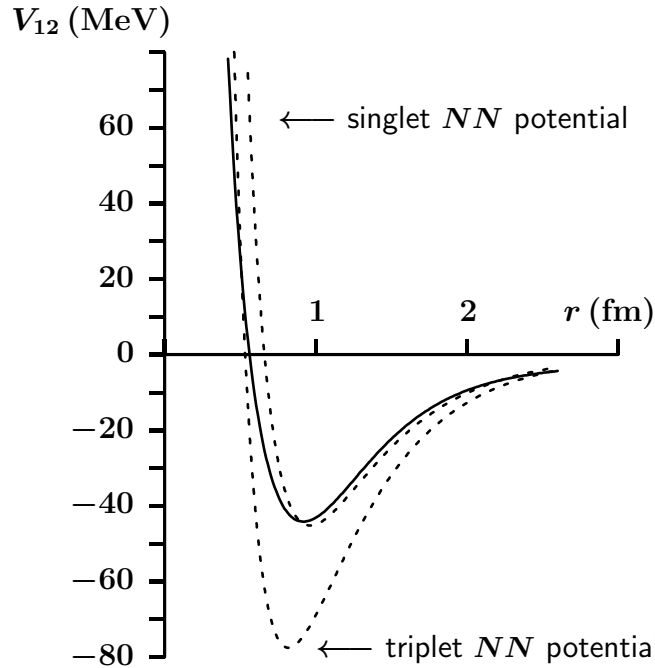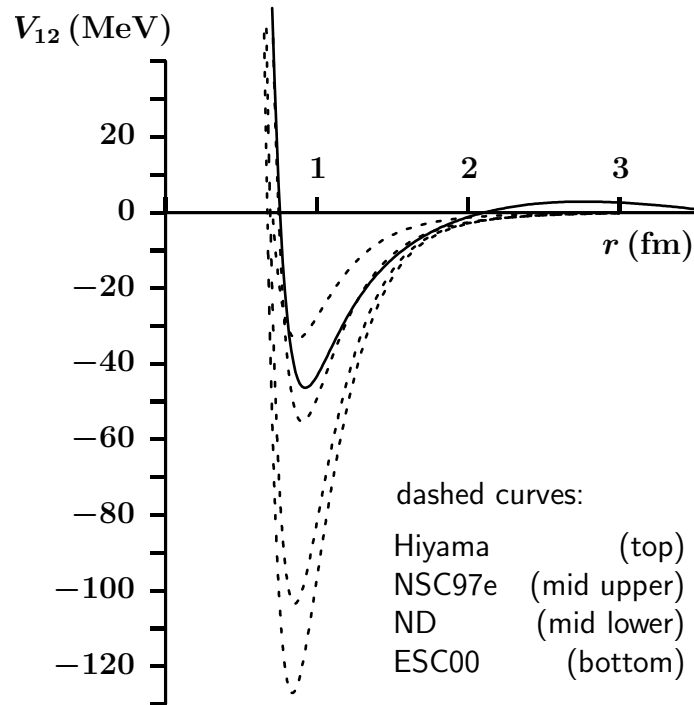
Figure 7.5: The singlet $\Lambda\Lambda$-potential (solid curve) numerically recovered using Eq. (7.28) with the approximate (guessed) wave function (7.44) of the hypernucleus $^{6}_{\Lambda\Lambda}$He and with its experimentally known ground-state energy $E = -7.25\,\mathrm{MeV}$. For the sake of comparison, three versions of the Nijmegen soft-core one-boson-exchange $\Lambda\Lambda$-potential, namely, NSC97e, ND, and ESC00 as well as the potential used by Hiyama et al. in Ref. [95] are shown by the dashed curves.

Chapter 8

General Conclusions

This study involved the investigation into the Lambda-nuclear and the multi-Lambda systems. It was motivated by the lack of understanding of how the hyperons interact with nucleons and with each other, which is important for developing adequate models in nuclear astrophysics. The main results are summarized and possible future work is briefly discussed.

8.1 Single Lambda-nuclear systems

The Jost matrix method is an approach that allows us to find the spectral points (bound states and resonant states) and the scattering states in a unified way, hence the S-matrix can also be obtained. The relationship between the S-matrix residues and the Jost matrices also allows us to determine the Asymptotic Normalization Constants(ANC) as well as the Nuclear Vertex Constants(NVC) parameters. The relevant background material were presented in Chapter 2. Chapter 3 further present the background material for low energy scattering parameters.

In Chapter 5 we present the new results obtained using the method provided in Chapter 2. Besides the background material in Chapter 3 the second part of results were also presented in Section 3.5.

In Chapter 5 the wide range of hypernuclei two-body Λ plus nuclear core systems were investigated using the same potential model as in Ref.[53]. Since the Jost functions are not single valued functions of E, a complex analysis approach was used to by treating the Jost functions as single valued functions by defining them on the complex surface called the Riemann surface consisting of the physical sheets and unphysical sheets. For a given hypernuclei, all their possible bound states on the physical sheet and resonances states energies on the unphysical sheet were obtained from the direct calculations of the Jost functions.To check if no bound states is not missing, we used the Chew-Frautschi

plots(spectral points on the $E - \ell$ plane). In order to achieve this, the two-body radial Schrodinger equation was transformed into an equivalent system of first-order differential equations for the functions that asymptotically tend to the Jost functions. We also calculated the S-matrix residues and their corresponding Asymptotic normalization Constants and the Nuclear Vertex Constants.

In Chapter 3 the method based on power series effective-range expansion was presented, in order to look for low energy parameters. The Jost functions were factorized in such way that they form certain combination of the channel momenta times an analytic single-valued function of the energy E. The remaining energy-dependent factors were now defined on single energy plane which does not have any branching points anymore.For these energy-dependent functions, a system of first-order differential equations is obtained. Then, using the fact that the functions are analytic, they are expanded in the power series to obtain a system of differential equations that determine the expansion coefficients. When expansion coefficients are obtained for the expansion around the energy $E_0 = 0$, the coefficients are then used to calculate the effective range parameters. In Section 3.5, for the same set of hypernuclear systems, these parameters were obtained for the expansion of the effective-range function up to the order of $\sim k^8$ and for three values of the angular momentum, $\ell = 0, 1, 2$. The S-wave scattering lengths and effective radii reported in Ref.[53], agree with our results only for the hyper-nuclear systems with weak Λ-core binding.

8.2   Multi-Lambda systems

In Chapter 6 we investigated the multi-hyperon systems $\Lambda\Lambda$, $\Lambda\Lambda\Lambda$, and $\Lambda\Lambda\Lambda\Lambda$ with a feature that none of their subsystems can actually form a bound system. This study was motivated by the work done on the multi-neutron systems of Ref.[44], since neutron and Λ-particle both are neutral and both have the same spin $1/2$.

We used the hyperspherical approach method, presented in Chapter 4, which is based on the expansion of the N-body wave function (for a given total angular momentum J) within the hyper-spherical harmonics, $Y_{[L]}^J(\Omega)$. Within the hyperspherical approach, the wave function is expanded on an infinite series over hyperspherical harmonics, we then end up with an infinite system of coupled hyperradial equations, which is truncated in practical calculations. We used the hyperradial equations to locate the spectral points (the resonance state energies) for the system considered. The numerical results obtained are presented on Section 6.5.

The $\Lambda\Lambda$-potential were multiplied by a numerical factor $g > 1$, and gradually increasing it to trace the movement of the corresponding resonance pole until it reaches the threshold energy. The critical values of g at which the spectral points pass the threshold and become bound states were found for each system. These values are listed in the last column of Table 6.1.Thus found critical value of g (with which a bound state just appears)

characterizes the "readiness" of the system to be bound. As we move from the system $\Lambda\Lambda\Lambda$ to $\Lambda\Lambda\Lambda\Lambda$, the minimal critical value of g is decreasing and that may interpreted as a tendency and an indication that a large enough system of Λ-particles could be bound.

8.3 Reconstruction of the Multi-Lambda systems potential

In Chapter 7 a method suggested a way to directly obtain the two-body potential, using available information on a system where the two bodies in question are included were explored. It has been showed in Section 7.2.1 and Section 7.2.2 via examples on how can we analytically and numerically recover the two body potential for the two body systems ep and np. For ep system, it was a direct recovery using the bound ground state hydrogen atom wavefunction and its corresponding binding energy into the two-body Schrodinger equation.

In Section 7.3 a three body system background material were presented. A triton system data (nnp) was used as an example to illustrate how to recover the two-body nn potential from a three body bound system in section 7.3.1 using a guessed wavefunction constructed within the hyperspherical approach. The recovered potential were obtained and compared with the known NN singlet and triplet Malfliet-Tjon NN-potentials in Figure.7.4. The last part of this work was to try and construct the $\Lambda\Lambda$ potential using the same approach used for three-body system as in Section 7.3.1. In this case the the double-Λ hypernuclei experimental information were useful. Similarly, an approximate (guessed) wave function was used for the hypernucleus $_{\Lambda\Lambda}^{6}$He in the three-body model $\Lambda\Lambda\alpha$ together with its corresponding binding energy $|E| = 7.25$ MeV determined in the NAGARA experiment [96]. The $\Lambda\Lambda$-potential recovered from the wave function (7.44) is shown in Fig. 7.5 and compared with three different Nijmegen $\Lambda\Lambda$-potentials, as well as the potential used by Hiyama et al. in Ref. [95] in the same figure.

8.4 Conclusion

In general, the calculations made in Chapter 3 and Chapter 5(and Ref.[54]), their results reasonable reproduced the results reported in Ref.[53] and Ref.[71]. In Chapter 3, further effective-range parameters for up to the order of $\sim k^8$ for three of the angular momentum values were calculated. Furthermore, the spectral points (bound states and resonance states) for a given hypernulear system were obtained by being traced via Chew-Frautschi plots (on the $E - \ell$ plane), and they are reported in Chapter 5. Hence, it can be claimed that the results obtained in Chapter3 and Chapter5(and Ref.[54]) are reliable and comparable with some of the results reported before.

In Chapter 6, the trajectories of the calculated resonance spectral points on the complex energy plane for the considered multi-Λ systems are reported. The critical values of g which strengthens the potential in order for the spectral points to pass the threshold and becomes bound states were found. This calculations gives us an indication that a

large enough system of Λ-particles may be bound.

A proposed method is presented in Chapter7 (and Ref.[98]) that can be used to construct the two-body potential using an approximate (guessed) wave function. The accuracy of the method is demonstrated using the examples of the bound systems ep, np, nnp, and $\Lambda\Lambda\alpha$.

8.5   Future work

The work presented here leads to further investigations in the field of hypernuclear physics. An understanding of how the hyperons interact with nucleons and with each other is crucial for developing adequate models in nuclear astrophysics. However it is not easy to develop adequate models since the experimental data on Λ hypernuclei are poorer,both in quantity and quality than the data available on normal nuclei.

Further work on single Λ-nuclear systems should take into the account the $\Lambda N - \Sigma N$ coupling when doing the calculations. So far, the majority of theoretical and experimental works in the field of hyper-nuclear systems were concentrated on the bound states of the Λ particles in various nuclei. The resonances (quasi-bound states) are still waiting for an adequate attention from both the theoreticians and experimentalists.

Appendix A

Nuclear vertex constant

Let H be the hamiltonian of relative Λ-nucleus motion. If the plane waves are normalized to the δ-function, $\langle \vec{k'}|\vec{k}\rangle = \delta(\vec{k'} - \vec{k})$, the scattering amplitude f at the energy z is given by

$$\mathsf{f}(z, \vec{k'}, \vec{k}) = -(2\pi)^2 \mu \langle \vec{k'}|T(z + i0)|\vec{k}\rangle \ , \tag{A.1}$$

where T is the operator obeying the equation

$$T = V + VGV \tag{A.2}$$

with the propagator $G(z) = (z - H)^{-1}$. This propagator can be written in the form of the Berggren spectral expansion[99],

$$G(z) = \sum_n \frac{|n\rangle\langle n|}{z - \mathcal{E}_n} + \sum_r \frac{|\psi_r^+\rangle\langle\psi_r^-|}{z - \mathcal{E}_r} + \mathcal{G}(z) \ , \tag{A.3}$$

which involves singular terms corresponding to bound states $|n\rangle$ and resonances $|\psi_r\rangle$ as well as a background term $\mathcal{G}(z)$. The state-vectors $|\psi_r^\pm\rangle$ are related to each other via the operation of time reversal[100]. Berggren showed[99, 101] that the two sets of resonant states $|\psi_r^+\rangle$ and $|\psi_r^-\rangle$ together constitute a so-called bi-orthogonal set, such that

$$\langle\psi_r^-|\psi_{r'}^+\rangle = \delta_{rr'} \ .$$

The states $|\psi_r^\pm\rangle$ can be normalize to unity using either a regularization procedure[99] or complex rotation of the coordinate[102].

Substituting the expansion (A.3) into Eq. (A.2), we obtain

$$\langle\vec{k'}|T(z)|\vec{k}\rangle = \sum_n \frac{\langle\vec{k'}|V|n\rangle\langle n|V|\vec{k}\rangle}{z - \mathcal{E}_n} + \sum_r \frac{\langle\vec{k'}|V|\psi_r^+\rangle\langle\psi_r^-|V|\vec{k}\rangle}{z - \mathcal{E}_r}$$

$$+ \ \langle\vec{k'}|V|\vec{k}\rangle + \langle\vec{k'}|V\mathcal{G}(z)V|\vec{k}\rangle \ . \tag{A.4}$$

94

Apparently, the T-matrix has first-order poles at all the spectral points ($\mathcal{E}_n$ or $\mathcal{E}_r$), where its residue is either

$$\mathrm{Res}\,[T(z), \mathcal{E}_n] = \langle \vec{k'}|V|n\rangle\langle n|V|\vec{k}\,\rangle \tag{A.5}$$

or

$$\mathrm{Res}\,[T(z), \mathcal{E}_r] = \langle \vec{k'}|V|\psi_r^+\rangle\langle \psi_r^-|V|\vec{k}\,\rangle \ . \tag{A.6}$$

It is well-known (see, for example, Chapter 10 of Ref.[103]) that the scattering T-matrix can be found as

$$\langle \vec{k'}|T(z+i0)|\vec{k}\,\rangle = \langle \vec{k'}|V|\vec{k}+\rangle = \langle \vec{k'}-|V|\vec{k}\,\rangle \ , \tag{A.7}$$

where $|\vec{k}\pm\rangle$ are the scattering states (related to each other via the time reversal in the same way as $|\psi_r^\pm\rangle$). In the case of a bound state, the time reversal operation leaves the state vector unchanged, i.e. $|n+\rangle = |n-\rangle = |n\rangle$ (this is because a bound state formally lives forever, i.e. remains the same when time $t \to \pm\infty$). Therefore, the residues (A.5) and (A.6) are products of the T-matrices describing virtual formation and decay of the corresponding discrete states. Symbolically, these transition operators for a resonance
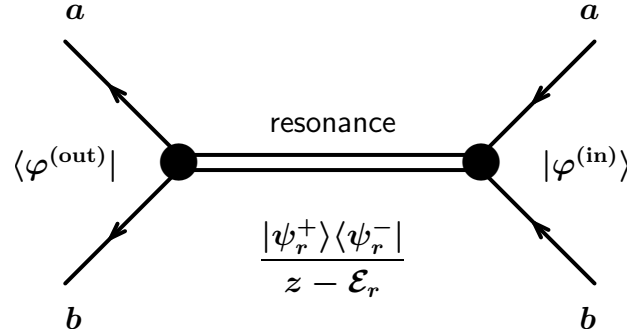
Figure A.1: Symbolic representation of a collision process $a + b \to a + b$ that goes from the in-coming asymptotic state $|\varphi^{(\mathrm{in})}\rangle$ to the out-going asymptotic state $\langle\varphi^{(\mathrm{out})}|$ via formation and subsequent decay of a resonant state $|\psi_r\rangle$ (which corresponds to a pole of the S-matrix at a complex energy $\mathcal{E}_r = \mathcal{E}_R - i\Gamma/2$). The filled circles represent the so-called vertex constants, i.e. the amplitudes of formation and decay of the resonance.

are represented in Fig. A.1 by filled circles. Both momenta, $\vec{k'}$ and $\vec{k}$, are complex and correspond to the energy of a given state,

$$\frac{k'^2}{2\mu} = \frac{k^2}{2\mu} = z \ , \tag{A.8}$$

where z is either $\mathcal{E}_n$ or $\mathcal{E}_r$. With the condition (A.8), the formation and decay amplitudes are constants, which are called vertex constants. They are mainly used in nuclear physics and therefore are known as Nuclear Vertex Constants with a traditional acronym NVC.

95

Apparently, the S-matrix and the T-matrix have exactly the same poles, and their residues differ by a constant factor. We can therefore evaluate NVC by finding the residues of the S-matrix. First of all, because of the rotational invariant, all the spectral states (bound and resonant) are characterized by definite values of the angular momentum ℓ and its z-component m (as we stated earlier, we ignore the spin effects). The partial wave amplitudes $\mathsf{f}_\ell(z)$ do not depend on m and are defined via the expansion

$$\mathsf{f}(z, \vec{k}', \vec{k}) = 4\pi \sum_{\ell m} \mathsf{f}_\ell(z) Y_{\ell m}(\hat{\vec{k}'}) Y^*_{\ell m}(\hat{\vec{k}}) , \qquad (A.9)$$

where k', k, and z are related via the on-shell condition (A.8).

Multiplying Eq. (A.4) by $-(2\pi)^2\mu$, we obtain the corresponding equation for the scattering amplitude. Then we multiply this equation by $Y^*_{\ell m}(\hat{\vec{k}'}) Y_{\ell m}(\hat{\vec{k}})$ and integrate over the angles of vectors $\vec{k}'$ and $\vec{k}$. This gives

$$\mathsf{f}_\ell(z) = -(2\pi)^2\mu \sum_d \frac{\langle klm|V|d^+\rangle\langle d^-|V|klm\rangle}{z - \mathcal{E}_d} + \mathcal{B}(z) , \qquad (A.10)$$

where the states $|klm\rangle$ are defined via the expansion

$$|\vec{k}\rangle = \sqrt{4\pi} \sum_{\ell m} |klm\rangle Y^*_{\ell m}(\hat{\vec{k}}) , \qquad (A.11)$$

the operator $|d^+\rangle\langle d^-|$ stands for a generic discrete state projector (either $|n\rangle\langle n|$ or $|\psi_r^+\rangle\langle\psi_r^-|$), and $\mathcal{B}(z)$ represents the resulting background terms of Eq. (A.4). The summation in Eq. (A.10) runs over the discrete states having the same angular momentum ℓ.

The NVC are usually defined via the residues of the T-matrix (see, for example, Refs. [53, 104]). While the normalization of the scattering amplitude is defined uniquely (its square gives the observable cross section), the normalization of the T-matrix depends on the normalization of the plane waves. We therefore define NVC via the amplitude,

$$G_{d\to ab}(\ell)G_{ab\to d}(\ell) \overset{\text{def}}{=} -\frac{2\pi}{\mu} \lim_{z\to\mathcal{E}_d} (z - \mathcal{E}_d)\mathsf{f}_\ell(z) = \frac{i\pi}{\mu\kappa_d} \lim_{z\to\mathcal{E}_d} (z - \mathcal{E}_d)s_\ell(z) , \qquad (A.12)$$

where $G_{ab\to d}(\ell)$ and $G_{d\to ab}(\ell)$ are the NVC for the formation (from the fragments a and b) and decay of the discrete state d, $\kappa_d = \sqrt{2\mu\mathcal{E}_d}$, and s_ℓ is the partial wave S-matrix,

$$s_\ell(z) = 1 + 2ik\mathsf{f}_\ell(z) . \qquad (A.13)$$

The product $G_{d\to ab}(\ell)G_{ab\to d}(\ell)$ corresponds to the two factors in the numerator on the right hand side of Eq. (A.10). These factors are not independent from each other. Indeed, the second factor can be written as $\langle d^-|V|klm\rangle = \langle d^-|klm\rangle\mathcal{V}(k,\ell)$, where $\mathcal{V}(k,\ell)$ is the

96

potential in the momentum representation (a real function). Taking into account that $\langle d^-|klm\rangle = \langle klm|d^-\rangle^*$ and that the time reversal is equivalent to complex conjugation of the wave function combined with the inversion of the momentum (see chapter 6 of Ref. [103]), as well as using the symmetry property $Y_{\ell m}(-\hat{\vec{k}}) = (-1)^\ell Y_{\ell m}(\hat{\vec{k}})$, we find that $\langle d^-|V|klm\rangle = (-1)^\ell \langle klm|V|d^+\rangle$ and thus

$$G_{d\to ab}(\ell)G_{ab\to d}(\ell) = (-1)^\ell G_{d\to ab}^2(\ell) \ , \tag{A.14}$$

which finally gives

$$G_{d\to ab}^2(\ell) = (-1)^\ell \frac{i\pi}{\mu\kappa_d}\mathrm{Res}\left[s_\ell(z),\mathcal{E}_d\right] \ . \tag{A.15}$$

If $|d\rangle$ is a bound state, then $k = i|\kappa|$. As can be deduced from Fig. 1 of Ref.[63], the partial-wave S-matrix, $s_\ell(z)$, is real on the real negative axis of the physical sheet of the energy Riemann-surface. According to Eq. (A.13) the amplitude $\mathsf{f}_\ell(z)$ is also real on that axis. This implies that the product $G_{d\to ab}(\ell)G_{ab\to d}(\ell)$ is real at all bound state spectral points.

Appendix B

Relation between the S-matrix residues and the ANC

Using the so called Jost solutions $\chi_\ell^{(\pm)}(E, r)$ of the radial Schrödinger equation (5.1) that are defined by the boundary conditions

$$\chi_\ell^{(\pm)}(E, r) \xrightarrow[r\to\infty]{} h_\ell^{(\pm)}(kr) \xrightarrow[r\to\infty]{} (\mp i)^{\ell+1} e^{\pm ikr} , \tag{B.1}$$

the Jost functions (5.6) in the asymptotic behaviour (5.7) of a regular solution $u_\ell(E, r)$ can be written as

$$f_\ell^{(\text{in/out})}(E) = \pm \frac{i}{2k} W\left[\chi_\ell^{(\pm)}, u_\ell\right] , \tag{B.2}$$

where $W[f, g] = fg' - f'g$ is a Wronskian of two functions, and $W[h_\ell^{(-)}(kr), h_\ell^{(+)}(kr)] = 2ik$. It follows from Eq. (B.2) that

$$\dot{f}_\ell^{(\text{in})}(E) = \frac{i}{2k}\left[W(\chi_\ell^{(+)}, \dot{u}_\ell) + W(\dot{\chi}_\ell^{(+)}, u_\ell)\right] + W(\chi_\ell^{(+)}, u_\ell)\frac{d}{dE}\left(\frac{i}{2k}\right) ,$$

where the dot over the functions means the derivative over E. At a spectral point, $\mathcal{E}_d = k_d^2/(2\mu)$, the last term in this equation vanishes because the functions u_ℓ and $\chi_\ell^{(+)}$ are linearly dependent, or simply because their Wronskian is proportional to the vanishing Jost function. Therefore

$$\dot{f}_\ell^{(\text{in})}(\mathcal{E}_d) = \frac{i}{2k_d}\left\{W\left[\chi_\ell^{(+)}(\mathcal{E}_d, r), \dot{u}_\ell(\mathcal{E}_d, r)\right] + W\left[\dot{\chi}_\ell^{(+)}(\mathcal{E}_d, r), u_\ell(\mathcal{E}_d, r)\right]\right\} . \tag{B.3}$$

Our task now is to express the Wronskians on the right hand side of this equation in terms of the discrete state wave function. In order to achieve this, consider the equations

$$\left[\frac{d^2}{dr^2} + k^2 - \frac{\ell(\ell+1)}{r^2} - U(r)\right] u_\ell(E, r) = 0 ,$$

$$\left[\frac{d^2}{dr^2} + \tilde{k}^2 - \frac{\ell(\ell+1)}{r^2} - U(r)\right] \chi_\ell^{(+)}(\tilde{E}, r) = 0 ,$$

98

at two different energies E and $\tilde{E}$. Multiplying the first of them by $\chi_\ell^{(+)}(\tilde{E}, r)$, the second by $u_\ell(E, r)$, and subtracting the second from the first, we obtain

$$u_\ell''(E, r)\chi_\ell^{(+)}(\tilde{E}, r) - u_\ell(E, r)\chi_\ell''^{(+)}(\tilde{E}, r) + (k^2 - \tilde{k}^2)u_\ell(E, r)\chi_\ell^{(+)}(\tilde{E}, r) = 0 \ ,$$

which means that

$$\frac{d}{dr}W\left[\chi_\ell^{(+)}(\tilde{E}, r), u_\ell(E, r)\right] = (\tilde{k}^2 - k^2)u_\ell(E, r)\chi_\ell^{(+)}(\tilde{E}, r) \ . \tag{B.4}$$

The differentiation of this equation over the energy E gives

$$\frac{d}{dr}W\left[\chi_\ell^{(+)}(\tilde{E}, r), \dot{u}_\ell(E, r)\right] = -2\mu u_\ell(E, r)\chi_\ell^{(+)}(\tilde{E}, r) + (\tilde{k}^2 - k^2)\dot{u}_\ell(E, r)\chi_\ell^{(+)}(\tilde{E}, r) \ .$$

If $E = \tilde{E} = \mathcal{E}_d$, then $k^2 - \tilde{k}^2 = 0$, and thus

$$\frac{d}{dr}W\left[\chi_\ell^{(+)}(\mathcal{E}_d, r), \dot{u}_\ell(\mathcal{E}_d, r)\right] = -2\mu u_\ell(\mathcal{E}_d, r)\chi_\ell^{(+)}(\mathcal{E}_d, r) \ . \tag{B.5}$$

Similarly, by differentiating Eq. (B.4) over $\tilde{E}$ and putting $E = \tilde{E} = \mathcal{E}_d$, we obtain

$$\frac{d}{dr}W\left[\dot{\chi}_\ell^{(+)}(\mathcal{E}_d, r), u_\ell(\mathcal{E}_d, r)\right] = 2\mu u_\ell(\mathcal{E}_d, r)\chi_\ell^{(+)}(\mathcal{E}_d, r) \ . \tag{B.6}$$

When $r \to 0$, both $u_\ell(\mathcal{E}_d, r)$ and $\chi_\ell^{(+)}(\mathcal{E}_d, r)$ behave as the Riccati-Bessel function, $\sim (k_d r)^{\ell+1}$. According to the boundary conditions (5.5), the function $u_\ell(\mathcal{E}_d, r)$ near the point $r = 0$ does not have any other energy-dependent (normalization) factor but $k_d^{\ell+1}$. Therefore after differentiation over the energy, the r-dependence remains the same,

$$\dot{u}_\ell(\mathcal{E}_d, r) \underset{r \to 0}{\sim} r^{\ell+1} \ .$$

This means that the functions $\dot{u}_\ell(\mathcal{E}_d, r)$ and $\chi_\ell^{(+)}(\mathcal{E}_d, r)$ are linearly dependent at short distances and thus

$$W\left[\chi_\ell^{(+)}(\mathcal{E}_d, r), \dot{u}_\ell(\mathcal{E}_d, r)\right] \underset{r \to 0}{\longrightarrow} 0 \ . \tag{B.7}$$

When $r \to \infty$, both $u_\ell(\mathcal{E}_d, r)$ and $\chi_\ell^{(+)}(\mathcal{E}_d, r)$ behave as the exponential function, $\sim \exp(+ik_d r)$. According to the boundary condition (B.1), the function $\chi_\ell^{(+)}(\mathcal{E}_d, r)$ at large r does not have any energy-dependent (normalization) factor. Therefore after differentiation over the energy, its r-dependence remains the same. For a bound state the momentum k_d is pure imaginary, $k_d = i|k_d|$, and this exponential function vanishes when $r \to \infty$. If the discrete state we are considering is a resonance, then $\text{Im}\, k_d < 0$. In such a case, we need to rotate the coordinate into the complex plane, $r = |r|\exp(i\theta)$, with such a rotation angle θ that $\text{Im}(k_d r) > 0$. In fact, this is how a resonance wave function can be normalized to unity, namely, by integrating its square from zero to infinity along a ray in the complex plane [102]. Therefore, we can assume that for any discrete state

99

$\exp(+ik_d r) \xrightarrow[r \to \infty]{} 0$ (where for resonances, r goes to infinity along a complex path). This implies that

$$W\left[\dot{\chi}_\ell^{(+)}(\mathcal{E}_d, r), u_\ell(\mathcal{E}_d, r)\right] \xrightarrow[r \to \infty]{} 0 . \tag{B.8}$$

Bearing in mind Eqs. (B.7, B.8) and integrating (for resonances along a complex path) Eq. (B.5) from 0 to r and Eq. (B.6) from r to ∞, we obtain

$$W\left[\chi_\ell^{(+)}(\mathcal{E}_d, r), \dot{u}_\ell(\mathcal{E}_d, r)\right] = -2\mu \int_0^r u_\ell(\mathcal{E}_d, r)\chi_\ell^{(+)}(\mathcal{E}_d, r)dr$$

and

$$W\left[\dot{\chi}_\ell^{(+)}(\mathcal{E}_d, r), u_\ell(\mathcal{E}_d, r)\right] = -2\mu \int_r^\infty u_\ell(\mathcal{E}_d, r)\chi_\ell^{(+)}(\mathcal{E}_d, r)dr .$$

Being substituted into Eq. (B.3), these Wronskians give

$$\dot{f}_\ell^{(\text{in})}(\mathcal{E}_d) = \frac{\mu}{ik_d} \int_0^\infty u_\ell(\mathcal{E}_d, r)\chi_\ell^{(+)}(\mathcal{E}_d, r)dr . \tag{B.9}$$

Comparing the asymptotics (B.1) and (5.7), where $f_\ell^{(\text{in})}(\mathcal{E}_d) = 0$, we see that

$$u_\ell(\mathcal{E}_d, r) = f_\ell^{(\text{out})}(\mathcal{E}_d)\chi_\ell^{(+)}(\mathcal{E}_d, r) . \tag{B.10}$$

Therefore

$$\dot{f}_\ell^{(\text{in})}(\mathcal{E}_d) = \frac{\mu}{ik_d} f_\ell^{(\text{out})}(\mathcal{E}_d) \int_0^\infty \left[\chi_\ell^{(+)}(\mathcal{E}_d, r)\right]^2 dr . \tag{B.11}$$

Let $\phi_\ell(\mathcal{E}_d, r)$ be the normalized wave function of a discrete state

$$\int_0^\infty \left[\phi_\ell(\mathcal{E}_d, r)\right]^2 dr = 1 ,$$

with the asymptotic behaviour

$$\phi_\ell(\mathcal{E}_d, r) \xrightarrow[r \to \infty]{} \mathcal{A}_\ell e^{+ik_d r} , \tag{B.12}$$

where $\mathcal{A}_\ell$ is the asymptotic normalization constant (ANC). Then, comparing the asymptotics (B.12) and (B.1), we see that it is related to the Jost solution as

$$\phi_\ell(\mathcal{E}_d, r) = i^{\ell+1}\mathcal{A}_\ell \chi_\ell^{(+)}(\mathcal{E}_d, r) . \tag{B.13}$$

Using this, we finally obtain the derivative of the Jost function,

$$\dot{f}_\ell^{(\text{in})}(\mathcal{E}_d) = (-1)^{\ell+1}\frac{\mu}{ik_d}\frac{f_\ell^{(\text{out})}(\mathcal{E}_d)}{\mathcal{A}_\ell^2} . \tag{B.14}$$

Since at each spectral point the Jost function $f_\ell^{(\text{in})}(E)$ has a simple zero, the S-matrix has a simple pole, and the corresponding residue is related to the ANC as follows:

$$\text{Res}\left[s_\ell(E), \mathcal{E}_d\right] = \frac{f_\ell^{(\text{out})}(\mathcal{E}_d)}{\dot{f}_\ell^{(\text{in})}(\mathcal{E}_d)} = (-1)^{\ell+1}\frac{ik_d}{\mu}\mathcal{A}_\ell^2 . \tag{B.15}$$

100

Alternatively, the S-matrix can be considered as a function of the momentum k. In such a case, near the pole k_d it behaves as $s_\ell \approx \mathcal{C}_\ell/(k - k_d)$, where $\mathcal{C}_\ell = \mathrm{Res}\,[s_\ell, k_d]$ is the corresponding residue. It is easy to see that

$$\mathrm{Res}\,[s_\ell, k_d] = \frac{\mu}{k_d}\mathrm{Res}\,[s_\ell, \mathcal{E}_d] = i(-1)^{\ell+1}\mathcal{A}_\ell^2 \ . \tag{B.16}$$

Appendix C

Effective-range parameters

In Sec. 3.4 it was shown that the effective-range function

$$\mathcal{F}(E) = k^{2\ell+1} \cot \delta_\ell(k) \tag{C.1}$$

is the ratio of two power-series of variable $E = k^2/2\mu$:

$$\mathcal{F}(E) = \frac{a_0 + a_1 E + a_2 E^2 + \cdots}{b_0 + b_1 E + b_2 E^2 + \cdots} . \tag{C.2}$$

Expanding this function in the Maclaurin series,

$$\mathcal{F}(E) = \mathcal{F}(0) + \mathcal{F}'(0)E + \mathcal{F}''(0)\frac{E^2}{2} + \mathcal{F}'''(0)\frac{E^3}{6} + \mathcal{F}^{(4)}(0)\frac{E^4}{24} + \cdots , \tag{C.3}$$

we can obtain the effective range parameters on the right hand side of Eq. (1.2),

$$\mathsf{a}_\ell = -1/\mathcal{F}(0) , \qquad \mathsf{r}_\ell = \mathcal{F}'(0)/\mu , \tag{C.4}$$

$$\mathsf{P}_\ell = -\frac{\mu \mathcal{F}''(0)}{8\,[\mathcal{F}'(0)]^3} , \qquad \mathsf{Q}_\ell = \frac{\mu^2 \mathcal{F}'''(0)}{48\,[\mathcal{F}'(0)]^5} , \qquad \mathsf{L}_\ell = -\frac{\mu^3 \mathcal{F}^{(4)}(0)}{384\,[\mathcal{F}'(0)]^7} , \tag{C.5}$$

where

$$\mathcal{F}(0) = \frac{a_0}{b_0} , \qquad \mathcal{F}'(0) = \frac{a_1}{b_0} - \frac{a_0 b_1}{b_0^2} , \tag{C.6}$$

$$\mathcal{F}''(0) = \frac{2a_2}{b_0} + \frac{2a_0 b_1^2}{b_0^3} - \frac{2a_0 b_2}{b_0^2} - \frac{2a_1 b_1}{b_0^2} , \tag{C.7}$$

$$\mathcal{F}'''(0) = \frac{6a_3}{b_0} + \frac{6a_1 b_1^2}{b_0^3} - \frac{6a_0 b_1^3}{b_0^4} - \frac{6a_0 b_3}{b_0^2} - \frac{6a_1 b_2}{b_0^2} - \frac{6a_2 b_1}{b_0^2} + \frac{12a_0 b_1 b_2}{b_0^3} , \tag{C.8}$$

$$\mathcal{F}^{(4)}(0) = \frac{24a_4}{b_0} + \frac{24a_0b_2^2}{b_0^3} + \frac{24a_2b_1^2}{b_0^3} - \frac{24a_1b_1^3}{b_0^4} + \frac{24a_0b_1^4}{b_0^5} - \frac{24a_0b_4}{b_0^2} - \frac{24a_1b_3}{b_0^2}$$

$$- \frac{24a_2b_2}{b_0^2} - \frac{24a_3b_1}{b_0^2} + \frac{48a_0b_1b_3}{b_0^3} + \frac{48a_1b_1b_2}{b_0^3} - \frac{72a_0b_1^2b_2}{b_0^4} \ . \tag{C.9}$$

Appendix D

Expansion of the Riccati Functions

The Riccati–Bessel and Riccati–Neumann functions can be factorized asthe Riccati–Bessel and Riccati–Neumann functions as shown in equations and can be factorized as

$$j_\ell(kr) = k^{\ell+1}\tilde{j}_\ell(E, r) \qquad y_\ell(kr) = k^{\ell+1}\tilde{y}_\ell(E, r) \tag{D.1}$$

where the tilded functions depend on k^2. Since these functions are holomorphic, they can be expanded in taylor series at an arbitrary point $E = E_0$,

$$\tilde{j}_\ell(E, r) = \sum_{n=0}^{\infty}(E - E_0)^n g_{\ell n}(E_0, r) \qquad \tilde{y}_\ell(E, r) = \sum_{n=0}^{\infty}(E - E_0)^n t_{\ell n}(E_0, r), \tag{D.2}$$

where the coefficients are given by the derivatives

$$g_{\ell n}(E_0, r) = \frac{1}{n!}\left[\frac{d^n}{dE^n}\tilde{j}_\ell(E, r)\right]_{E=E_0} = \frac{1}{n!}\left[\frac{d^n}{dE^n}\frac{j_\ell(kr)}{k^{\ell+1}}\right]_{E=E_0} \tag{D.3}$$

$$t_{\ell n}(E_0, r) = \frac{1}{n!}\left[\frac{d^n}{dE^n}\tilde{y}_\ell(E, r)\right]_{E=E_0} = \frac{1}{n!}\left[\frac{d^n}{dE^n}k^\ell y_\ell(kr)\right]_{E=E_0} \tag{D.4}$$

the following relations can be used to find the derivatives,

$$\frac{d}{dz}\frac{j_\ell(z)}{z^{\ell+1}} = -\frac{j_{\ell+1}(z)}{z^{\ell+1}} \quad \text{and} \quad \frac{d}{dz}[z^\ell y_\ell(z)] = z^\ell j_{\ell-1}(z). \tag{D.5}$$

After a simple but lengthy algebra, we finally obtain[mathfunction]

$$g_{\ell n}(E_0, r) = \frac{1}{n!}\left[\left(-\frac{\mu r}{\hbar^2}\right)^n \frac{j_{\ell+n}(kr)}{k^{\ell+n+1}}\right]_{E=E_0}, \tag{D.6}$$

$$t_{\ell n}(E_0, r) = \frac{1}{n!}\left(\frac{\mu r}{\hbar^2}\right)^n [k^{\ell-n}y_{\ell-n}(kr)]_{E=E_0}. \tag{D.7}$$

These functions should be the same for all sheets of the Riemann surface , $i.e.$ for any choice of the signs of channel momenta. The matrices γ_n and η_n of equations (3.28) and (3.29) are diagonal with each row having the functions (D.6) and (D.7) with μ and k for the corresponding channel.

Bibliography

[1] E. Gadiloi P.E Hodgson, E. Gadioli. *Introductory Nuclear Physics*. Oxford University Press, (1997).

[2] M.Danysz. Hyperfragments. *Nuovo Cimento suppl*, **4**(609), (1956).

[3] Hoai Le, Johann Haidenbauer, Ulf-G. Meissner, and Andreas Nogga. Jacobi no-core shell model for p-shell hypernuclei. *The European Physical Journal*, **A56**(12), (2020).

[4] L. Tolos and L. Fabbietti. Strangeness in nuclei and neutron stars. *Progress in Particle and Nuclear Physics*, **112**:103770, (2020).

[5] A. Gal, E. V. Hungerford, and D. J. Millener. Strangeness in nuclear physics. *Rev. Mod. Phys.*, **88**:035004, (2016).

[6] Stefano Gandolfi, Alexandros Gezerlis, and J. Carlson. Neutron matter from low to high density. *Annual Review of Nuclear and Particle Science*, **65**(1):303–328, (2015).

[7] Debarati Chatterjee and Isaac Vidana. Do hyperons exist in the interior of neutron stars? *The European Physical Journal*, **A52**(2), (2016).

[8] S. Weissenborn, D. Chatterjee, and J. Schaffner-Bielich. Hyperons and massive neutron stars: Vector repulsion and su(3) symmetry. *Phys. Rev.*, **C85**:065802, (2012).

[9] Kenneth S. Krane. *Introductory nuclear physics*. John Wiley and Sons, Inc., (1988).

[10] Emiko Hiyama and Kazuma Nakazawa. Structure of $s = -2$ hypernuclei and hyperon–hyperon interactions. *Annual Review of Nuclear and Particle Science*, **68**:131–159, (2018).

[11] E. Hiyama. Weakly bound states in light hypernuclei. *Few-Body-Systems*, **34**:79–84, (2004).

[12] O. Hashimoto and H. Tamura. Spectroscopy of Λ hypernuclei. *Progress in Particle and Nuclear Physics*, **57**(2):564–653, (2006).

[13] H. Nemura and for QCD. Central and tensor lambda-nucleon potentials from lattice qcd. (2010).

[14] Fridolin Weber. Strangeness in neutron stars. *Journal of Physics G: Nuclear and Particle Physics*, **27**(3):465, (2001).

[15] T.R. Saito, D. Nakajima, C. Rappold, Sébastien Bianchin, O. Borodina, Vakkas Bozkurt, B. Göküzüm, Myroslav Kavatsyuk, Eunjeo Kim, Yuanxin Ma, F. Maas, S. Minami, B. Özel Tashenov, Patrick Achenbach, S. Ajimura, T. Aumann, Carlos Ayerbe Gayoso, H.C. Bhang, C. Caesar, and W. Trautmann. Production of hypernuclei in peripheral hi collisions: The hyphi project at gsi. *Nuclear Physics*, **A881**:218–227, (2012).

[16] M. Danysz, K. Garbowska, J. Pniewski, T. Pniewski, J. Zakrzewski, E. Fletcher, J. Lemonne, P. Renard, J. Sacton, W. Toner, Diarmuid O'Sullivan, and T. Shah. Observation of a double hyperfragment. *Physical Review Letters*, **11**:29–32, (1963).

[17] M. Danysz, K. Garbowska, J. Pniewski, T. Pniewski, J. Zakrzewski, E.R. Fletcher, J. Lemonne, P. Renard, J. Sacton, W.T. Toner, Diarmuid O'Sullivan, T.P. Shah, A. Thompson, P. Allen, Sr.M. Heeran, A. Montwill, J.E. Allen, M.J. Beniston, Donald Davis, and P.V. March. The identification of a double hyperfragment. *Nuclear Physics*, **49**:121–132, (1963).

[18] Shigeki Aoki, S. Bahk, K. Chung, S.H. Chung, H. Funahashi, Chang Hahn, T. Hara, S. Hirata, K. Hoshino, M. Ieiri, Toru Iijima, Kohzoh Imai, T. Ishigami, Y. Itow, M. Kazuno, K. Kikuchi, C. Kim, D. Kim, J. Kim, and Chunsil Yoon. Direct observation of sequential weak decay of a double hypernucleus. *Progress of Theoretical Physics*, **85**:1287–1298, (1991).

[19] C. Dover, D. Millener, A Gal, and Donald Davis. Interpretation of a double hypernucleus event. *Physical review: Nuclear physics*, **C44**:1905–1909, (1991).

[20] Hiroshi Takahashi, J.K. Ahn, H. Akikawa, Shigeki Aoki, K. Arai, S.Y. Bahk, Kyungmin Baik, B. Bassalleck, J.H. Chung, M.S. Chung, Donald Davis, T. Fukuda, K. Hoshino, A. Ichikawa, M. Ieiri, Kohzoh Imai, Y.H. Iwata, Y.S. Iwata, H. Kanda, and Longming Zhu. Observation of a $_{\Lambda\Lambda}^{6}$He double hypernucleus. *Physical Review Letters*, **87**:2125021–2125025, (2001).

[21] J. Ahn, H. Akikawa, Shigeki Aoki, K. Arai, S. Bahk, Kyungmin Baik, B. Bassalleck, J. Chung, M. Chung, Donald Davis, T. Fukuda, K. Hoshino, A. Ichikawa, M. Ieiri, Kohzoh Imai, K. Itonaga, Y. Iwata, Y. Iwata, H. Kanda, and L. Zhu. Double-Λ hypernuclei observed in a hybrid emulsion experiment. *Physical Review*, **C88**, (2013).

[22] Kazuma Nakazawa. Double-Λ hypernuclei via the Ξ-hyperon capture at rest reaction in a hybrid emulsion. *Nuclear Physics*, **A835**:207–214, (2010).

[23] H. Nemura, Y. Akaishi, and Y. Suzuki. Ab initio approach to s-shell hypernuclei $^3_\Lambda$H,$^4_\Lambda$H,$^4_\Lambda$He and $^5_\Lambda$He with a $\Lambda n - \Sigma n$ interaction. *Phys. Rev. Lett.*, **89**:142504, (2002).

[24] Emiko Hiyama, Masayasu Kamimura, Yasuo Yamamoto, Toshio Motoba, and Thomas A. Rijken. S=-1 hypernuclear structure. *Progress of Theoretical Physics Supplement*, **185**:106–151, (2010).

[25] L. Contessi, N. Barnea, and A. Gal. Resolving the Λ hypernuclear overbinding problem in pionless effective field theory. *Phys. Rev. Lett.*, **121**:102502, (2018).

[26] L. Contessi, M. Schäfer, N. Barnea, A. Gal, and J. Mareš. The onset of $\Lambda\Lambda$ hypernuclear binding. *Physics Letters*, **B797**:134893, (2019).

[27] Diego Lonardoni, Alessandro Lovato, Stefano Gandolfi, and Francesco Pederiva. Hyperon puzzle: Hints from quantum monte carlo calculations. *Phys. Rev. Lett.*, **114**:092301, (2015).

[28] Hoai Le, Johann Haidenbauer, Ulf-G. Meißner, and Andreas Nogga. Implications of an increased Λ-separation energy of the hypertriton. *Physics Letters*, **B801**:135189, (2020).

[29] K. Miyagawa and W. Glöckle. Hypertriton calculation with meson-theoretical nucleon-nucleon and hyperon-nucleon interactions. *Phys. Rev.*, **C48**:2576–2584, (1993).

[30] K. Miyagawa, H. Kamada, W. Glöckle, and V. Stoks. Properties of the bound $\Lambda(\Sigma)$nn system and hyperon-nucleon interactions. *Phys. Rev.*, **C51**:2905–2913, (1995).

[31] A. Nogga. Light hypernuclei based on chiral and phenomenological interactions. *Nuclear Physics*, **A914**:140–150, (2013). XI International Conference on Hypernuclear and Strange Particle Physics (HYP2012).

[32] A. Nogga. Light hypernuclei based on chiral and phenomenological interactions. *Nuclear Physics*, **A914**:140–150, (2013). XI International Conference on Hypernuclear and Strange Particle Physics (HYP2012).

[33] J. Haidenbauer and U.-G. MeiBner and A. Nogga. Hyperon-nucleon interaction within chiral effective field theory revisited. *The European Physical Journal*, **A56**(3), (2020).

[34] A Gal, J.M Soper, and R.H Dalitz. A shell-model analysis of Λ binding energies for the p-shell hypernuclei iii. further analysis and predictions. *Annals of Physics*, **113**(1):79–97, (1978).

[35] D. J. Millener, A. Gal, C. B. Dover, and R. H. Dalitz. Spin dependence of the Λ n effective interaction. *Phys. Rev.*, **C31**:499–509, (1985).

[36] D.J. Millener. Shell-model calculations for *p*-shell hypernuclei. *Nuclear Physics*, **A881**:298–309, (2012). Progress in Strangeness Nuclear Physics.

[37] A. Gal and D.J. Millener. Neutron-rich hypernuclei:$^6_\Lambda$H,and beyond. *Physics Letters*, **B725**(4):445–450, (2013).

[38] Bing-Nan Lu, Emiko Hiyama, Hiroyuki Sagawa, and Shan-Gui Zhou. Superdeformed Λ hypernuclei within relativistic mean field models. *Phys. Rev.*, **C89**:044307, (2014).

[39] Bing-Nan Lu, Emiko Hiyama, Hiroyuki Sagawa, and Shan-Gui Zhou. Superdeformed Λ hypernuclei within relativistic mean field models. *Phys. Rev.*, **C89**:044307, (2014).

[40] Dillon Frame, Timo A. Lähde, Dean Lee, and Ulf-G. Meissner. Impurity lattice monte carlo for hypernuclei. *The European Physical Journal*, **A56**(10), (2020).

[41] Bruce R. Barrett, Petr Navrátil, and James P. Vary. Ab initio no core shell model. *Progress in Particle and Nuclear Physics*, **69**:131–181, (2013).

[42] K. Amos S.A Rakityansky, S.A Sofianos. A method for calculating the Jost functions for analytical potentials. *Nuovo Cimento*, **B111**:363–378, (1996).

[43] S.A Sofianos S.A Rakityansky. Exact method for locating potential resonances and Regge trajectories. *J. Phys.A:Math.Gen*, **A30**(10):3725–3737, (1997).

[44] G. P Vermaak S. A Sofianos, S.A Rakityansky. Subthreshold resonances in few-neutron systems. *Nuclear and Particle Physics*, **23**(11):1619–1629, (1997).

[45] SA Rakityansky and SA Sofianos. Jost function for coupled partial waves. *Journal of Physics: Mathematical and General*, **A31**(22):5149, (1998).

[46] S A Rakityansky and N Elander. Multi-channel analog of the effective-range expansion. *Journal of Physics A: Mathematical and Theoretical*, **44**(11):115303, (2011).

[47] M. Hussein, W. Li, and S. Wuster. Canonical quantum potential scattering theory. *J. Phys. A: Math. Theory.*, **41**:475207, (2008).

[48] D.J. Millenerz A. Gal, E.V. Hungerfordy. Strangeness in nuclear physics. *arXiv:1605.00557v2 [nucl-th]*, (2016).

[49] C. Providencia A. Polls I. Bombaci D. Logoteta, I. Vidana. Effect of hyperonic three-body forces on the maximum mass of neutron stars. *Journal of Physics: Conference Series*, **342**:012006, (2012).

[50] K. Saito T. Katayama. Hyperons in neutron stars. *Phys. Lett.*, **B747**:43–47, (2015).

[51] I. Bombaci. The hyperon puzzle in neutron stars. *arXiv:1601.05339v1 [nucl-th]*, (2016).

[52] R.E. Tribble A. Sattarov A.M. Mukhamedzhanov, R.P. Schmitt. Aastrophysical factor for the radiative capture reaction $\alpha + d \rightarrow {}^6\text{Li} + \gamma$. *Phys. Rev.*, **C52**:3483–3487, (1995).

[53] L. Blokhintsev, Vasily Eremenko, B. Irgaziev, and Yu Orlov. Vertex constants(asymptotic normalization coefficients) and mean-square radii of hypernuclei in the potential model. *Bulletin of the Russian Academy of Sciences: Physics*, **71**:408–414, (2007).

[54] Rakityansky S. A. and Gopane I. M. Effective-range parameters and vertex constants for Λ-nuclear systems. *International Journal of Modern Physics E*, **26**(04):1750014, (2017).

[55] Nouredine Zettili. Quantum mechanics: Concepts and applications. *Quantum Mechanics: Concepts and Applications, by Nouredine Zettili, pp. 664. ISBN 0-471-48944-1. Wiley-VCH , October 2001.*, **71**, (2001).

[56] R. Jost. "uber die falschen nullstellen der eigenwerte der s-matrix". *Helv. Phys. Acta, v. XX, pp. 256-266*, (1947).

[57] J. Mathews and L.R Walker. *Mathematical Methods of Physics*. W.A. Benjamin., New York, (1964).

[58] S. Rakityansky and Nils Elander. Analyzing the contribution of individual resonance poles of the s -matrix to two-channel scattering. *Int. J. Quantum Chem.*, **106**:1105–29, (2006).

[59] S.A Rakityansky. *Jost Functions in Quantum Mechanics: A Unified Approach to Scattering, Bound, and Resonant State Problems*. Switzerland AG: Springer Nature, (2022).

[60] Milton Abramowitz. *Handbook of Mathematical Functions, With Formulas, Graphs, and Mathematical Tables,*. Dover Publications, Inc., New York, USA, (1974).

[61] S. Rakityansky and S. Sofianos. Jost function for coupled channels. *Few-Body Syst. Suppl.*, pages 93–96, (1999).

[62] S. Rakityansky. Unified treatment of bound, scattering, and resonant states in one-dimensional semiconductor nanostructures. *Phys. Rev.*, **B68**, (2003).

[63] S. Rakityansky, S. Sofianos, and Nils Elander. Pade approximation of the s-matrix as a way of locating quantum resonances and bound states. *J. Phys. A: Math. Theor.*, **A40**:pp. 14857–14869, (2007).

[64] S. Rakityansky and SA Sofianos. Jost function for coupled partial waves. *J. Phys.*, **A31**:5149–75, (1998).

[65] S. Massen, S. Sofianos, S. Rakityansky, and Shinsho Oryu. Effective interactions: Resonances and off-shell characteristics. *HNPS Proceedings*, **10**:93, (2019).

[66] S. Rakityansky. Modified transfer matrix for nanostructures with arbitrary potential profile. *Phys. Rev.*, **B70**, (2004).

[67] S. Rakityansky and Nils Elander. Analytic structure and power-series expansion of the jost matrix. *Few-Body Systems*, **54**, (2012).

[68] K.M. Watson M.L. Goldberger. *Collision Theory.* John Wiley and Sons, New York, London, Sydney, (1967).

[69] A.M. Perelomov A.I. Baz, Ya.B. Zeldovich. Scattering, reactions and decay in nonrelativistic quantum mechanics. *Israel Program for Scientific Translations: Jerusalem*, (1969).

[70] S. Rakityansky and Nils Elander. Generalized effective-range expansion. *Journal of Physics A: Mathematical and Theoretical*, **42**:225302, (2009).

[71] L. Blokhintsev, Vasily Eremenko, B. Irgaziev, and Yu Orlov. Characteristics of scattering of Λ hyperons from nuclei within the potential model. *Bulletin of the Russian Academy of Sciences: Physics*, **72**:811–816, (2008).

[72] Andrea Lombardi, Federico Palazzetti, L. Peroncelli, Gaia Grossi, Vincenzo Aquilanti, and Mikhail Sevryuk. Few-body quantum and many-body classical hyperspherical approaches to reactions and to cluster dynamics. *Theoretical Chemistry Accounts*, **117**:709–721, (2007).

[73] D.H. Davis and J. Pniewski. "hypernuclei". *Contemporary Physics*, **27**:91, (1986).

[74] Curtis Gerald and Patrick Wheatley. Applied numerical analysis. (2023).

[75] S.C. Frautschi. Regge poles and s-matrix theory. (frontiers in physics). (2023).

[76] H. Togashi, E. Hiyama, Y. Yamamoto, and M. Takano. Equation of state for neutron stars with hyperons using a variational method. *Physical Review*, **C93**, (2016).

[77] R.G. Newton. "scattering theory of waves and particles". *New York: McGraw-Hill*, (1967).

[78] R.I. Jibuti and N.B. Krupennikova. *"The Method of Hyperspherical Functions in the Quantum Mechanics of Few Bodies", [in Russian] Metsniereba, Tbilisi*, (1984).

[79] A.M. Gorbatov, Pavel Komarov, Yury Krylov, A.V. Bursak, V.L. Skopich, P.Yu Nikishov, and Elena Kolganova. Multineutron systems in the hyperspherical basis. *Soviet Journal of Nuclear Physics-Ussr*, **50**:218–223, (1989).

[80] Yu.F. Smirnov A.M. Shirokov and S.A. Zaytsev. *"Modern Problems in Quantum Theory", (Ed. V.I. Savrinm and O.A. Khrustalev), (Moscow)*, (1998).

[81] A. Shirokov, George Papadimitriou, A. Mazur, I. Mazur, R. Roth, and J. Vary. Prediction for a four-neutron resonance. *Physical Review Letters*, **117**, (2016).

[82] Hidekatsu Nemura, Yasuyuki Suzuki, Yoshikazu Fujiwara, and Choki Nakamoto. Study of light lambda- and lambda lambda-hypernuclei with the stochastic variational method and effective lambda n potentials. *Progress of Theoretical Physics*, **103**, (1999).

[83] Georges Audi, A.H. Wapstra, and Cidalia Thibault. The ame2003 atomic mass evaluation. *Nuclear Physics*, **A729**:337–676, (2003).

[84] Ingo Sick and Dirk Trautmann. On the rms radius of the deuteron. *Nuclear Physics*, **A637**:559–575, (1996).

[85] Rudi Malfliet and J.A. Tjon. Solution of the faddeev equations for the triton problem using local two-particle interactions. *Nuclear Physics*, **A127**:161–168, (1969).

[86] G. Payne, J. Friar, B. Gibson, and I. Afnan. Configuration space faddeev calculations. i. triton ground state properties. *Phys. Rev.*, **C22**, (1980).

[87] V. K.Khersonskii D. A. Varshalovich, A. N. Moskalev. *Quantum Theory of Angular Momentum*. World Scientific: Singapore, New Jersey, Hong Kong, (1988).

[88] S. Yakovlev. Weak asymptotics of the wave function for an n-particle system and asymptotic filtration. *Theoretical and Mathematical Physics*, **206**:68–83, (2021).

[89] Y. C. Tang K. Wildermuth. *A Unified Theory of the Nucleus*. (1977).

[90] István Angeli and Krassimira Marinova. Table of experimental nuclear ground state charge radii: An update. *Atomic Data and Nuclear Data Tables*, **99**:69–95, (2013).

[91] Georges Audi, Wang Meng, A.H. Wapstra, Filip Kondev, M. MacCormick, Xing Xu, and B. Pfeiffer. The ame2012 atomic mass evaluation. *Chinese Physics*, **C36**:1287, (2012).

[92] V. Stoks and Th Rijken. Soft-core baryon-baryon potentials for the complete baryon octet. *Physical Review*, **C59**, (1999).

[93] Toshio Motoba Taiichi Yamada Emiko Hiyama, Masayasu Kamimura and Yasuo Yamamoto. Three- and four-body cluster models of hypernuclei using the g-matrix Λn interaction. *Progress of Theoretical Physics*, **97**(6):881–899, (1997).

[94] I. Filikhin and A. Gal. Faddev-yakubovsky calculations for light $\Lambda\Lambda$ hypernuclei. *Nuclear Physics*, **A707**:491–509, (2002).

[95] E. Hiyama, M. Kamimura, T. Motoba, T. Yamada, and Y. Yamamoto. Four-body cluster structure of $a = 7 - 10$ double-Λ hypernuclei. *Phys. Rev.*, **C66**:024007, (2002).

[96] H. Takahashi et al. Observation of a $^{6}_{\Lambda\Lambda}$He Double Hypernucleus. *Phys. Rev. Lett.*, **87**(21):212502, (2001).

[97] I. N. Filikhin and S. L. Yakovlev. $^{6}_{\Lambda\Lambda}$He and $^{9}_{\Lambda\Lambda}$Be systems in the three-body cluster model treated on the basis of differential faddeev equations. *Physics of Atomic Nuclei*, Vol.**63**(3):pp. 336–342, (2000).

[98] Rakityansky S.A. Belyaev, V.B. and I.M. Gopane. Recovering the two-body potential from a given three-body wave function. *Few-Body Systems*, **64**, (2022).

[99] Tore Berggren. On the use of resonant states in eigenfunction expansions of scattering and reaction amplitudes. *Nucl.Phys.*, **A109**:265–287, 1968.

[100] T. Berggren. On resonance contributions to sum rules in nuclear physics. *Phys.Lett.*, **44**:23–25, (1973).

[101] T. Berggren. On a probabilistic interpretation of expansion coefficients in the non-relativistic quantum theory of resonant states. *Phys.Lett.*, **B33**:547–549, (1970).

[102] T. Rescigno and CW McCurdy. Normalization of resonance wave functions and the calculation of resonance widths. *Physical review.*, **A34**:1882–1887, 1986.

[103] J.R. Taylor. Scattering theory. *Dover Publications, Inc., Mineola, New York*, (2000).

[104] E.I. Dolinski L.D. Blokhintsev, I. Borbei. Nuclear vertex constants. *Sov.J.Part.Nucl.*, **8**:485, (1977).